NASA TECHNICAL NOTE

NASA TN D-7563

NASA TN D-7563

FLIGHT-TEST INVESTIGATION OF THE AERODYNAMIC CHARACTERISTICS AND FLOW INTERFERENCE EFFECTS ABOUT THE AFT FUSELAGE OF THE F-111A AIRPLANE

by Norman V. Taillon

Flight Research Center
Edwards, Calif. 93523

NATIONAL AERONAUTICS AND SPACE ADMINISTRATION • WASHINGTON, D. C. • FEBRUARY 1974

1. Report No.	2. Government Accession No.	3. Recipient's Catalog No.
NASA TN D-7563		

4. Title and Subtitle	5. Report Date
FLIGHT-TEST INVESTIGATION OF THE AERODYNAMIC CHARACTERISTICS AND FLOW INTERFERENCE EFFECTS ABOUT THE AFT FUSELAGE OF THE F-111A AIRPLANE	February 1974
	6. Performing Organization Code
7. Author(s)	8. Performing Organization Report No.
Norman V. Taillon	H-717
	10. Work Unit No.
9. Performing Organization Name and Address	766-76-01-00
NASA Flight Research Center P. O. Box 273 Edwards, California 93523	11. Contract or Grant No.
	13. Type of Report and Period Covered
12. Sponsoring Agency Name and Address	Technical Note
National Aeronautics and Space Administration Washington, D. C. 20546	14. Sponsoring Agency Code

15. Supplementary Notes

16. Abstract

Static pressure measurements were made on the aft fuselage of an F-111A airplane to determine local flow characteristics and engine/airframe interaction effects. Data were obtained over the Mach number range from 0.5 to 2.0. Aspiration effects associated with low ejector nozzle expansion ratios reduced the local pressure coefficients particularly on the interfairing but also extending to the trailing edge of the nacelle. The presence of afterbodies also affected the behavior of the air flowing into and about the ejector nozzle.

Pressures about the aft fuselage were improved by an increase in primary nozzle area at a supersonic speed.

A comparison of wind-tunnel and flight-test results showed generally good agreement, although there was a large disparity in pressure level about the ejector nozzle. However, the shape of the data curves and the local flow behavior were basically similar.

17. Key Words (Suggested by Author(s))	18. Distribution Statement
Aircraft/engine integration Flow interference F-111A airplane	Unclassified - Unlimited Cat. 01

19. Security Classif. (of this report)	20. Security Classif. (of this page)	21. No. of Pages	22. Price*
Unclassified	Unclassified	77	$3.75

* For sale by the National Technical Information Service, Springfield, Virginia 22151

FLIGHT-TEST INVESTIGATION OF THE AERODYNAMIC CHARACTERISTICS AND FLOW INTERFERENCE EFFECTS ABOUT THE AFT FUSELAGE OF THE F-111A AIRPLANE

Norman V. Taillon
Flight Research Center

INTRODUCTION

The rapid expansion of the operational envelopes of military and commercial aircraft and the stringent requirement for maximum propulsion efficiency at critical points within the envelopes have placed upon the airplane designer a demand for improvements in the employment of available thrust. The search for new techniques has led toward the development of variable-geometry exhaust nozzles and the use of boundary layer bleed flow for thrust augmentation of internally mounted engines. Thus the engine and airplane have been integrated into a single propulsion system.

The components of the propulsion system, however, inevitably have an aerodynamic influence upon each other. These interactions take the form of airframe-generated constraints on auxiliary nozzle flow requirements and exhaust flow aspiration influence on adjacent structure. From the outset, then, design considerations must include steps to integrate the engine with the airplane in order to minimize unfavorable interaction effects. Careful aft fuselage design, extensive and varied local flow studies, wind-tunnel tests of hot-flow models, and empirical data from flight tests of advanced airplanes may all prove to be useful.

A significant amount of wind-tunnel data was obtained for the F-111A airplane in the studies of references 1 to 5, for example. Reference 1 indicated that 40 percent to 50 percent of the entire airplane drag at transonic speeds may be attributed to the aft fuselage. In addition, the blow-in-door nozzle was tested in isolated form in the studies of references 6 and 7, and the effects of interference drag were included in an analytical procedure in reference 8. Little is known, however, about local flow and interaction effects in full-scale flight. The NASA Flight Research Center has conducted flight tests of an F-111A airplane that was extensively instrumented about the aft fuselage and ejector nozzle. This report discusses the aerodynamic characteristics and flow interference effects revealed in that investigation, and the effect of flight variables.

SYMBOLS

Physical quantities in this report are given in the International System of Units and parenthetically in U.S. Customary Units. Calculations and measurements were made in U.S. Customary Units. Factors relating the two systems are presented in reference 9.

A	area, m^2 (ft^2)
C_p	pressure coefficient, $\frac{p - p_\infty}{q}$
h	overall height of airplane, m (ft)
l	overall length of airplane, m (ft)
M	Mach number
p	local static pressure, kN/m^2 (lb/ft^2)
p_i	impact pressure, kN/m^2 (lb/ft^2)
p_t	total pressure, kN/m^2 (lb/ft^2)
q	free-stream dynamic pressure, $\frac{1}{2}\rho V^2$, kN/m^2 (lb/ft^2)
R	Reynolds number, $\frac{\rho V}{\mu}$, per m (ft)
T	total temperature, °K (°R)
V	airplane velocity, m/sec (ft/sec)
W	weight-flow rate, kN/sec (lb/sec)
x	axial distance coordinate, m (ft)
z	vertical distance coordinate, m (ft)
α	airplane angle of attack, deg
δ	boundary layer thickness, m (ft)
μ	free-stream viscosity, kg/m-sec (lb/ft-sec)
ρ	free-stream density, kg/m^3 (lb/ft^3)
φ	angular position coordinate, looking forward, deg

$\omega\sqrt{\tau}$ corrected secondary weight flow, $\frac{W_s}{W_p}\sqrt{\frac{T_s}{T_p}}$

Subscripts:

av	average
int	internal surface
n	ejector nozzle
p	primary nozzle
s	secondary flow (boundary layer bleed duct)
∞	free-stream condition

DESCRIPTION OF THE AIRPLANE

The F-111A airplane used in this investigation was one of several preproduction models. It was characterized by a high wing with sweep variable from 16° to 72°. The horizontal tail surfaces were all movable. The airplane was capable of supersonic flight at sea level as well as at high altitudes and could loiter for a sustained period at subsonic speed. A photograph and a three-view drawing of the airplane are presented in figures 1 and 2, respectively. Detailed physical characteristics are included in reference 10.

The F-111A airplane was powered by two internally mounted Pratt & Whitney TF30 P-1 afterburning turbofan engines. Each engine provided 46.7 kilonewtons (10,500 pounds) of thrust at sea level in the military power setting and 82.3 kilonewtons (18,500 pounds) of thrust at full reheat power. Thrust was variable within each of the five sequentially ignited stages of afterburning.

To promote operational efficiency throughout the extended flight envelope, a principal feature of the engine was an ejector nozzle (fig. 3) fitted aft of the primary nozzle. At lower speeds and nozzle expansion ratios, tertiary air was admitted to the ejector nozzle through free-floating blow-in doors upon demand created by the depressed ejector nozzle pressures associated with underexpanded nozzle flow. Free-floating interleaved sections (tail feathers) formed the aft end of the ejector nozzle and operated in conjunction with the blow-in doors to control the expansion of the primary nozzle flow.

Boundary layer bleed air, separated from the engine inlet flow by a splitter plate and ducted about the engine (fig. 4), was used to cool the ejector nozzle and to augment the ejector nozzle flow. A portion of this flow normally went through apertures in the bulkhead to which the blow-in doors were hinged; however, as indicated in the figure, these apertures were closed during this flight-test program.

The fuselage was terminated by a fairing (interfairing) between the engines and by afterbodies (speed bumps) which formed a fairing of the elevon roots and actuator assemblies.

INSTRUMENTATION AND ACCURACY

Extensive instrumentation was installed about the aft fuselage to aid in evaluating the complicated flow field and in defining interaction effects. Flow was assumed to be symmetrical, thus only the left half of the fuselage and the left engine were instrumented.

In this report static pressures are divided into the functional groups listed below and illustrated in figures 5(a) to 5(c). A sketch of the pertinent group is included with each data figure. (Circled numbers refer to figure 5.)

Nacelle, upper and lower surfaces – Two rows of five orifices on each surface. Six-probe rakes at $\varphi = 20^\circ$ and 140°. $x/l = 0.867$. (1) (5)

Interfairing, left side and base – Eight orifices on the side; either two or three orifices on the base, varying with configuration. (2) (3)

Speed bump – Two orifices on the inside surface near the root and tip. (4)

Ejector nozzle shroud, external – Six rows of five orifices each, spaced evenly about the nozzle on the extended centerline of the blow-in doors. (6)

Ejector nozzle shroud, internal – Two rows of three orifices each at $\varphi = 75^\circ$ and 135°. Also two four-probe rakes at $\varphi = 105^\circ$ and 170°. (6)

Blow-in doors, external and internal – One row of three external orifices on the centerline of the doors at $\varphi = 85^\circ$ and 145°. Also individual orifices at $\varphi = 80^\circ$ and 140° on the internal surfaces of these doors. (7)

Primary nozzle base – Individual orifices on the boattail at $\varphi = 350^\circ$ and 80°. $x/l = 0.903$ (fig. 4).

Boundary layer bleed duct – Total temperature and total pressure sensors and static pressure orifices at $\varphi = 0^\circ$ and 180°. $x/l = 0.870$ (fig. 4).

Individual pressure measurements were obtained from static pressure orifices installed flush with the local surface and connected by tubing to one of two differential pressure transducers through multiplexing valves (Scanivalves) in the interfairing. Both transducers were referenced to a common reservoir. The reservoir pressure was measured by an absolute pressure transducer mounted in a third Scanivalve. This Scanivalve was also used to measure total and impact pressures. Each Scanivalve could measure 48 pressures in rotation, completing the sequence in 2.5 seconds. The three Scanivalves were synchronized by a common timer and acted as

subcommutators to a similar number of channels of an onboard pulse code modulation (PCM) system. The ratio of the PCM system sampling rate to the Scanivalve sampling rate was 10; consequently, each Scanivalve measurement was sampled 10 times by the PCM system commutator.

Data from the PCM system were telemetered to a ground receiving station during flight for recording, and critical parameters were monitored in real time on a strip chart recorder. Data were reduced by an automatic data processing method in which the average of the last six of the ten PCM system samples was used as the value of each data point. This procedure eliminated the samples obtained when pressures were adjusting to new values.

All data were obtained under steady-state flight conditions.

The accuracy of the following measurements was estimated to be:

Mach number	±0.008
Altitude, m (ft)	±33.5 (±110)
Angle of attack, deg	±0.3
Total temperature, °K (°R)	±2.8 (±5.0)
Impact pressure, kN/m^2 (lb/ft^2)	±1.45 (±30.24)
Total pressure, kN/m^2 (lb/ft^2)	±1.45 (±30.24)
Free-stream total pressure, kN/m^2 (lb/ft^2)	±0.83 (±17.28)
Static pressure coefficient	±0.030
Blow-in-door position, percent open	±1.2
Tail-feather position, percent open	±1.2

Wind-Tunnel Model and Tests

Extensive tests have been made on a carefully detailed 1/12-scale model of the F-111 airplane in the 16-foot transonic wind tunnel at the NASA Langley Research Center (fig. 6). (Complete model dimensions are given in reference 2.) The positions of the blow-in doors were not measured on the model, however, and the primary nozzle area was fixed to represent a full-scale area of 0.34 square meter (3.65 square feet). The tail feathers were not movable but were represented by a solid turned surface. The model had a hot flow passage, variable over a range of total pressures for the primary jet (ref. 11), and separate cold flow passages, designated as bleed and secondary ducts, variable over a range of mass flows. The secondary flow duct discharged air directly into the ejector nozzle inside the blow-in doors; air from the bleed flow duct passed on the outside of the blow-in doors and entered the ejector nozzle only when the doors were open. As mentioned previously, the corresponding duct flow on the full-scale airplane was split at the leading edge of the blow-in doors to form the two flows represented separately in the model. The secondary passage was closed on the full-scale airplane, cutting off the flow to the inside of the blow-in doors; therefore, results from wind-tunnel tests in which secondary flow was used were not included in the comparative data.

Areas where static pressure measurements were obtained on the full-scale vehicle were duplicated on the model where possible to enable direct comparison of data. A large number of ejector nozzle, interfairing, and speed bump configurations were included in the wind-tunnel development program; however, because the flight vehicle was a preproduction airplane, with one of the earlier ejector nozzle designs tested only briefly in model form, only limited wind-tunnel results (unpublished) were available for comparison with the flight configuration.

In the wind-tunnel tests two runs were made at each test Mach number (0.5, 0.7, and 0.9), during which either the left engine primary nozzle total pressure ratio or the corrected weight-flow ratio for the bleed duct was varied incrementally while the other was held constant.

RESULTS AND DISCUSSION

External Flow

Blow-in-door positions are shown in figure 7 for three representative Mach numbers. At Mach 0.76 the engine demand for augmenting airflow was large, so the doors were almost fully open to supply the required flow. At Mach 1.61 the demand for additional air declined considerably, and the average door opening was approximately one-third of full travel. As Mach number increased to 2.01, the doors were nearly closed; the ejector nozzle was pressurized by the jet efflux, and only a small amount of augmenting airflow was required.

As shown in figure 8, nozzle tail feathers closed at the lower engine power setting ($M = 0.76$) and opened as power was increased to maintain full expansion of the jet flow. However, the tail feathers did not open beyond approximately 80 percent of full travel. This is attributed to interleaf friction.

The aft fuselage (engine nacelle) pressure coefficients became considerably less negative in the transition from subsonic to supersonic speed, as shown in figures 9(a) to 9(d). The peaks at $x/l = 0.86$ in figure 9(a) at the supersonic Mach numbers are attributed to local flow interactions not identifiable by source. Another local effect was the reduction in pressure coefficient about the trailing edge of the nacelle at the subsonic Mach number as a result of ejector nozzle aspiration. It is believed that aspiration tended to thin out the boundary layer, thus increasing the pressure coefficients at the leading edge of the ejector nozzle, particularly at $\varphi = 230^\circ$ (fig. 9(c)).

The rounded peaks near the trailing edge of the nacelle were probably caused by compression of the flow by a shallow wedge formed by remission of the boattail angle, as indicated in the accompanying sketches. This permitted the nacelle to be terminated in a zero-slope annulus about the boundary layer bleed duct.

As shown in figures 9(a) to 9(d), pressures measured on the external surface of the ejector nozzle typically resulted in an S-shaped curve, formed partially by the characteristic expansion of the flow about the truncated cone ejector nozzle shroud

and its subsequent rapid recompression. Some secondary expansions at the trailing edge of the shroud, notably at subsonic speed, are believed to have been caused by low pressures within the nozzle and the likelihood of leakage between nozzle leaves.

Figures 10(a) and 10(b) show pressure curves for the blow-in door, ejector nozzle, interfairing, and speed bump where the proximity of the engine and adjacent structure suggested the likelihood of flow interference. The pressure coefficients at $\varphi = 85^\circ$ (fig. 10(a)) on the ejector nozzle showed less variation than at other axial locations, particularly at supersonic Mach numbers. This resulted from the influence of the interfairing (fig. 10(b)) and from shielding by the fuselage base, which together tended to normalize flow in this area, as shown by the similarity of ejector nozzle, blow-in-door, and interfairing pressures at common fuselage locations.

A similar restraint on pressure coefficient variation is shown in figure 10(a) for the ejector nozzle at $\varphi = 265^\circ$, where the speed bump exerted a somewhat smaller influence than the interfairing. The integrated values of the pressure coefficients at $\varphi = 85^\circ$ and 265° on the ejector nozzle did not materially differ from those at other axial locations; consequently, it can be inferred that interference effects diminished rapidly aft of the blow-in doors.

Local pressure coefficients at the roots of the interfairing and speed bump were directly affected by the aspiration of the ejector nozzle because the blow-in-door apertures were directly opposite the root pressure orifices, as shown in figure 10(b). Consequently, the large volume of augmenting airflow required at the subsonic speed lowered the local pressures at the root orifices. At supersonic speeds, where flow through the blow-in doors was diminished, the effects of aspiration disappeared.

Boattail effects and the mild effect of the jet flow were responsible for the reduction in pressure coefficient at the tip of the speed bump (fig. 10(b)). The interfairing was affected less because it was farther away laterally from the ejector nozzle and had a constant boattail angle. In general, however, pressures at the two speed bump orifices showed the same trend as pressures at orifices on the interfairing at comparable fuselage stations. Consequently, the two-point curve for the speed bump was faired to duplicate the general trend of the interfairing data.

Pressures obtained on both a flat and a recessed interfairing base for several Mach numbers are compared in figure 11. Essentially no difference in the aerodynamic effect of the two designs is shown.

Total pressure measurements obtained by using boundary layer rakes mounted near the nacelle trailing edge at $\varphi = 20^\circ$ and 140° (figs. 12(a) and 12(b)) showed that the nacelle lower surface maintained a lower total pressure than the upper surface, probably because of the injection into the trough between the engines of boundary layer air which had been separated by the inlet splitter plate and ducted to the bottom of the airplane. The relatively uniform boundary layer profile at $M = 0.76$ was attributed to the reduced thickness of the boundary layer as a result of the aspiration of the ejector nozzle through the fully opened blow-in doors.

Effective boundary layer thickness, δ, determined from flight tests at $M = 0.51$ is compared in figure 13 with similar results from the wind-tunnel-model tests of

reference 3. The thickness measurements for the airplane and the model were normalized to the boundary layer length as determined by the coordinate x of the rake locations. The thickness of the boundary layer was strongly influenced by the local fuselage geometry, as shown by the disparity in the data from the individual rakes, all of which were at different radial locations. It appears from the figure that the model boundary layer was reasonably scaled and would be useful for predicting full-scale effects.

The effect of angle of attack on aft fuselage external pressure coefficients at a Mach number of 0.70 is shown in figures 14(a) to 14(e). The pressure coefficients remained at essentially the same level as angle of attack increased, although a trend toward lower values on the upper surface and higher values on the lower surface may be detected. Nacelle rake measurements indicated that the increase in angle of attack had no significant influence on the boundary layer of the nacelle upper surface (fig. 15(a)). The increase in total pressure recorded on the lower surface of the nacelle (fig. 15(b)) is believed to have resulted from better alinement of the rake with the flow as angle of attack increased, since the rake was mounted perpendicular to the local surface. Figure 16 shows that the blow-in doors on the upper surface of the nacelle at $\varphi = 25^\circ$ and 325° opened a small amount as a result of the increase in angle of attack, thus relieving the demand on the door adjacent to the interfairing at $\varphi = 85^\circ$. The doors on the lower surface of the nacelle were not affected.

External-Internal Flow

The relationship between the engine nacelle and the ejector nozzle of the F-111A airplane was such that flow about the nacelle could be divided into two fractions: one which entered the ejector nozzle through the blow-in doors, while the other passed over the outside surface of the nozzle. Thus the flow would significantly influence not only the static pressures about the nozzle but also the pressures inside it. Other factors that affected external nozzle pressures, particularly at $\varphi = 85^\circ$, were shielding by the fuselage base and the injection of bleed flow into the shrouded area between the ejector nozzle and the interfairing, as previously mentioned. Therefore, local flow at $\varphi = 85^\circ$ was expected to have higher pressure losses than that at $\varphi = 145^\circ$, where it was relatively unobstructed.

Figure 17 presents static pressures on the nacelle, blow-in doors, and ejector nozzle at representative flight conditions and associated blow-in-door apertures. At a Mach number of 0.50 (fig. 17(a)), where the demand for ejector nozzle augmentation was large, the pressures on the blow-in doors were highly negative as a result of aspiration by the ejector nozzle. The aspiration effect also extended to the nacelle trailing edge. A partial pressure recovery then occurred inside the nozzle, but not enough to prevent the nozzle flow from overexpanding. Meanwhile, pressures on the external surface of the ejector nozzle at $\varphi = 85^\circ$ reflected the interaction effects between the nozzle and the interfairing, whereas the pressure coefficients at $\varphi = 145^\circ$ represent relatively unimpeded flow.

At a Mach number of 1.38 (fig. 17(b)), the blow-in doors closed to a small percentage of their maximum aperture. Aspiration effects were negligible, as indicated by the pressure level of the blow-in doors, and the nozzle was fully expanded. The

static pressures on the nacelle at $\varphi = 160^\circ$ were lower for this flight condition than their counterparts at $\varphi = 15^\circ$. This is consonant with the effect of Mach number shown in figure 9 for these nacelle locations.

As Mach number increased to 1.96 (fig. 17(c)), there was no demand for flow augmentation, and the blow-in doors closed. Pressure coefficients on the nacelle were again lower at $\varphi = 160^\circ$ than at $\varphi = 15^\circ$; this condition is also shown by the data for the blow-in doors. Pressures inside the nozzle were considerably higher than the free-stream values; therefore, the jet flow was underexpanded.

Total pressure rake measurements made on the nacelle at $\varphi = 20^\circ$ and 140° are compared in figure 18 with similar measurements obtained from the ejector nozzle rakes at $\varphi = 105^\circ$ and 170° to further illustrate the effects of interaction between the ejector nozzle and the adjacent airplane structure at $\varphi = 85^\circ$. Although one of the nozzle rakes was at $\varphi = 105^\circ$, it measured the flow entering the blow-in door centered at $\varphi = 85^\circ$.

Figure 18(a) shows that at a Mach number of 0.50 a moderate loss in total pressure occurred at the ejector nozzle rake when compared with the pressure at the nacelle rake. This was attributed to the influence of the fuselage base interfairing cavity exerted through the blow-in door. Inasmuch as the flow over the lower surface of the nacelle was also available to this blow-in door, figure 18(b) shows that the rake on the nacelle lower surface also measured a significantly higher total pressure than the ejector nozzle rake at $\varphi = 105^\circ$, thus confirming that the cavity was the origin of the pressure loss.

As Mach number increased to 1.38 (fig. 18(a)), the demand for flow augmentation dropped to a low level (blow-in door 13 percent open) and a large loss in pressure occurred at the ejector nozzle rake compared with the pressure at the nacelle rake. With a further increase in Mach number to 1.96 (blow-in door closed), the ejector rake showed pressures representative of the nozzle static pressures, except for that at the tip probe which was immersed in the primary jet flow.

Figure 18(b) shows that, at Mach 0.50 for the lower quadrant, there was no loss in total pressure as the flow moved in a nearly straight line from the nacelle to the ejector nozzle. The nacelle rake total pressures, however, fell off with increase in Mach number at a much higher rate than the pressures measured on the upper surface of the nacelle (fig. 18(a)). The loss in total pressure is attributed to the low energy bleed flow injected into the lower surface boundary layer. It is evident from this that the anticipated losses in the flow adjacent to the interfairing were realized but were balanced, particularly at supersonic speeds, by the boundary layer losses incurred on the bottom of the fuselage.

The efficiency of the ejector nozzle in expanding the primary jet flow to free-stream conditions by means of selective flow augmentation has been discussed for three representative Mach numbers. The ejector nozzle static pressure ratio shown in figure 19 was obtained by comparing pressures measured at the trailing-edge orifice with free-stream static pressures. The figure, which summarizes the installed nozzle performance over the test Mach number range, shows that the jet flow was overexpanded at Mach numbers approaching the speed of sound, fully expanded in the transonic speed range, and underexpanded at higher speeds. (Flight conditions for these data are shown in table 1.)

Internal Flow

Figure 20 presents internal pressure coefficients at three representative Mach numbers. At Mach 0.50 (fig. 20(a)) pressure was lower on the internal surface of the blow-in door, the primary nozzle boattail, and the ejector nozzle lip than in the bleed duct. Although it would appear that the higher pressure in the duct would decrease in the transition to the ejector nozzle, the two pressure levels are not directly comparable. Rather, the bleed duct flow would mix with tertiary flow upon leaving the confines of the duct. The combined flow would then come under the strong influence of ejector nozzle aspiration through the open blow-in door and mix with the primary flow to establish the pressure coefficients shown within the nozzle. It is evident, therefore, that drag on the primary nozzle boattail was not eliminated at subsonic speed by this ejector nozzle design. Only a moderate amount of compression was realized in the nozzle, although the blow-in doors were nearly fully open and aspiration was maximum, because the combined primary and augmenting mass flow was insufficient to pressurize the nozzle.

As Mach number increased to 1.38 (fig. 20(b)), the blow-in door was nearly closed, which reduced aspiration effects to a low level while admitting a small amount of flow augmentation. Under these conditions, pressures on the primary nozzle boattail and the inside surface of the blow-in door were slightly below free-stream level and flow was compressed to free stream in the nozzle.

At a Mach number of 1.96 (fig. 20(c)) the blow-in door was closed, which sealed the ejector nozzle against external flow. The primary nozzle jet stream pressurized the entire ejector nozzle so that rearward-facing surfaces would contribute to the net thrust.

Nozzle Flow Characteristics

Installed engine thrust would be expected to have a significant influence on aft fuselage pressure coefficients. In the absence of in-flight thrust measurements, however, primary nozzle total pressure ratio, $\frac{p_t}{p_\infty}$, may be used as a reliable indicator of thrust level. Figure 21(a) shows that an increase in nozzle pressure ratio forced the static pressures on the blow-in door and inside the ejector nozzle to less negative values. This is attributed to moderate pressurization of the ejector nozzle as the primary flow expanded. The effect on the position of the blow-in doors was mixed, with some opening and others closing, as shown in figure 21(b). The effect on the interfairing and speed bump was negligible, as shown in figure 21(c), and, similarly, the nacelle was unaffected (fig. 21(d)). Although ejector nozzle pressures also showed a trend toward less negative values (fig. 21(e)), it is unlikely that they were influenced appreciably by internal nozzle pressures; rather, they probably reflected the effects of minor variations in the local flow. It is concluded, therefore, that the effects of an increase in primary nozzle total pressure ratio at subsonic speed were limited to the internal surfaces of the ejector nozzle.

An increase in primary nozzle total pressure ratio at supersonic speed also resulted in less negative pressures on the blow-in doors and internal ejector nozzle,

as shown in figure 22(a). This forced the blow-in doors to close considerably (fig. 22(b)). Pressures on the forward part of the interfairing and speed bump approached free-stream values (fig. 22(c)), but the nacelle was essentially not affected (fig. 22(d)). The response of the static pressures on the external surface of the ejector nozzle was mixed, as shown in figure 22(e), but showed a general trend toward more negative values. It appears, therefore, that an increase in primary nozzle total pressure ratio had only a slightly greater effect at a supersonic speed than at a subsonic speed and that at both speeds the effect was highly localized.

Another parameter that affected aft fuselage pressure coefficients was the area of the primary nozzle, A_p. An increase in A_p at a supersonic speed (fig. 23(a)) resulted in an appreciable increase in pressure coefficients for the blow-in door and inside the ejector nozzle as the larger diameter jet flow more nearly filled the ejector nozzle. This caused the blow-in doors to close considerably (fig. 23(b)). Pressures on the interfairing and speed bump became uniformly less negative as the aspiration decayed (fig. 23(c)). The nacelle pressure coefficients, however, were not affected by the change in A_p, as shown in figure 23(d). The increase in nozzle area tended to mitigate the overexpansion of the flow about the ejector nozzle (fig. 23(e)). Although the slight increase in nozzle pressure ratio undoubtedly had an influence on the local pressures similar to that of primary nozzle area, the effect was believed to be minor.

Comparison of Flight and Wind-Tunnel Results

Figure 24(a) compares wind-tunnel and flight results for the nacelle at a Mach number of approximately 0.50. The agreement was good, although pressures determined from the flight data were generally slightly more negative than those from the wind-tunnel results. The reduction in flight-determined static pressure at the trailing edge of the nacelle, attributed to ejector nozzle aspiration effects, was closely approximated by model results.

Pressures on the interfairing (fig. 24(b)) showed good agreement, although it appears that the pressure loss on the forward interfairing caused by the influence of aspiration through the adjacent blow-in door was more highly localized on the airplane than on the model.

Some rather large differences between flight- and wind-tunnel-determined static pressure, characterized by a high degree of flow expansion about the ejector nozzle for the flight data, are shown in figure 24(c), although the shapes of the curves are similar. This lack of agreement is believed to have been caused by the previously noted differences in the construction and operational characteristics of the model and the full-scale ejector nozzle, magnified by the complexity of the local flow field. In addition there were the possibilities of leakage, particularly about the tail feathers, and of discrepancies in the mating of assembled parts of the flight nozzle.

At a Mach number of 0.70 pressure coefficients for the nacelle (fig. 25(a)) were in close agreement although, again, the flight results were slightly more negative than the model data. Interfairing pressures (fig. 25(b)) also agreed well, and the

trends of wind-tunnel and flight data were the same as for the lower Mach number (fig. 24(b)). Figure 25(c) indicates that ejector nozzle pressures are generally compatible, but the prominent expansion peak in the flight data was again not shown in the wind-tunnel data.

Flight and wind-tunnel results show good agreement at $M \approx 0.90$ for the nacelle upper surface (fig. 26(a)) but tend to exhibit somewhat different curves for the lower surface, as is true for the lower Mach numbers (figs. 24(a) and 25(a)). Pressures on the interfairing (fig. 26(b)) are again appreciably higher for the model than for the airplane. This discrepancy is believed to be caused by the previously mentioned differences in the effects of aspiration within the shrouded volume between the ejector nozzle and the interfairing for the model and the airplane. The flight data for the ejector nozzle (fig. 26(c)) were characterized by the previously discussed expansion peaks, which resulted in a substantially negative level of pressure distribution about the nozzle. The shapes of the model and flight data curves are, however, directly comparable.

The wind-tunnel and flight data in figures 24 to 26 show that pressures on the model nacelle remained about the same at the subsonic test Mach numbers, with the exception of the values for the lower surface at $M = 0.90$ which became, in general, substantially more negative. Similar pressures on the airplane tended to become gradually more negative as Mach number increased. The model results were generally slightly less negative than the flight results.

The effect of aspiration on the forward portion of the interfairing diminished on both the model and the airplane as the ejector nozzle demand for augmenting flow decayed with increasing Mach number. The relative shape of the curves indicated that aspiration effects were more highly localized on the airplane interfairing than on the model. The gentle, smooth curves of the model data suggested that the positive injection of bleed flow into the shrouded volume between the ejector nozzle and the interfairing tended to mitigate the aspiration effects. However, table 2, which presents boundary layer bleed duct total and static pressure ratios, shows that, at subsonic speeds where the demand for augmenting flow was large, the static pressures were lower than the free-stream pressure. Despite the extent of the aspiration effects, the model midinterfairing pressures tended to reach a consistent level for each of the Mach numbers considered. Flight-obtained pressures, however, clearly declined as Mach number increased.

Ejector nozzle pressures for the model showed about the same expansion-peak level as Mach number increased from 0.50 to 0.70 and a slightly greater expansion at Mach 0.90. The pressures for the airplane nozzle showed a similar trend. It appears, therefore, that although the pressure levels of the flight and wind-tunnel data were not in agreement, there were basic similarities in the behavior of the flow about the nozzle and in the shape of the curves.

CONCLUDING REMARKS

Aft fuselage and ejector nozzle static pressure measurements were made on an F-111A airplane to determine the effect of several flight conditions on local flow characteristics and to investigate flow interactions between the engine and the

adjacent structure. Data were obtained for Mach numbers from 0.5 to 2.0 and compared with results from wind-tunnel tests. It was found that ejector nozzle aspiration effects reduced static pressures particularly on the interfairing but also on the nacelle trailing edge at low speed and low nozzle expansion ratios, where nozzle demand for flow augmentation was maximum. As this demand was reduced at higher Mach numbers, however, the effects of aspiration diminished, and the pressure coefficients became more positive.

The presence of the interfairing affected the behavior of the air entering and flowing about the ejector nozzle through the blow-in door adjacent to the interfairing. A similar but lesser influence was observed between the nozzle and the speed bump.

An increase in primary nozzle area at a supersonic Mach number caused an increase in pressure inside the ejector nozzle and on the interfairing and speed bump, but had no effect on the nacelle. An increase in primary nozzle pressure ratio at subsonic and supersonic Mach numbers had generally similar results.

The ejector nozzle flow was overexpanded at subsonic speeds, fully expanded at moderately supersonic Mach numbers, and underexpanded at higher supersonic speeds.

Comparison of wind-tunnel and flight results showed generally good agreement at all the subsonic Mach numbers evaluated, although the flight data became more negative on the ejector nozzle with increasing subsonic Mach number. However, the shape of the data curves and the local flow behavior were basically similar.

Flight Research Center
National Aeronautics and Space Administration
Edwards, Calif., December 14, 1973

REFERENCES

1. Runckel, Jack F.: Jet-Exit and Airframe Interference Studies on Twin-Engine-Fuselage Aircraft Installations. NASA TM X-1274, 1966.

2. Schmeer, James W.; Lauer, Rodney F., Jr.; and Berrier, Bobby L.: Performance of Blow-In-Door Ejector Nozzles Installed on a Twin-Jet Variable-Wing-Sweep Fighter Airplane Model. NASA TM X-1383, 1967.

3. Re, Richard J.; Wilmoth, Richard G.; and Runckel, Jack F.: Investigation of Effects of Afterbody Closure and Jet Interference on the Drag of a Twin-Engine Tactical Fighter. NASA TM X-1382, 1967.

4. Wilmoth, Richard G.; Norton, Harry T., Jr.; and Corson, Blake W., Jr.: Effect of Engine-Interfairing Modifications on the Performance of a Powered Twin-Jet Fighter-Airplane Model at Mach 1.20. NASA TM X-1534, 1968.

5. Mercer, Charles E.; Pendergraft, Odis C., Jr.; and Berrier, Bobby L.: Effect of Geometric Variations on the Performance of a Twin-Jet Blow-In-Door Ejector Nozzle Installation. NASA TM X-1633, 1968.

6. Schmeer, James W.; Mercer, Charles E.; and Kirkham, Frank S.: Effect of Bypass Air on the Performance of a Blow-In-Door Ejector Nozzle at Transonic Speeds. NASA TM X-896, 1963.

7. Mercer, Charles E.; Schmeer, James W.; and Lauer, Rodney F., Jr.: Performance of Several Blow-In-Door Ejector Nozzles at Subsonic and Low-Supersonic Speeds. NASA TM X-1163, 1967.

8. Migdal, David; and Greathouse, William K.: Optimizing Exhaust-Nozzle/Airframe Thrust Minus Drag. SAE Paper 680294, 1968.

9. Mechtly, E. A.: The International System of Units - Physical Constants and Conversion Factors (Second Revision). NASA SP-7012, 1973.

10. Sisk, Thomas R.; Matheny, Neil W.; Kier, David A.; and Manke, John A.: A Preliminary Flying-Qualities Evaluation of a Variable-Sweep Fighter-Type Aircraft. NASA TM X-1583, 1968.

11. Runckel, Jack F.; and Swihart, John M.: A Hydrogen Peroxide Turbojet-Engine Simulator for Wind-Tunnel Powered-Model Investigations. NACA RM L57H15, 1957.

TABLE 1.– FLIGHT CONDITIONS FOR THE TEST MACH NUMBER RANGE

M	Altitude, m (ft)	α, deg	R, m (ft)	$\frac{p_{t_p}}{p_{s_\infty}}$	A_p, m^2 (ft^2)
0.501	3,283 (10,773)	3.24	7.986×10^6 (2.620×10^6)	1.980	0.35 (3.75)
0.699	3,114 (10,219)	3.18	11.326 (3.716)	1.928	0.35 (3.75)
0.911	9,320 (30,579)	4.05	7.759 (2.546)	3.118	0.64 (6.90)
1.005	9,593 (31,475)	4.61	8.300 (2.723)	3.560	0.54 (5.80)
1.195	9,293 (30,491)	5.44	10.211 (3.350)	4.052	0.61 (6.60)
1.291	9,367 (30,732)	3.93	10.960 (3.596)	4.389	0.63 (6.80)
1.570	13,592 (44,596)	5.66	7.352 (2.412)	6.724	0.53 (5.70)
1.796	13,560 (44,490)	4.56	8.449 (2.772)	7.636	0.56 (6.00)
2.006	13,448 (44,122)	4.42	9.604 (3.151)	9.601	0.52 (5.60)

TABLE 2.– BOUNDARY LAYER BLEED DUCT TOTAL AND STATIC PRESSURE RELATIONSHIPS

M	$\frac{p_{t_s}}{p_{s_{av}}}$	$\frac{p_{s_{av}}}{p_\infty}$
0.50	1.021	0.976
0.70	1.037	0.953
0.91	1.054	0.988
1.01	1.028	1.062
1.13	1.030	1.146
1.38	1.088	1.132
1.61	1.148	1.071
1.80	1.119	1.274
2.01	1.118	1.406

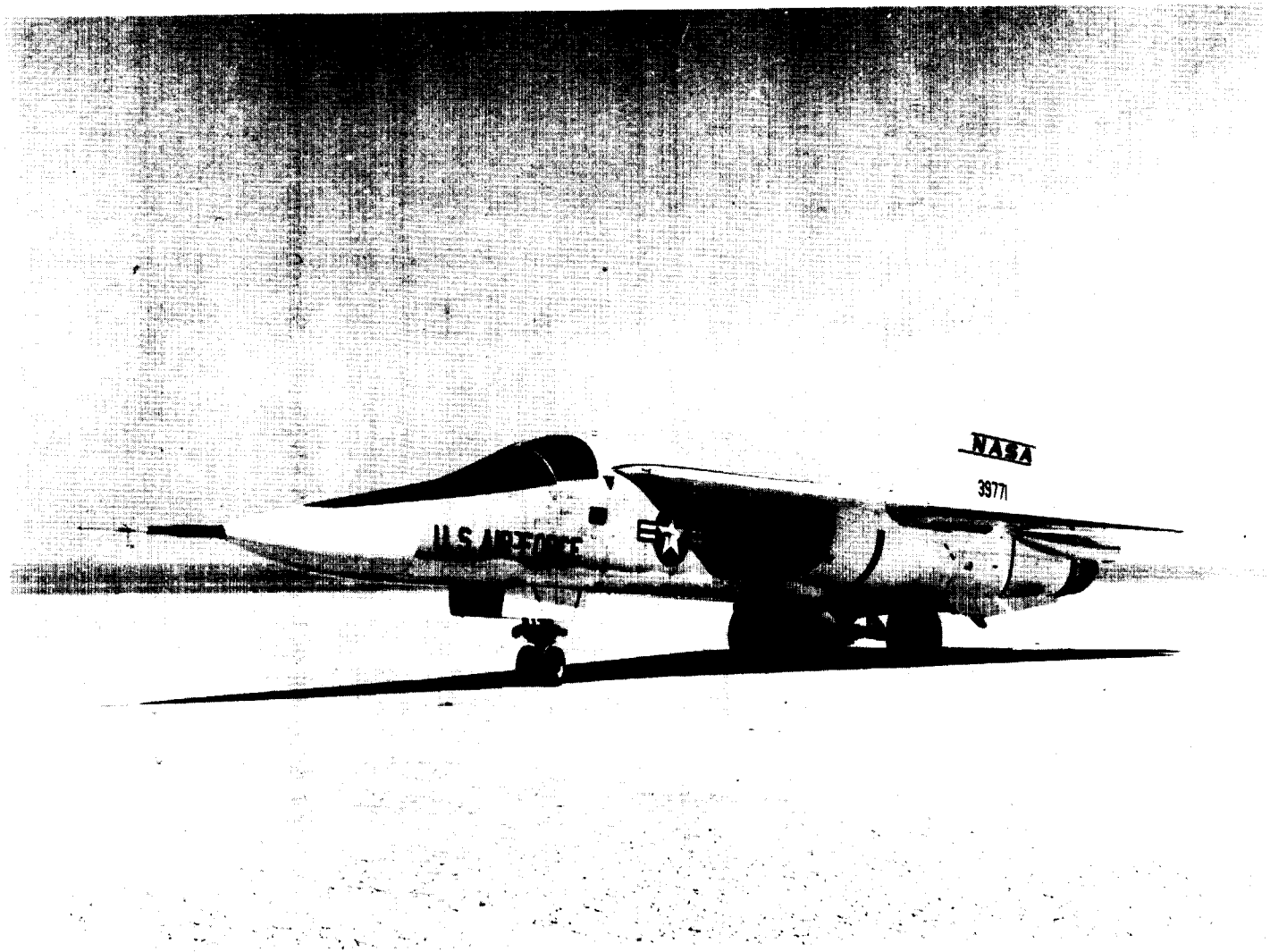

E-20273

Figure 1. F-111A airplane.

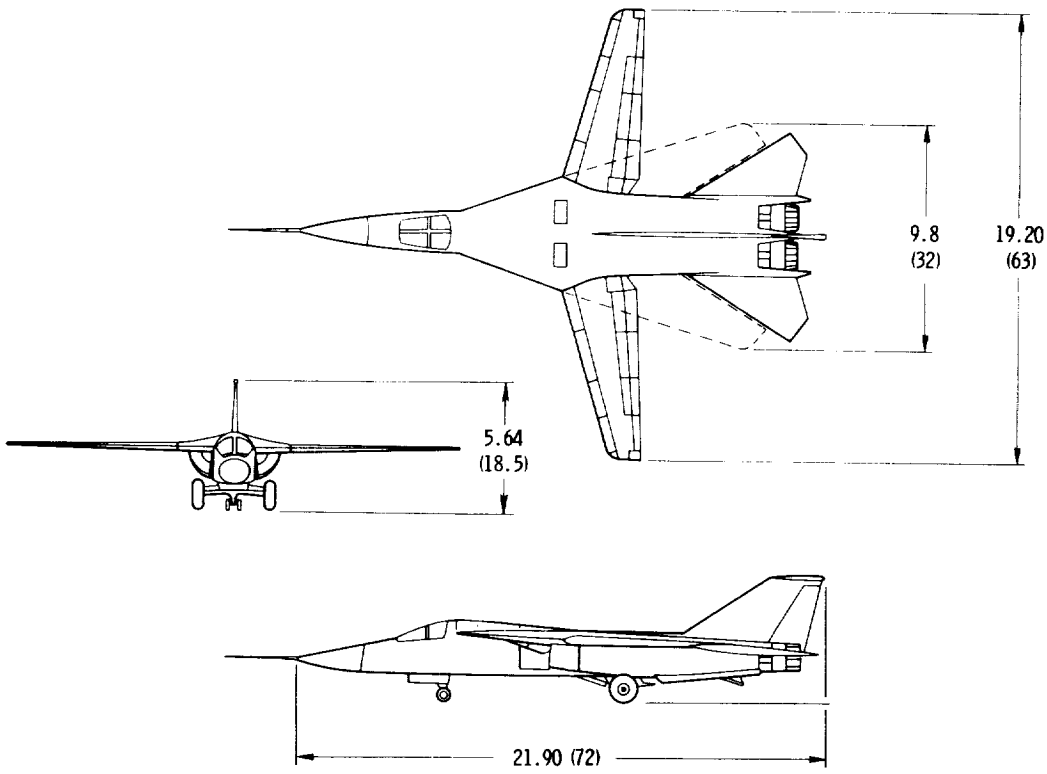

Figure 2. Three-view drawing of the F-111A airplane. Dimensions in meters (feet).

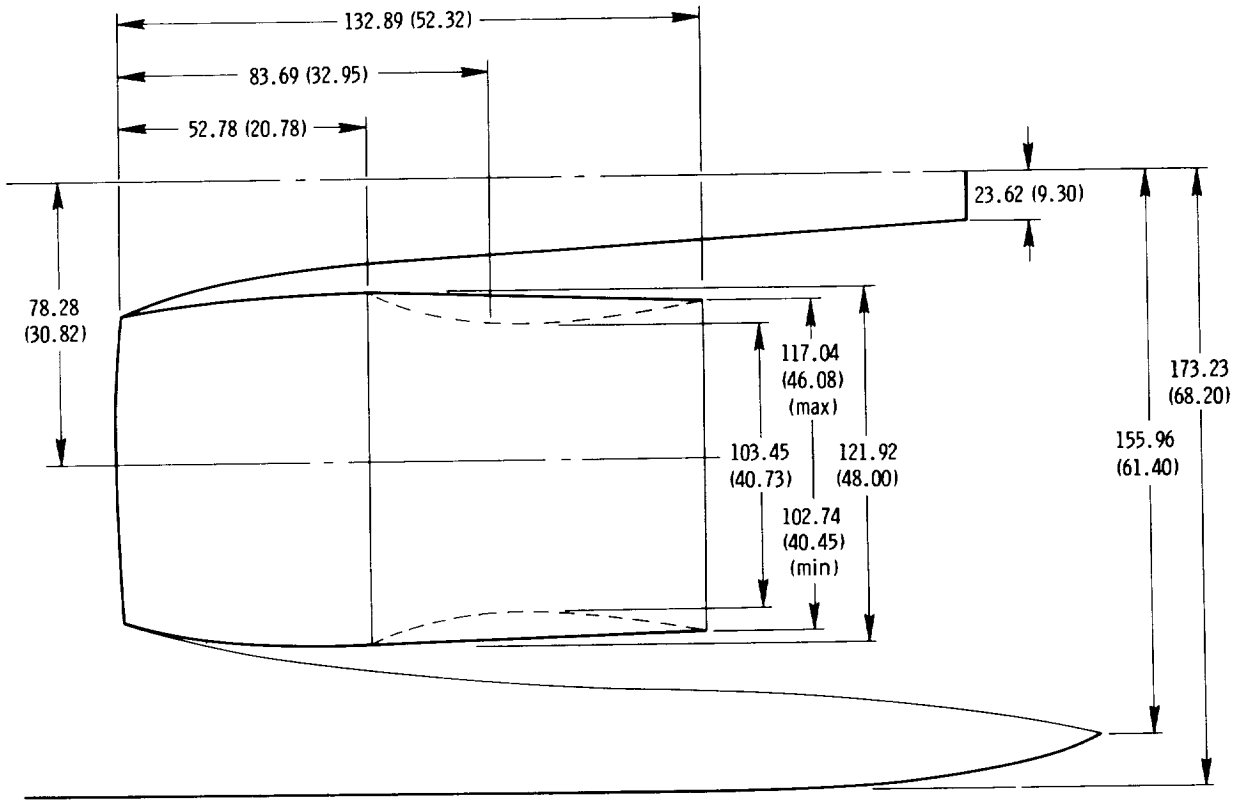

Figure 3. Ejector nozzle installation and dimensions (in centimeters (inches)).

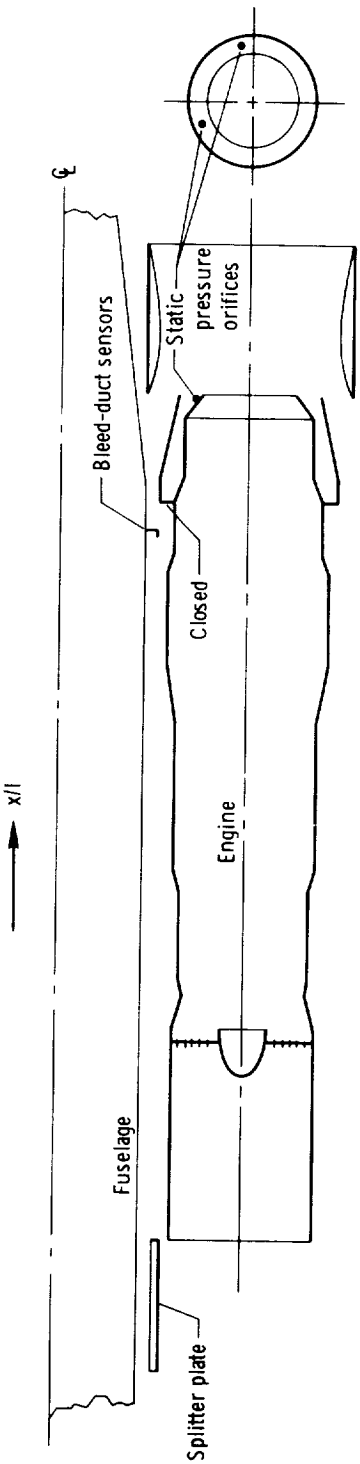

Figure 4. Boundary layer bleed duct. Top view.

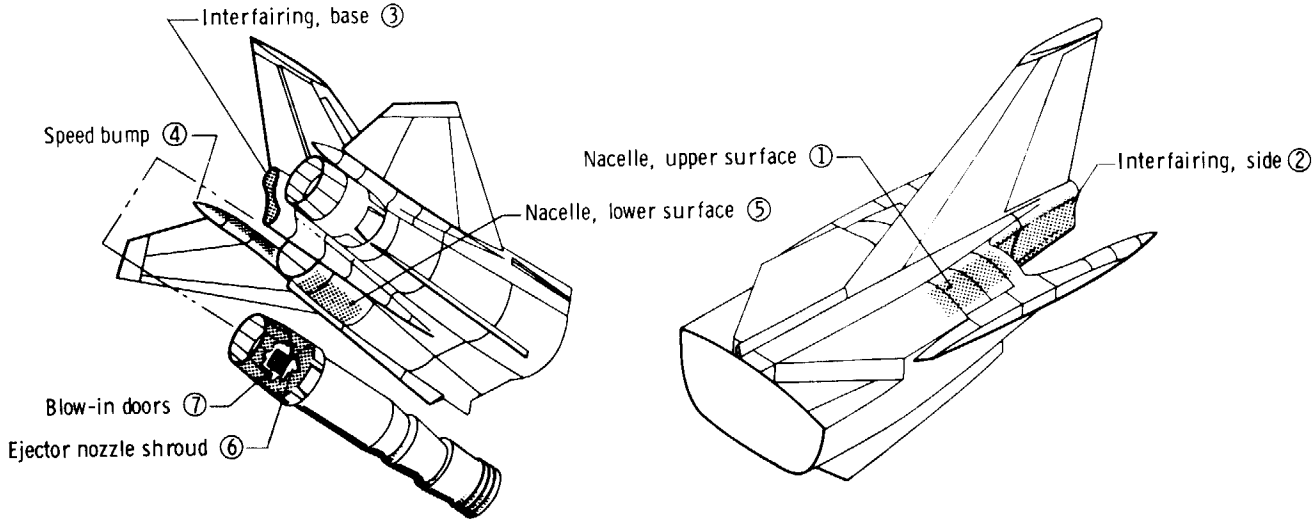

(a) General view. (Engines omitted for clarity.)

Figure 5. Instrumented areas of the aft fuselage.

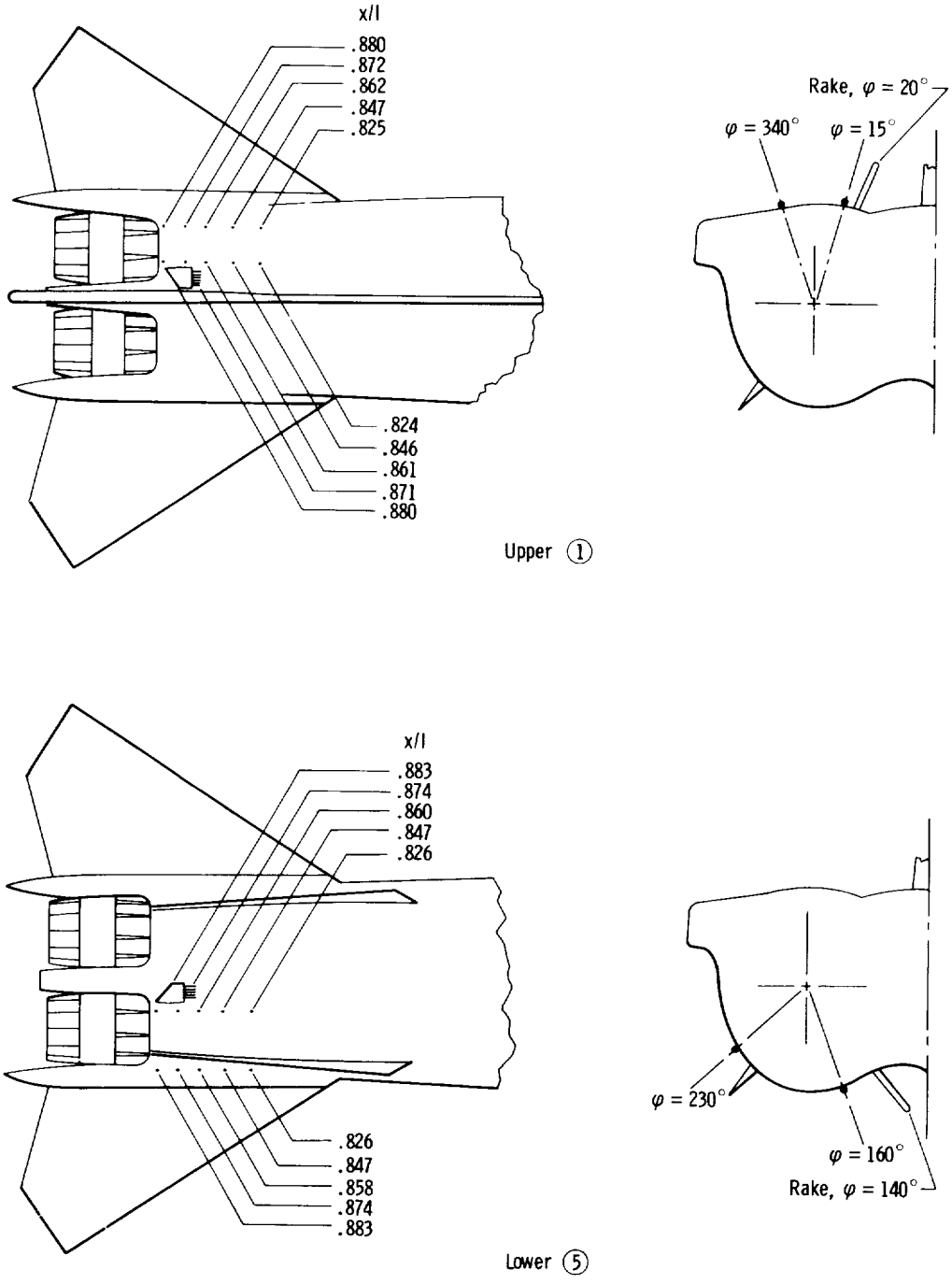

(b) Nacelle, upper and lower surfaces.

Figure 5. Continued.

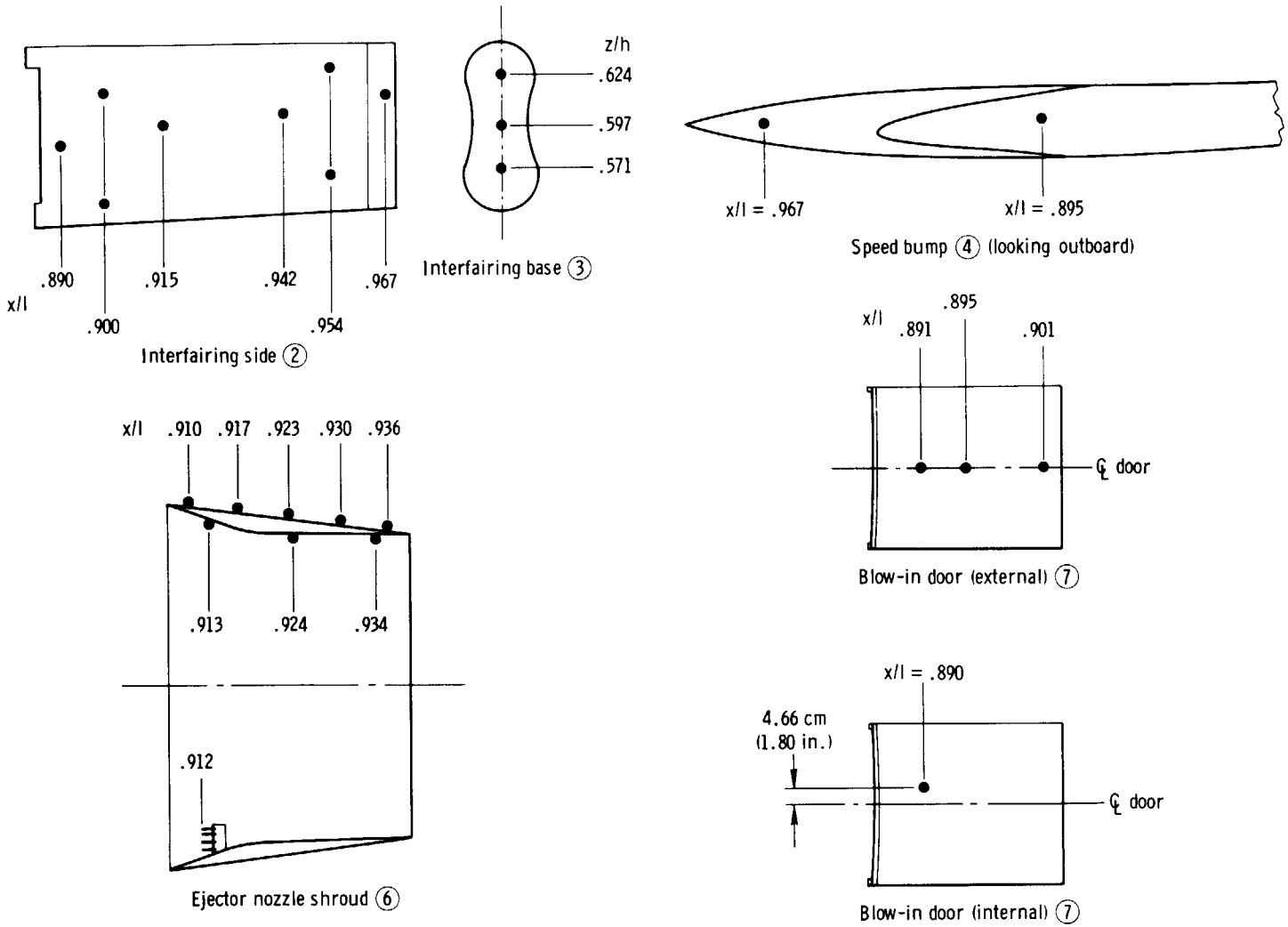

(c) Interfairing, speed bump, ejector nozzle shroud, and blow-in doors.

Figure 5. Concluded.

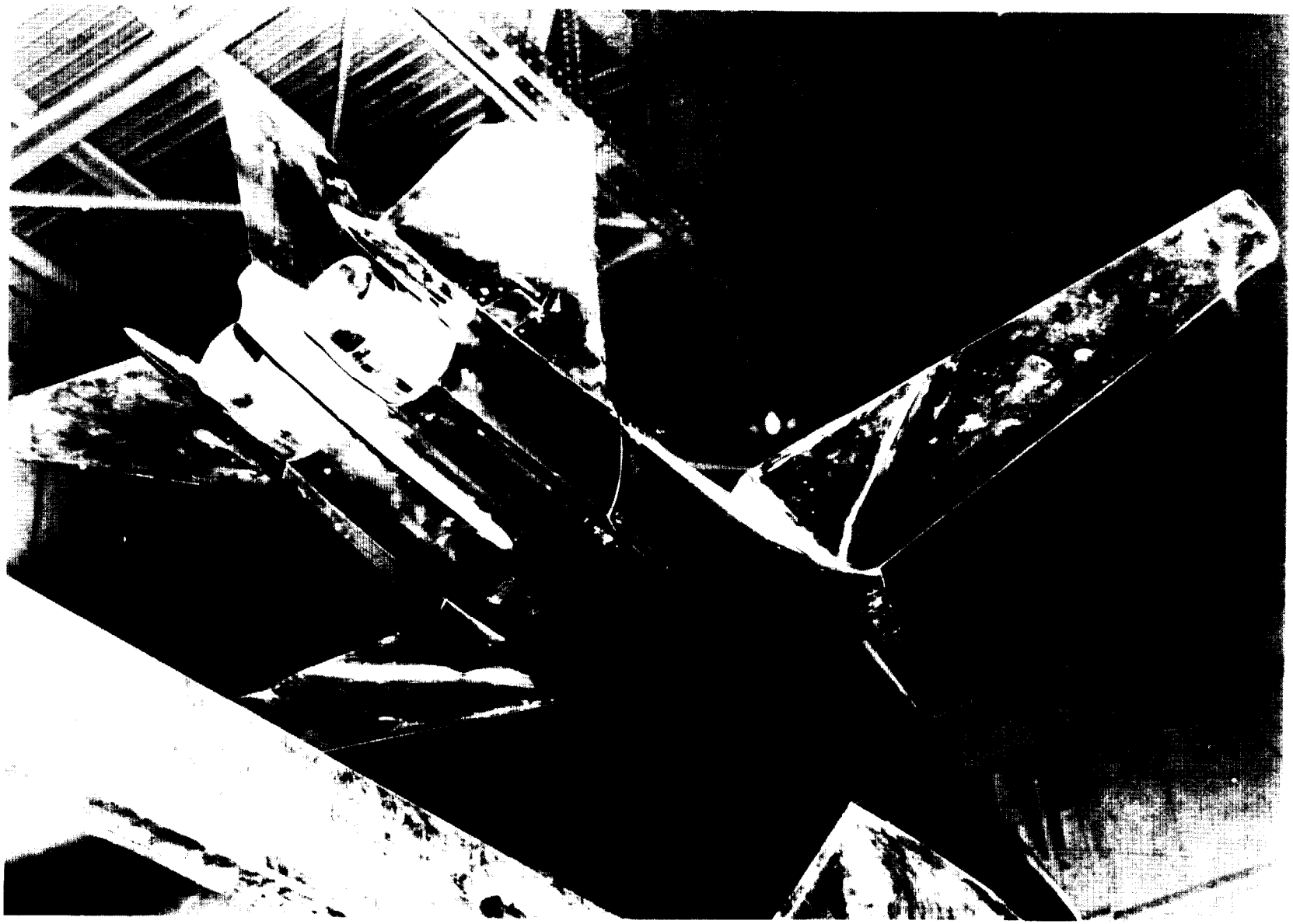

Figure 6. F-111 model mounted in the Langley Research Center 16-foot transonic wind tunnel.

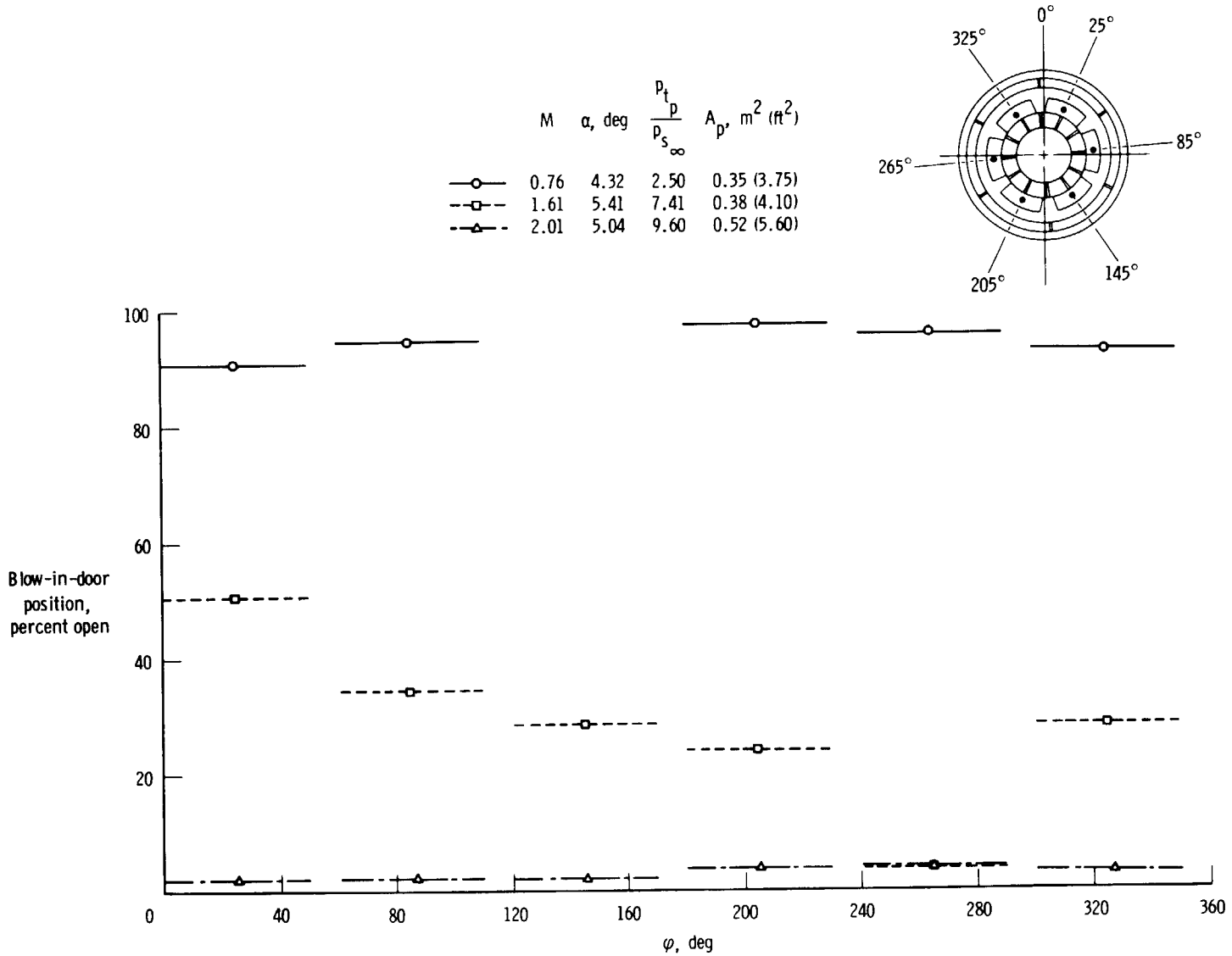

Figure 7. Blow-in-door positions for three representative Mach numbers.

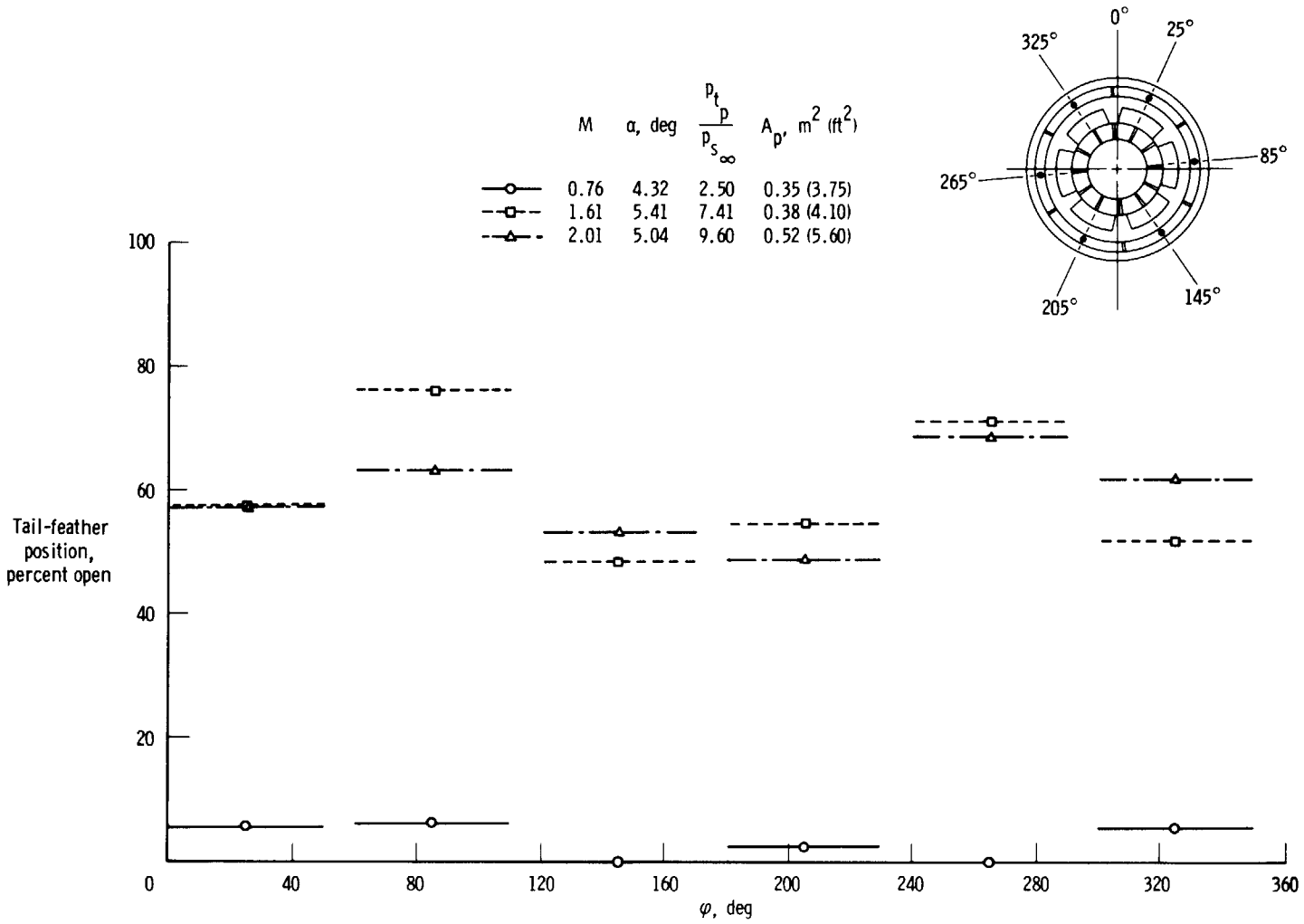

Figure 8. Tail-feather positions for three representative Mach numbers.

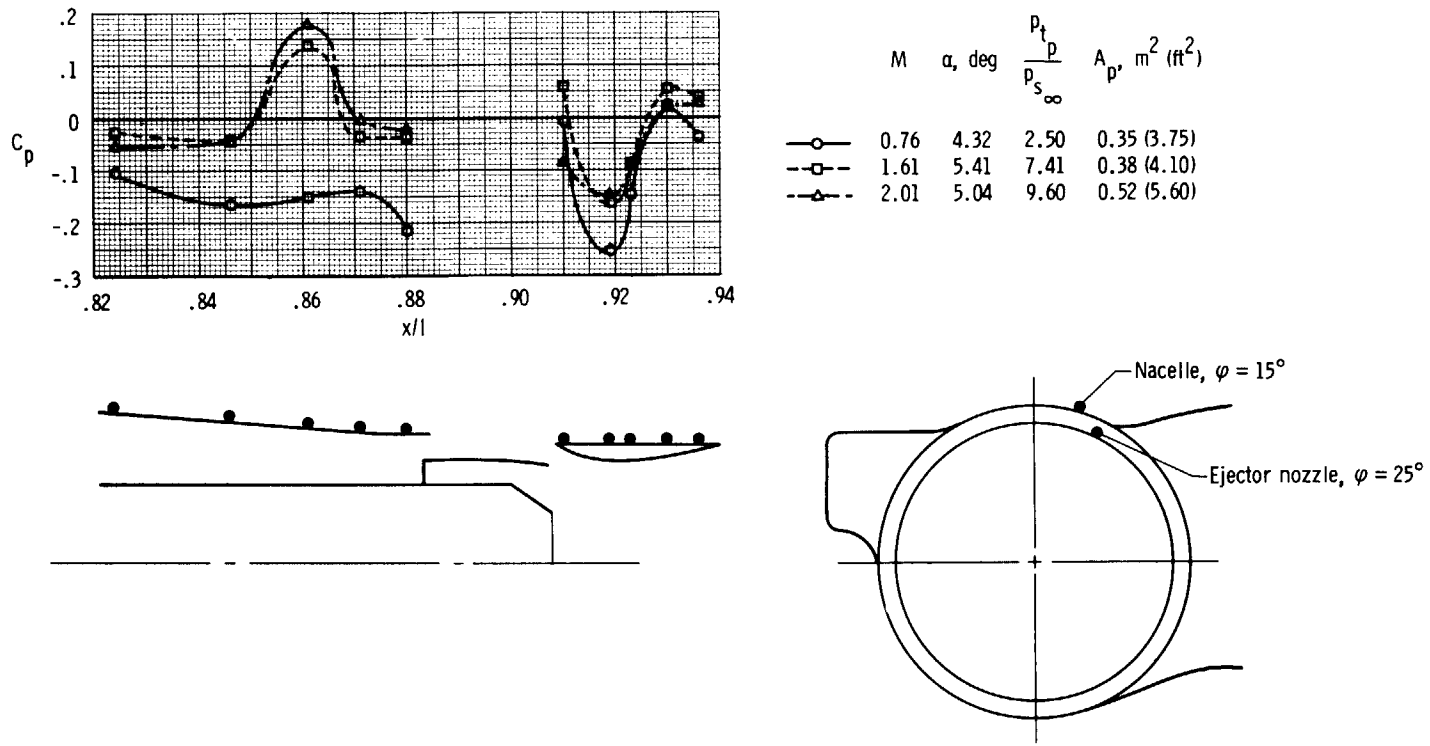

(a) Nacelle at $\varphi = 15°$ and ejector nozzle at $\varphi = 25°$.

Figure 9. Aft fuselage pressure coefficients at three representative Mach numbers.

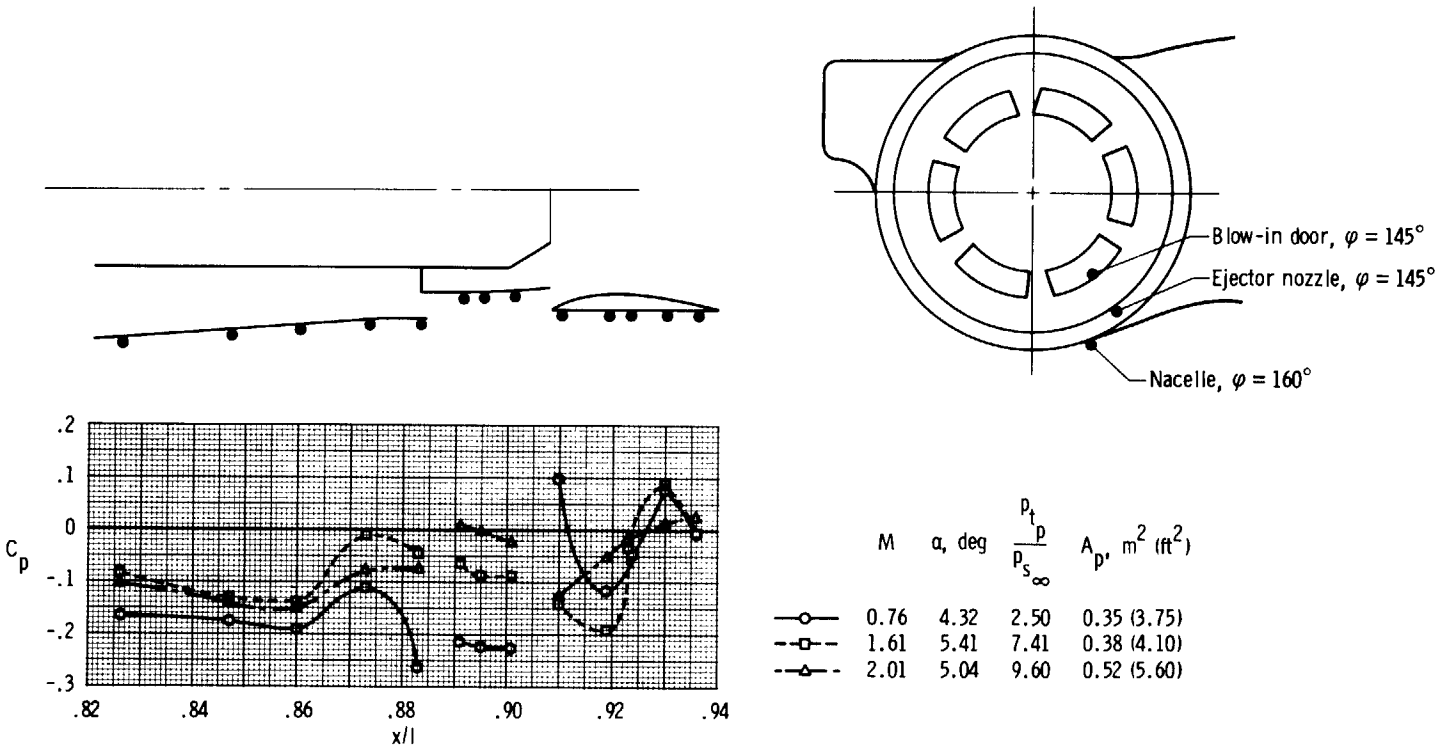

(b) Nacelle at $\varphi = 160°$, blow-in door at $\varphi = 145°$, and ejector nozzle at $\varphi = 145°$.

Figure 9. Continued.

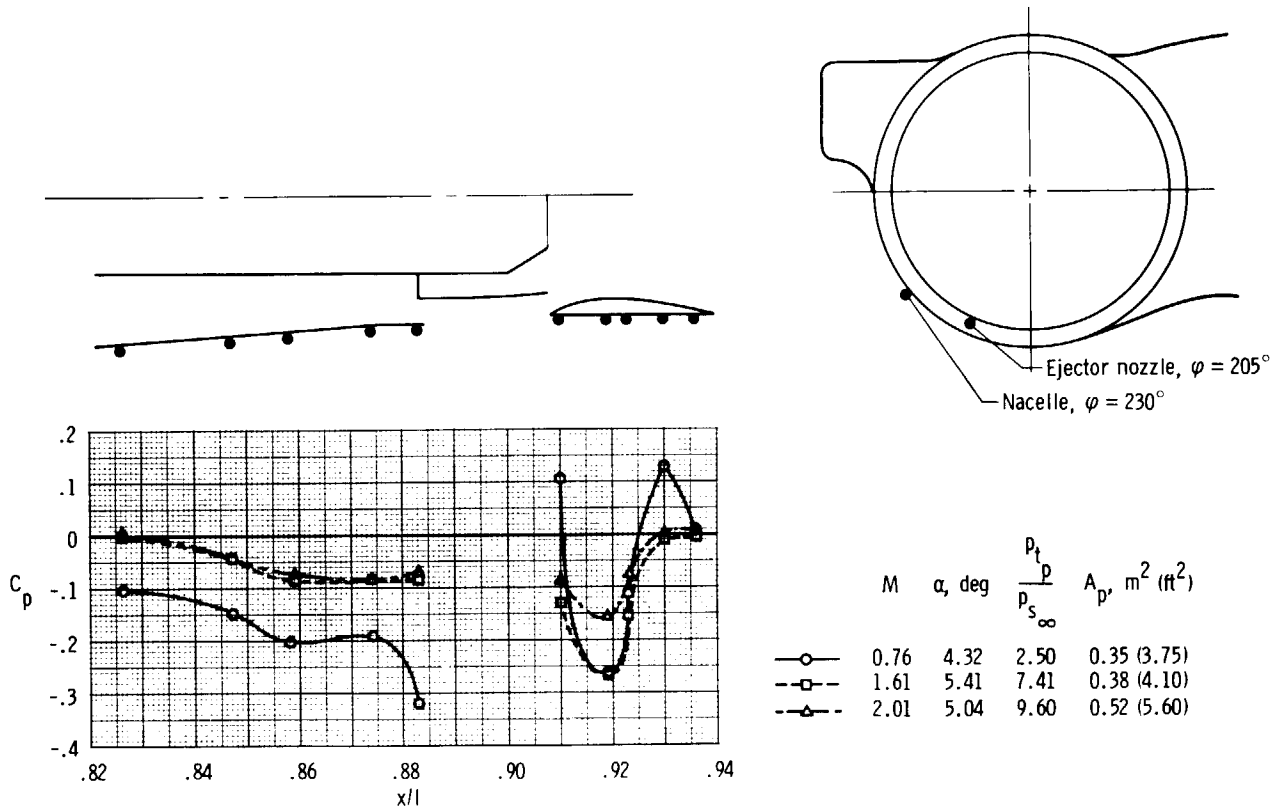

(c) Nacelle at $\varphi = 230°$ and ejector nozzle at $\varphi = 205°$.

Figure 9. Continued.

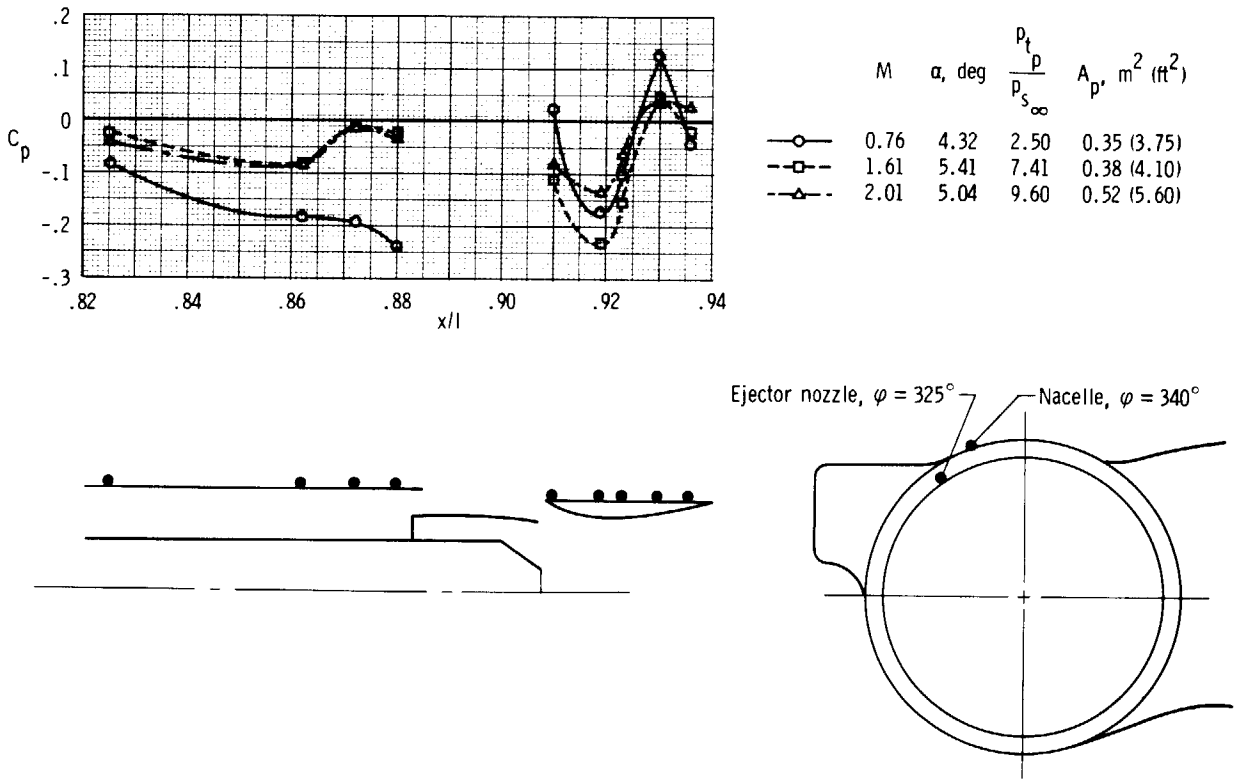

(d) Nacelle at $\varphi = 340°$ and ejector nozzle at $\varphi = 325°$.

Figure 9. Concluded.

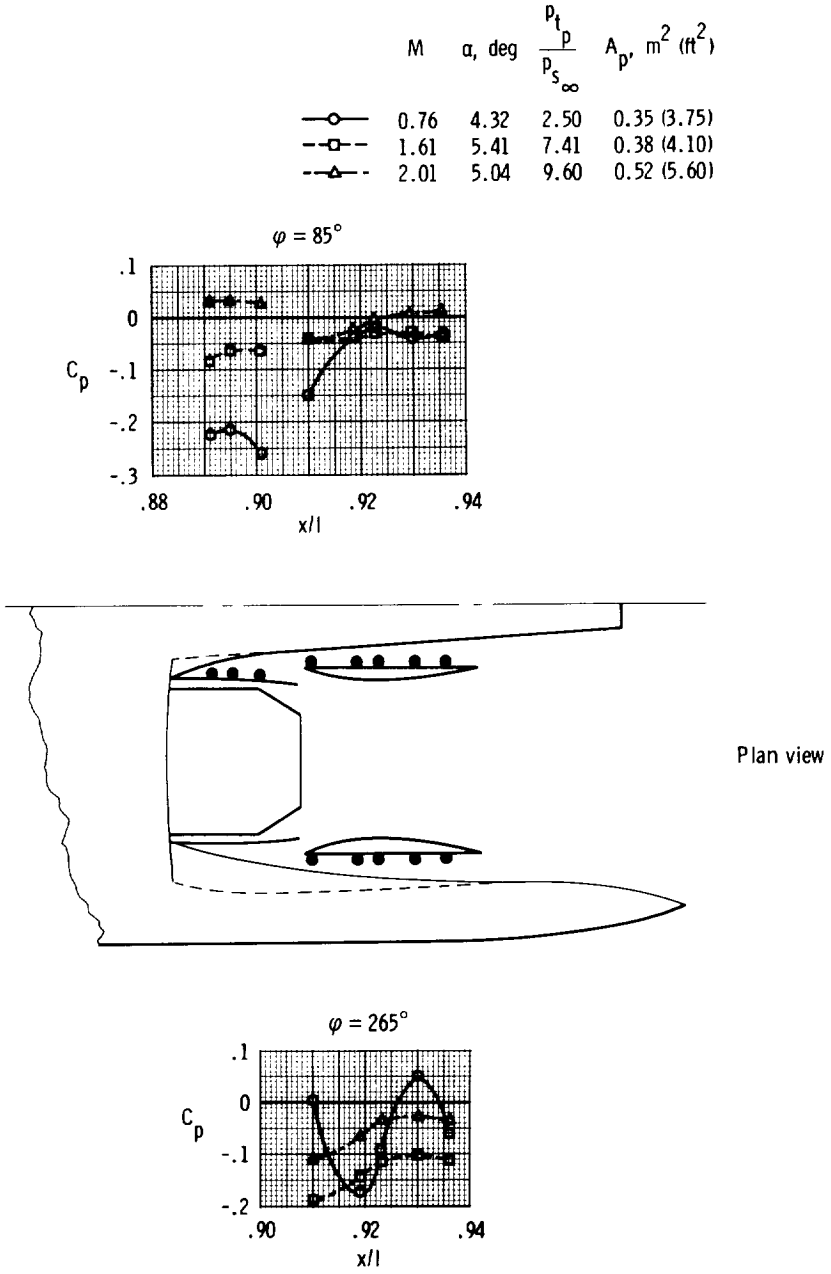

(a) Blow-in door and ejector nozzle.

Figure 10. Pressure coefficients on and adjacent to the ejector nozzle at three representative Mach numbers.

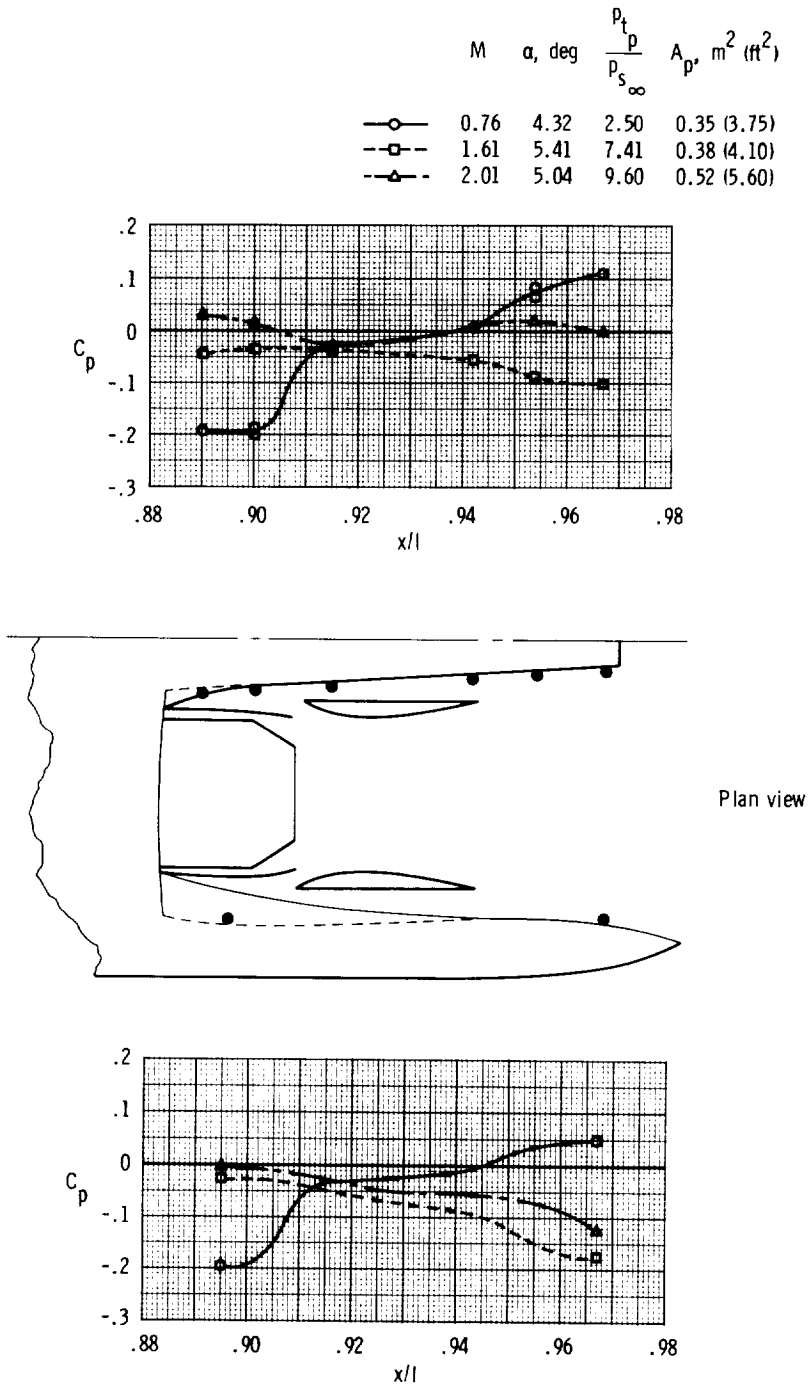

(b) Interfairing and speed bump.

Figure 10. Concluded.

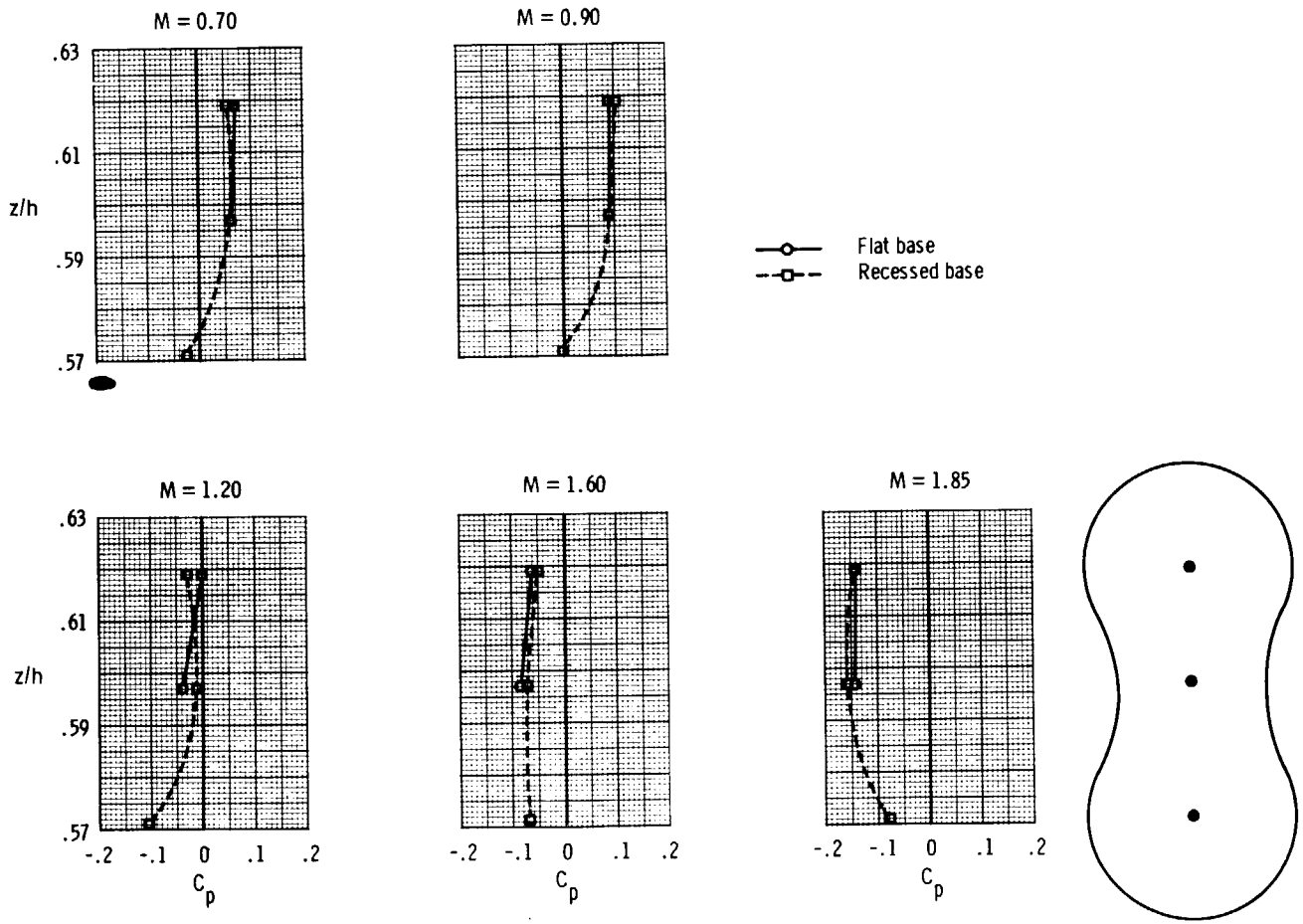

Figure 11. Comparison of pressure coefficients on a flat and a recessed interfairing base for several Mach numbers.

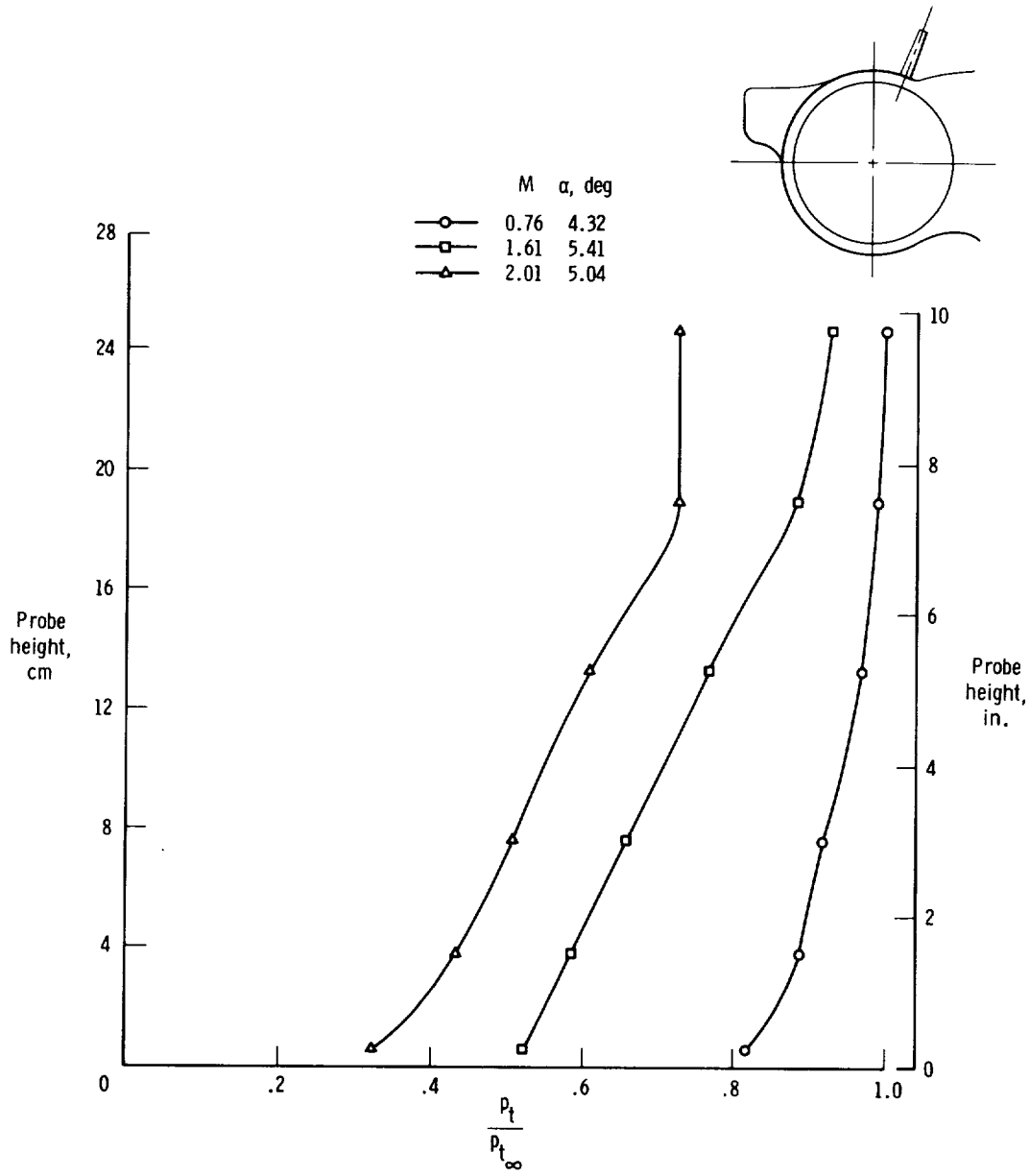

(a) $\varphi = 20°$.

Figure 12. Nacelle boundary layer rake measurements at three representative Mach numbers.

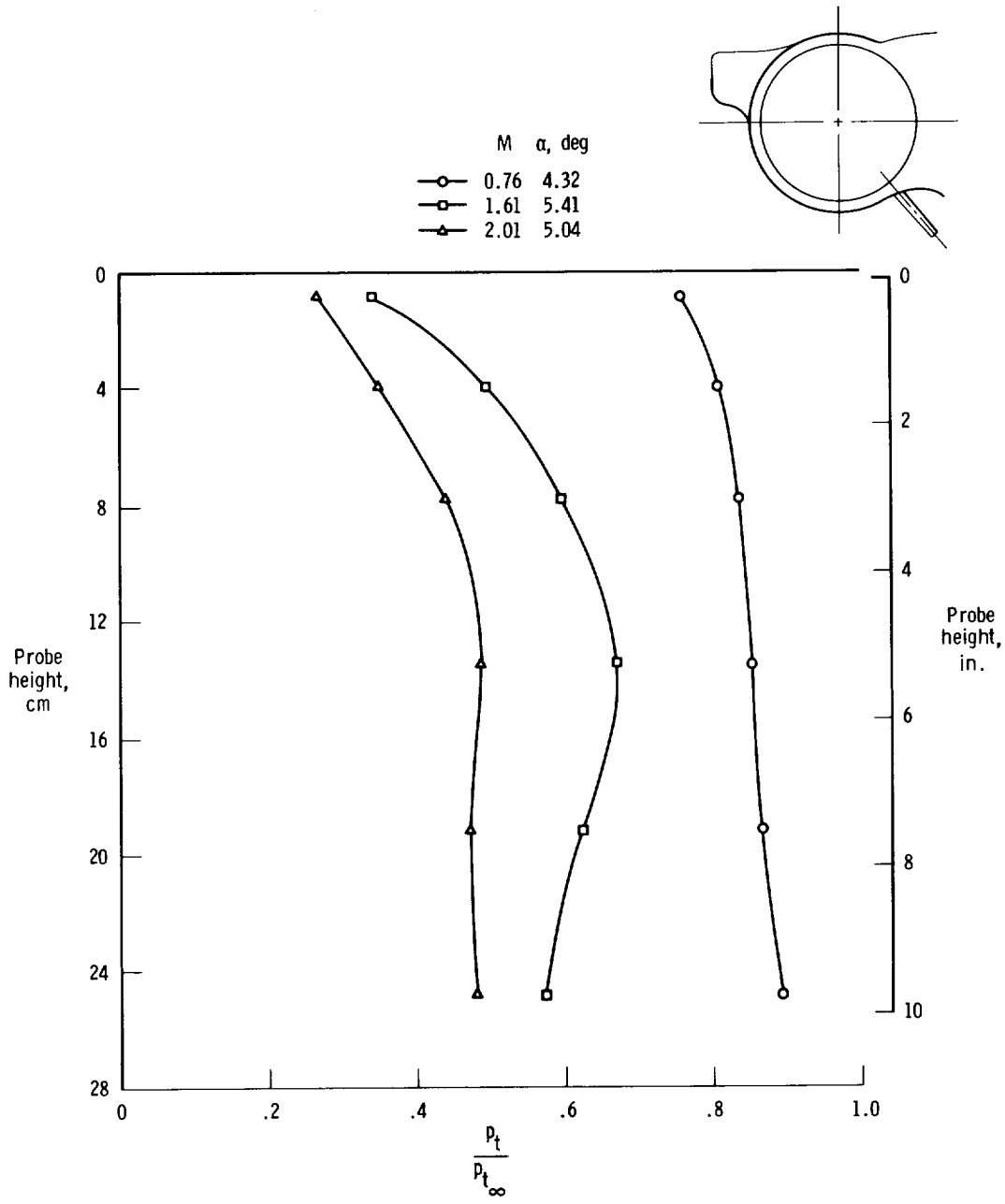

(b) $\varphi = 140°$.

Figure 12. Concluded.

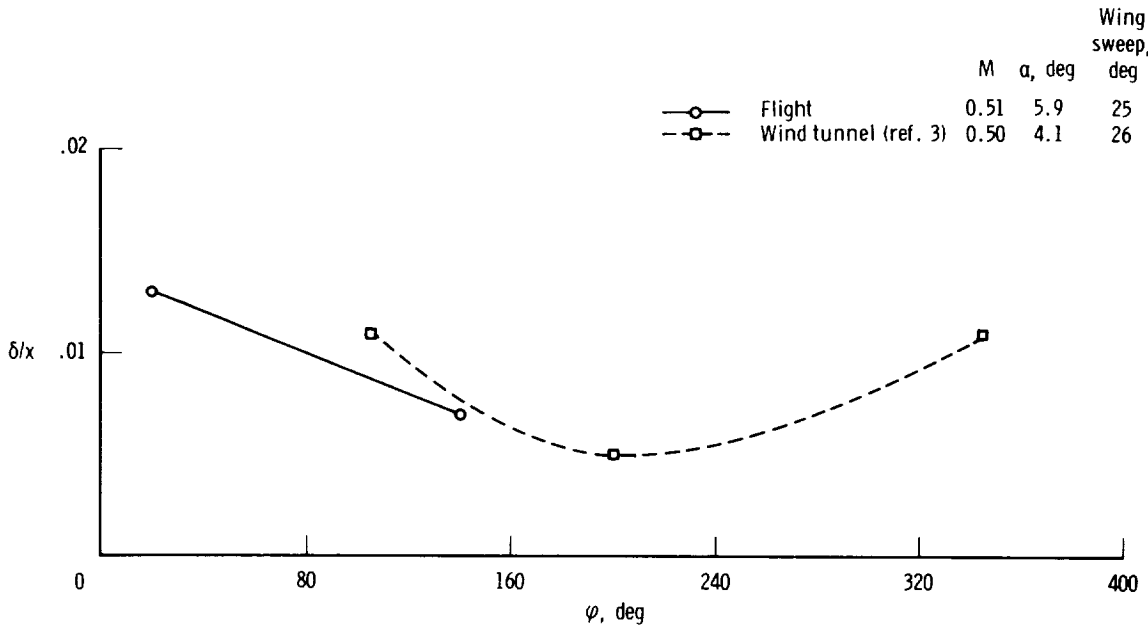

Figure 13. Comparison of flight and wind-tunnel-model effective boundary layer thickness.

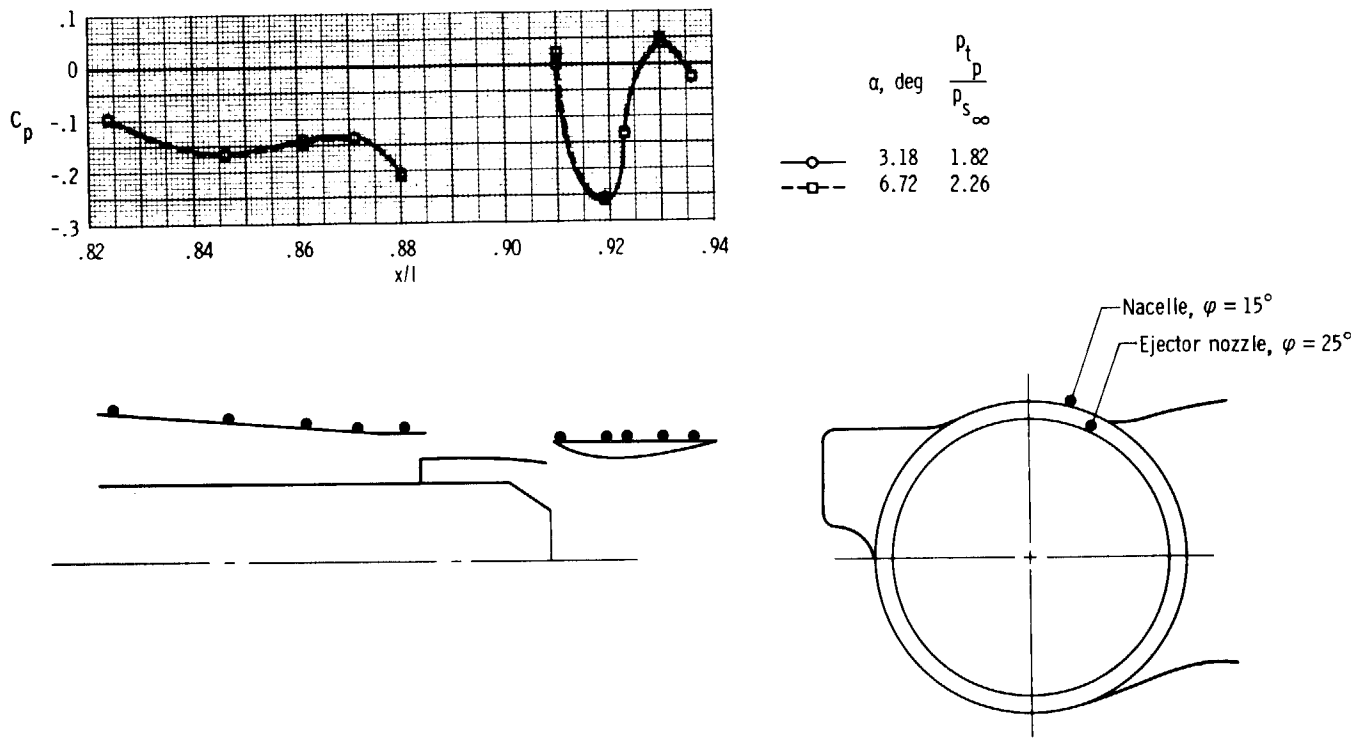

(a) Nacelle at $\varphi = 15°$ and ejector nozzle at $\varphi = 25°$.

Figure 14. Effect of angle of attack on the aft fuselage pressure coefficients. M = 0.70.

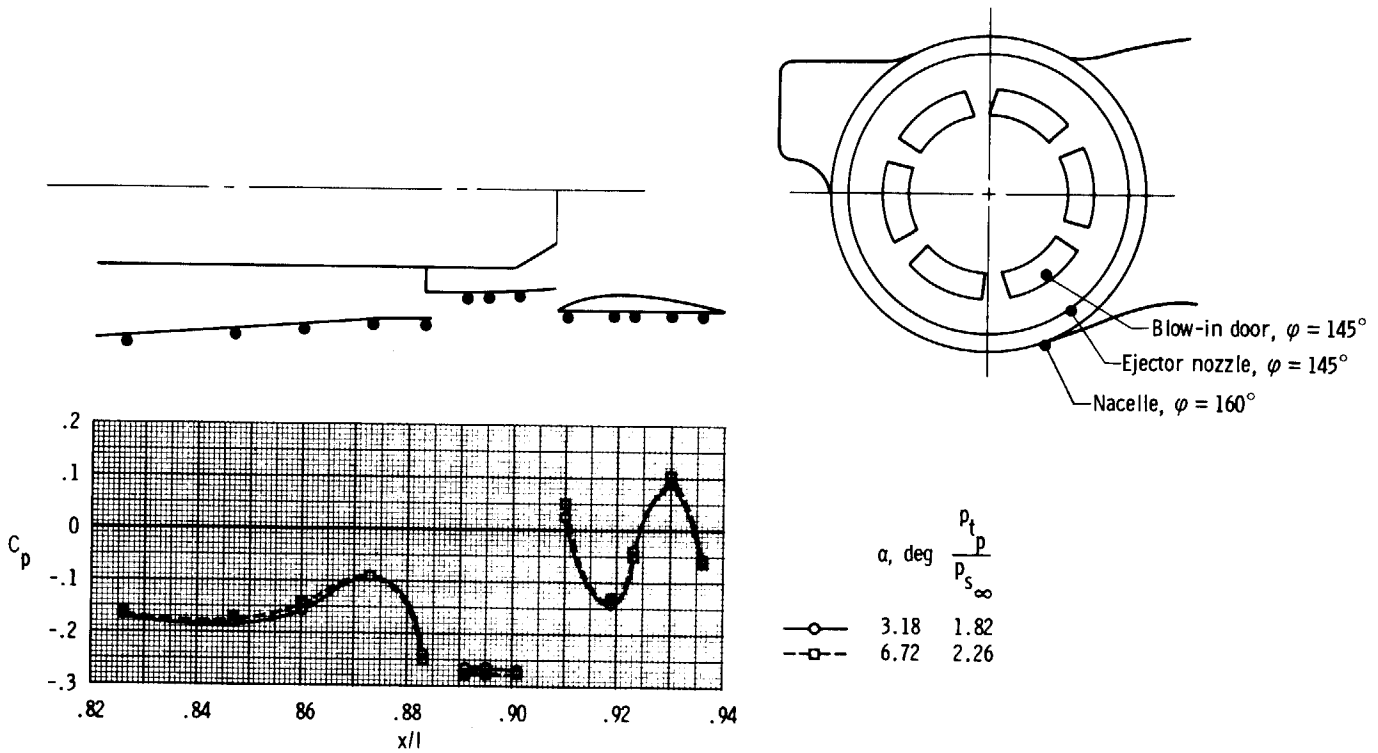

(b) Nacelle at $\varphi = 160°$, blow-in door at $\varphi = 145°$, and ejector nozzle at $\varphi = 145°$.

Figure 14. Continued.

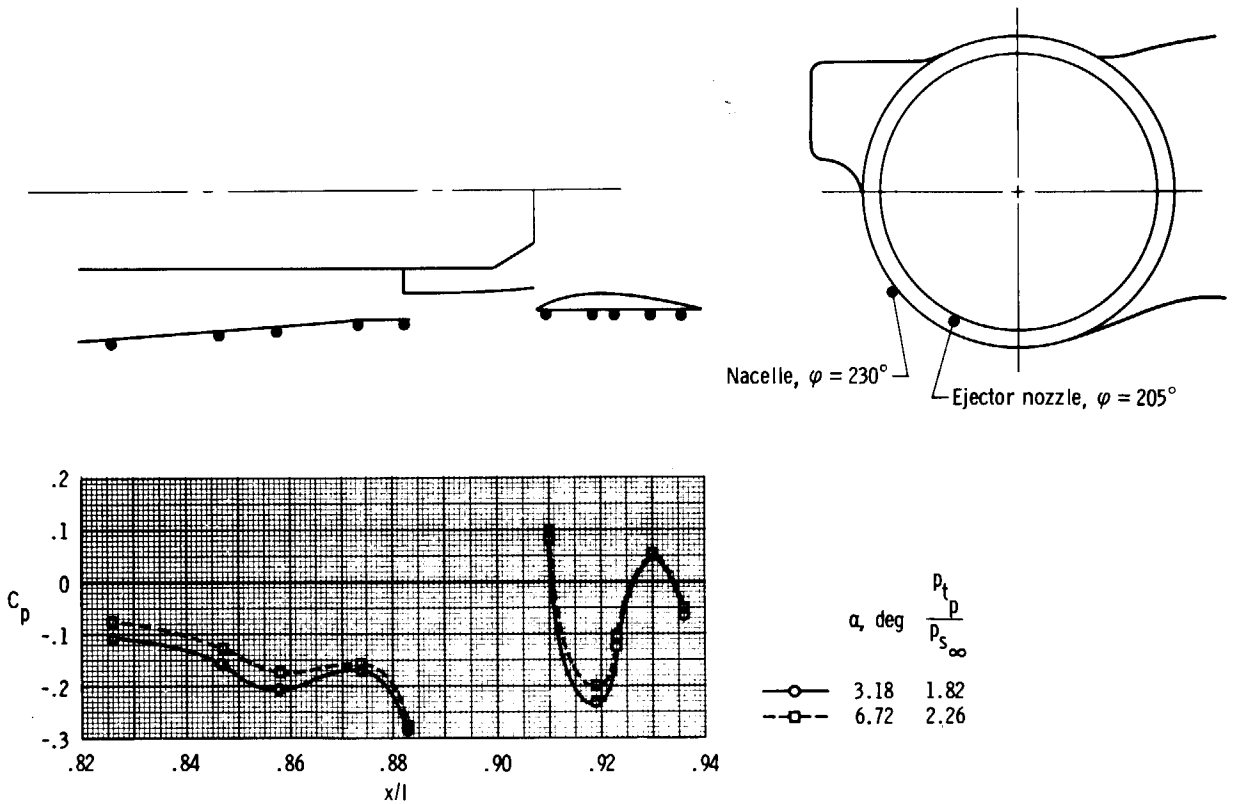

(c) Nacelle at $\varphi = 230°$ and ejector nozzle at $\varphi = 205°$.

Figure 14. Continued.

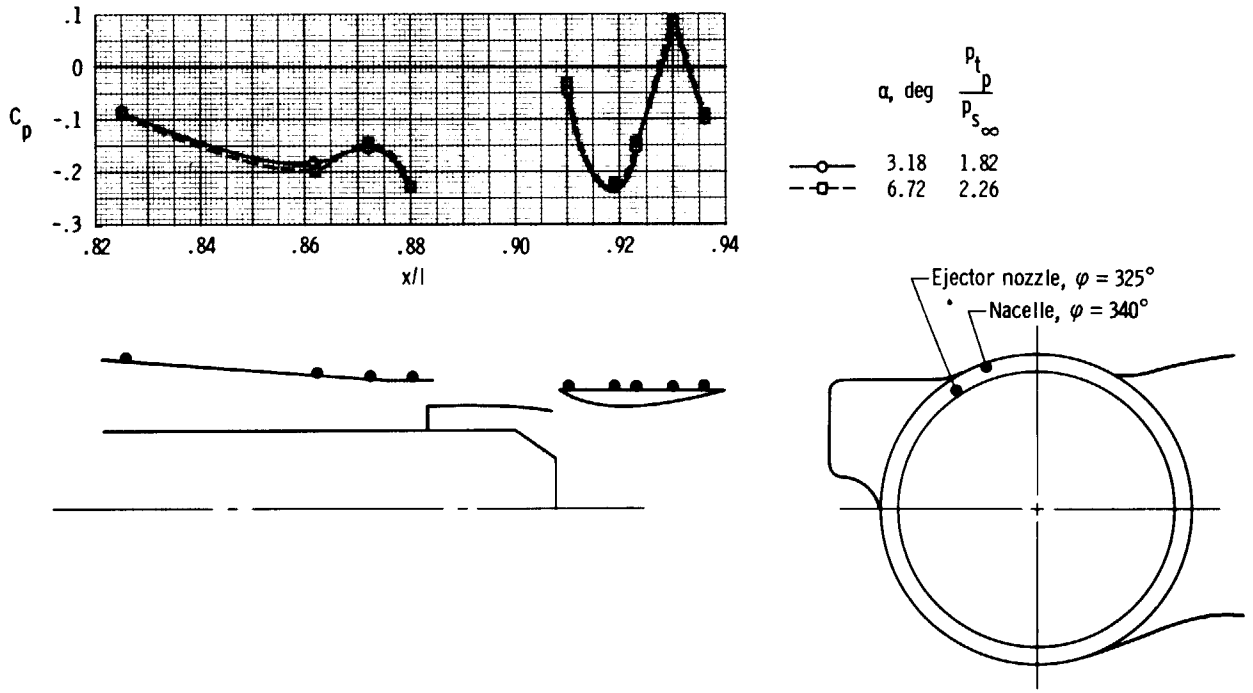

(d) Nacelle at $\varphi = 340°$ and ejector nozzle at $\varphi = 325°$.

Figure 14. Continued.

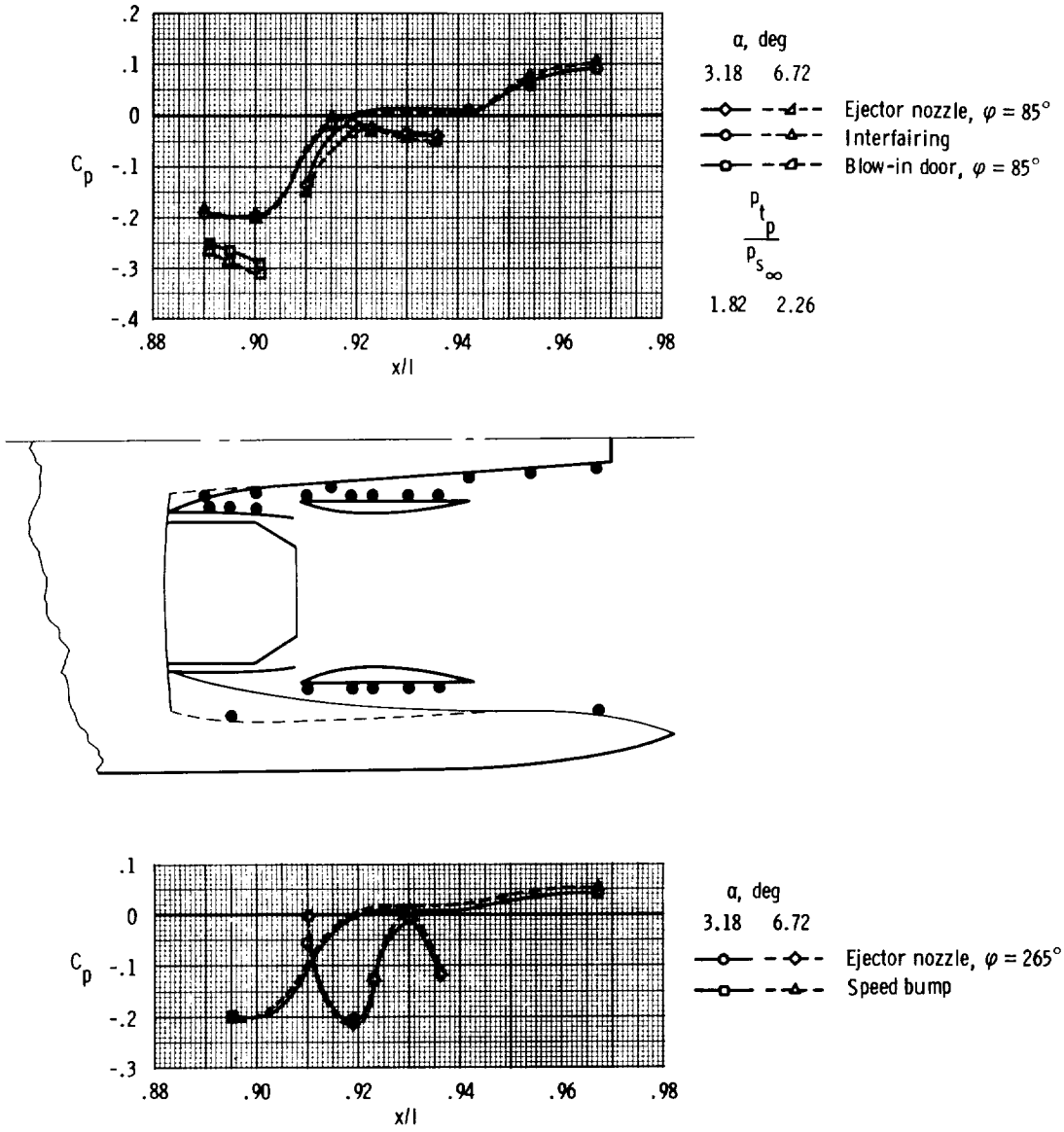

(e) Ejector nozzle at φ = 85° and 265°, blow-in door at φ = 85°, interfairing, and speed bump.

Figure 14. Concluded.

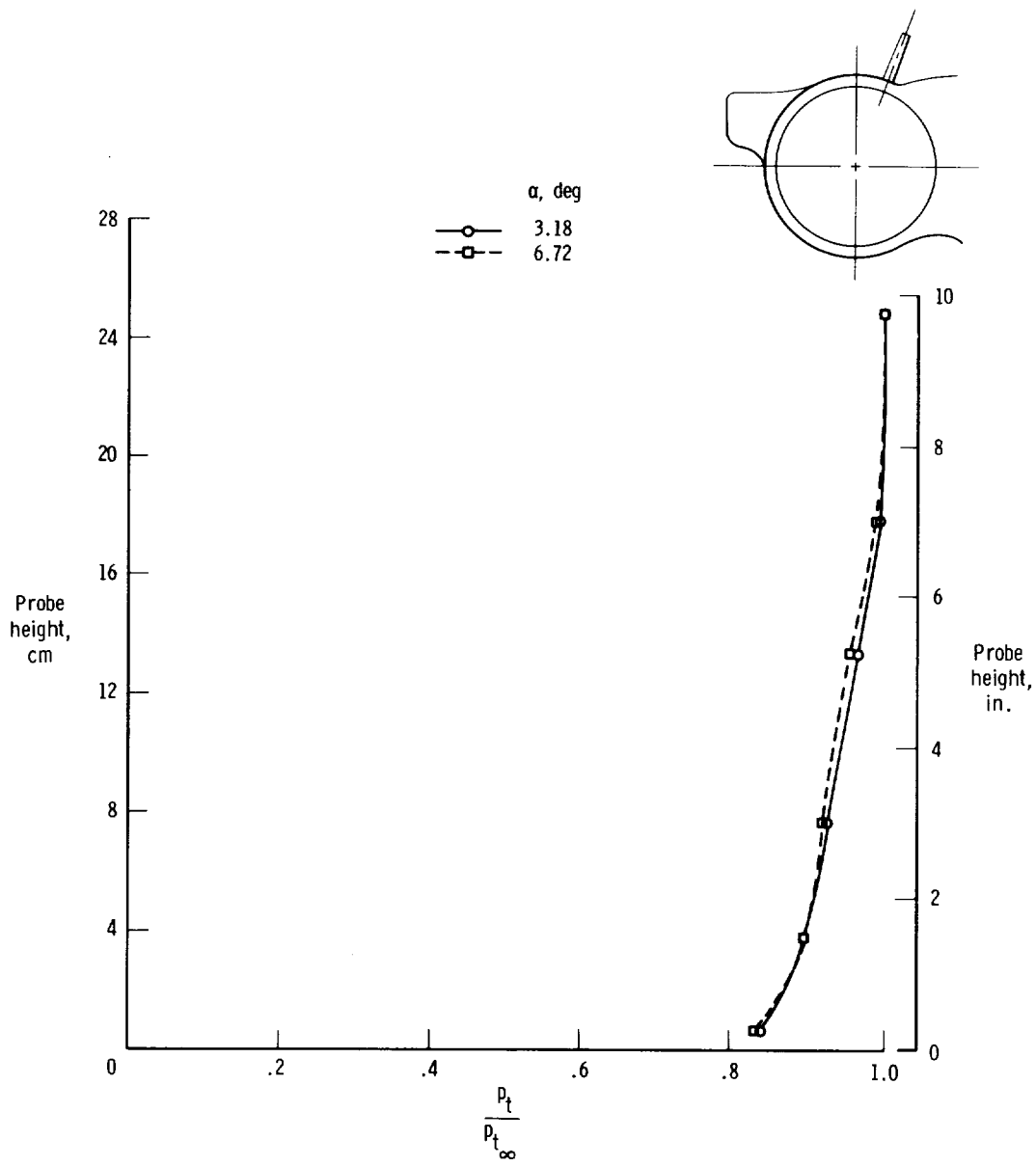

(a) $\varphi = 20°$.

Figure 15. Effect of angle of attack on boundary layer of the nacelle upper and lower surfaces. M = 0.70.

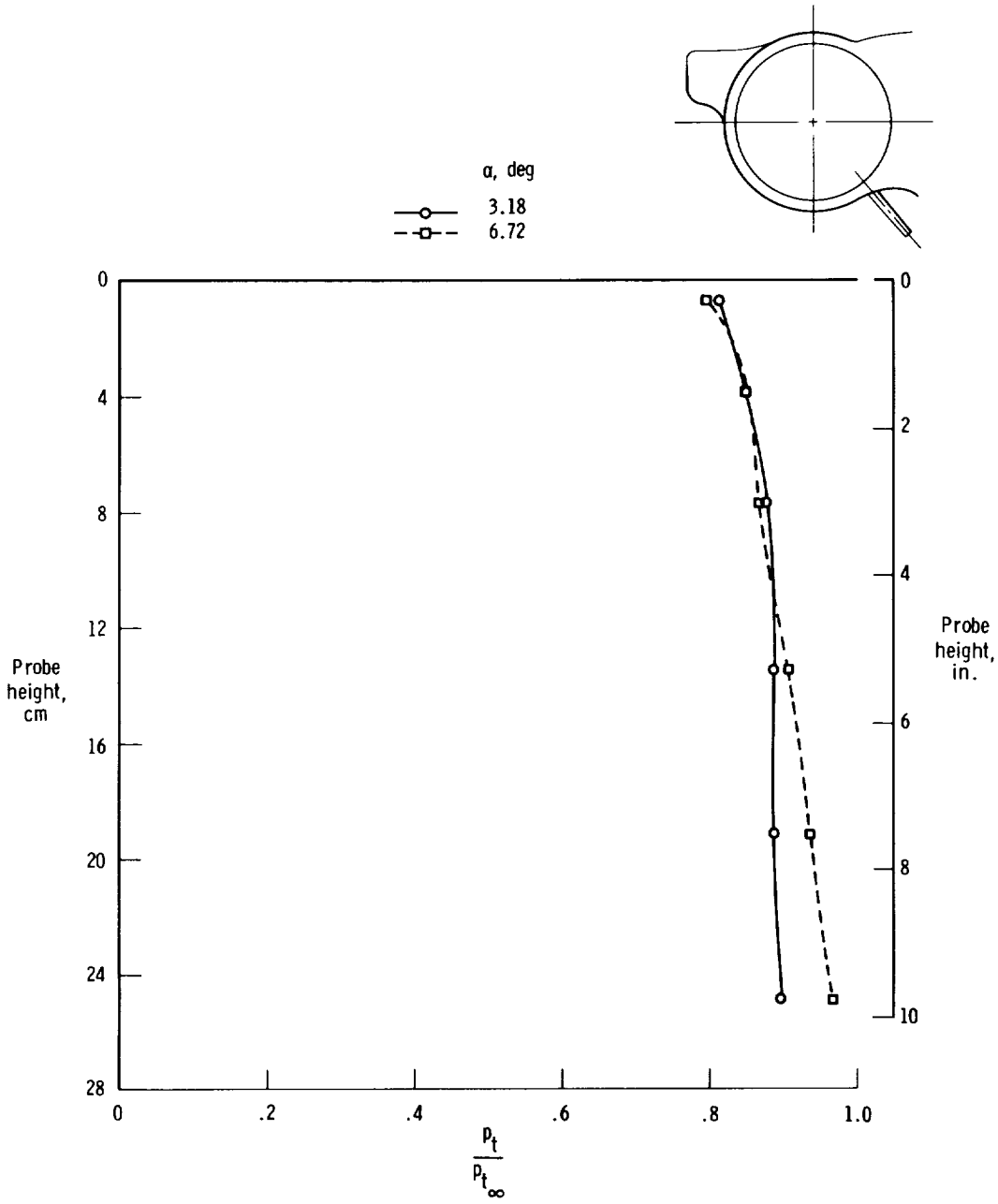

(b) $\varphi = 140°$.

Figure 15. Concluded.

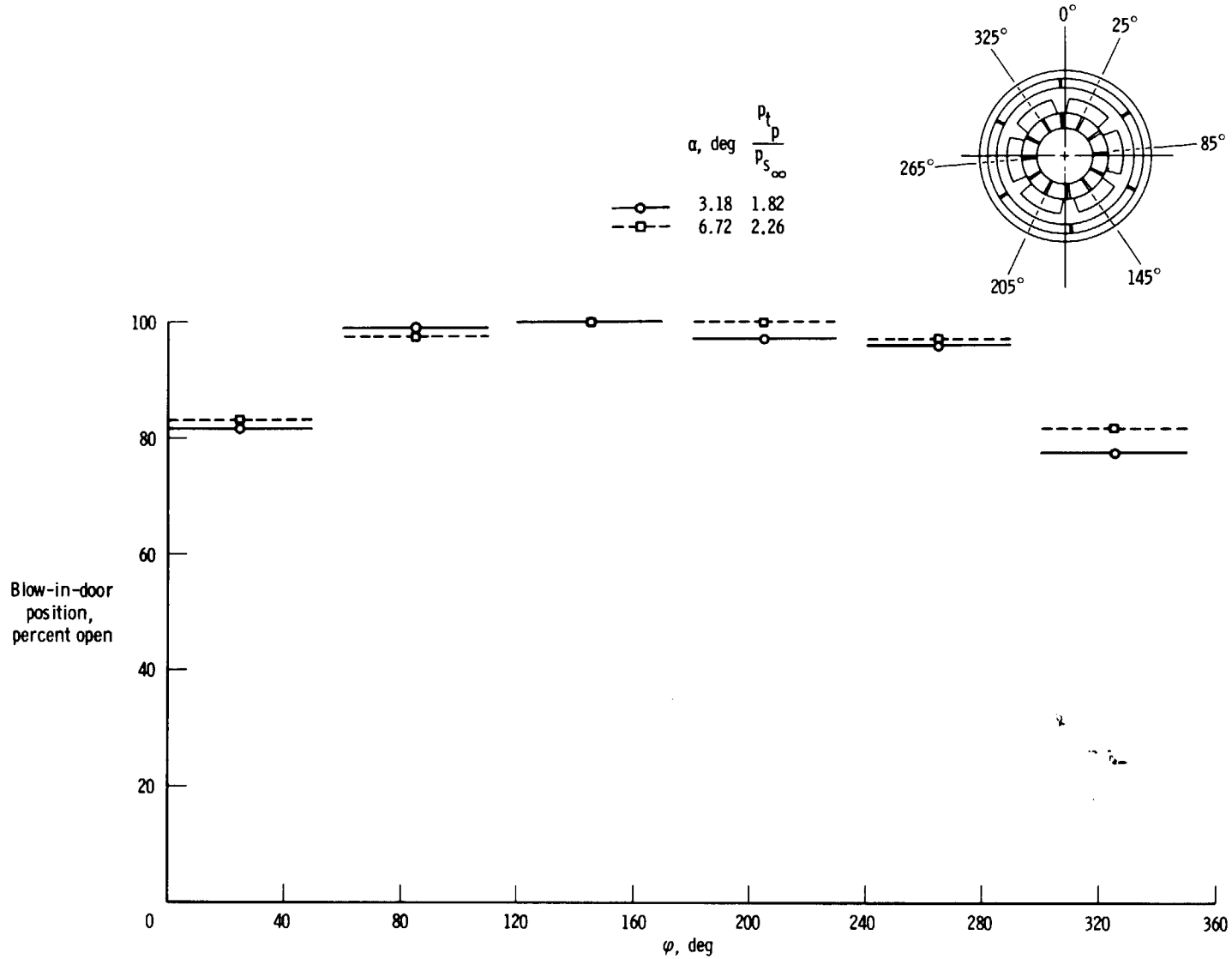

Figure 16. Effect of angle of attack on blow-in-door position. M = 0.70.

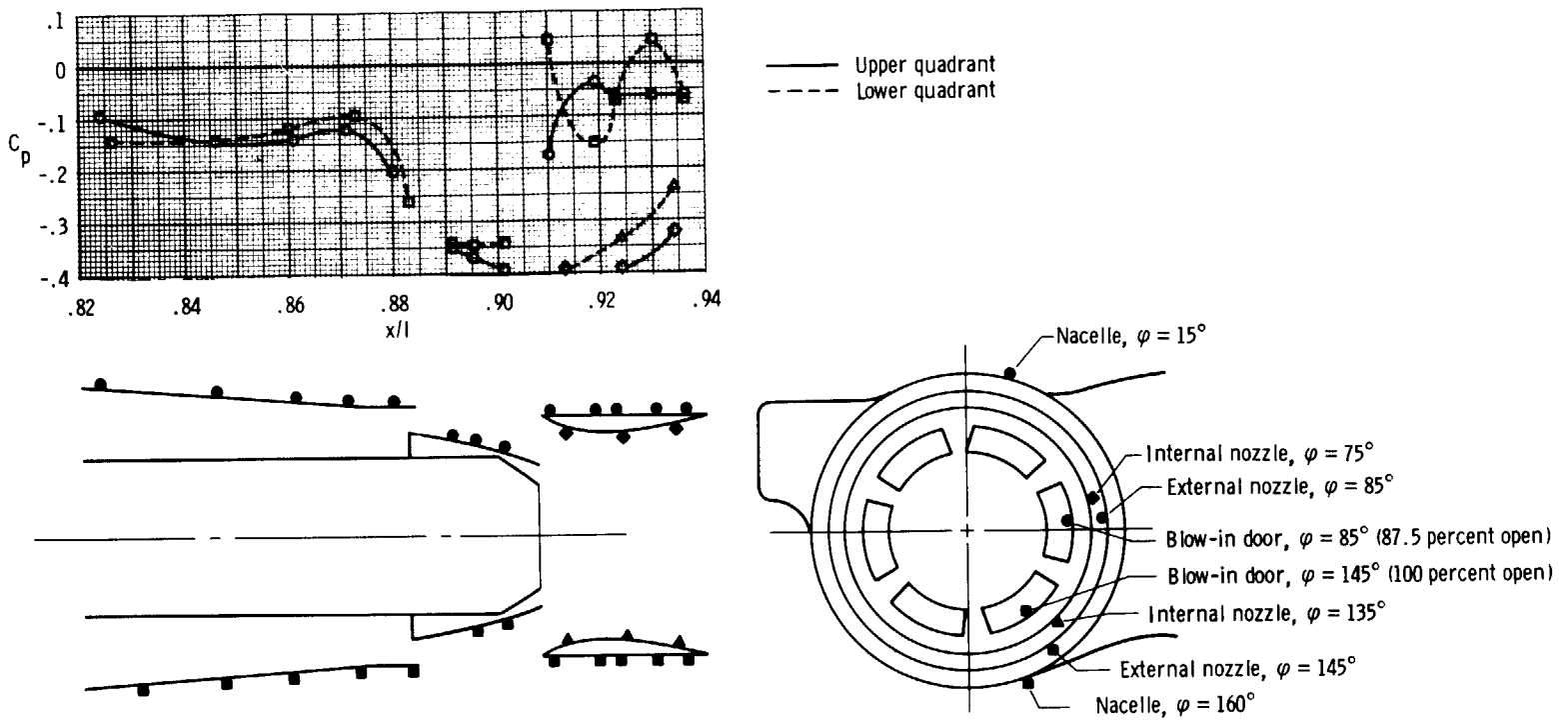

(a) M = 0.50, α = 2.10°.

Figure 17. External-internal pressure coefficients at three representative Mach numbers.

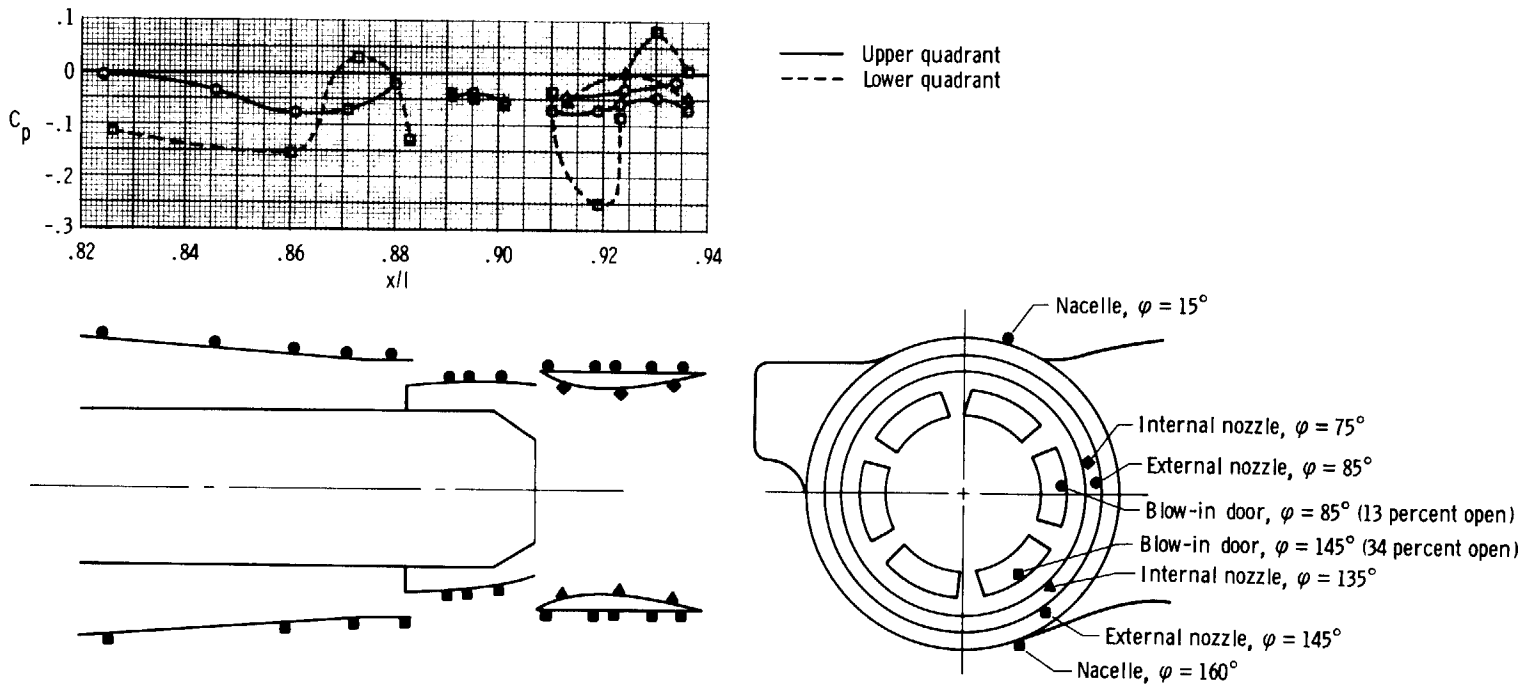

(b) M = 1.38, α = 3.00°.

Figure 17. Continued.

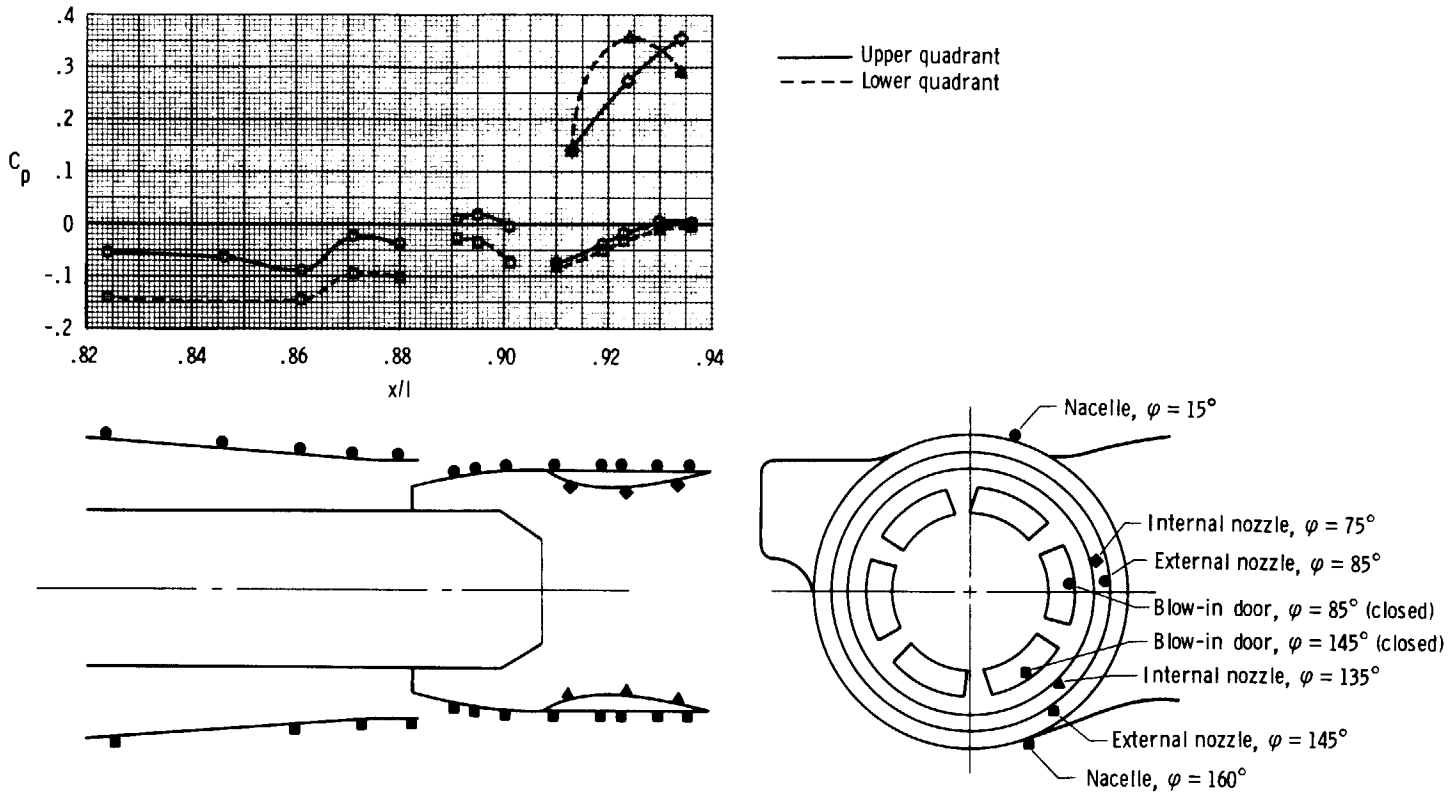

(c) M = 1.96, α = 3.49°.

Figure 17. Concluded.

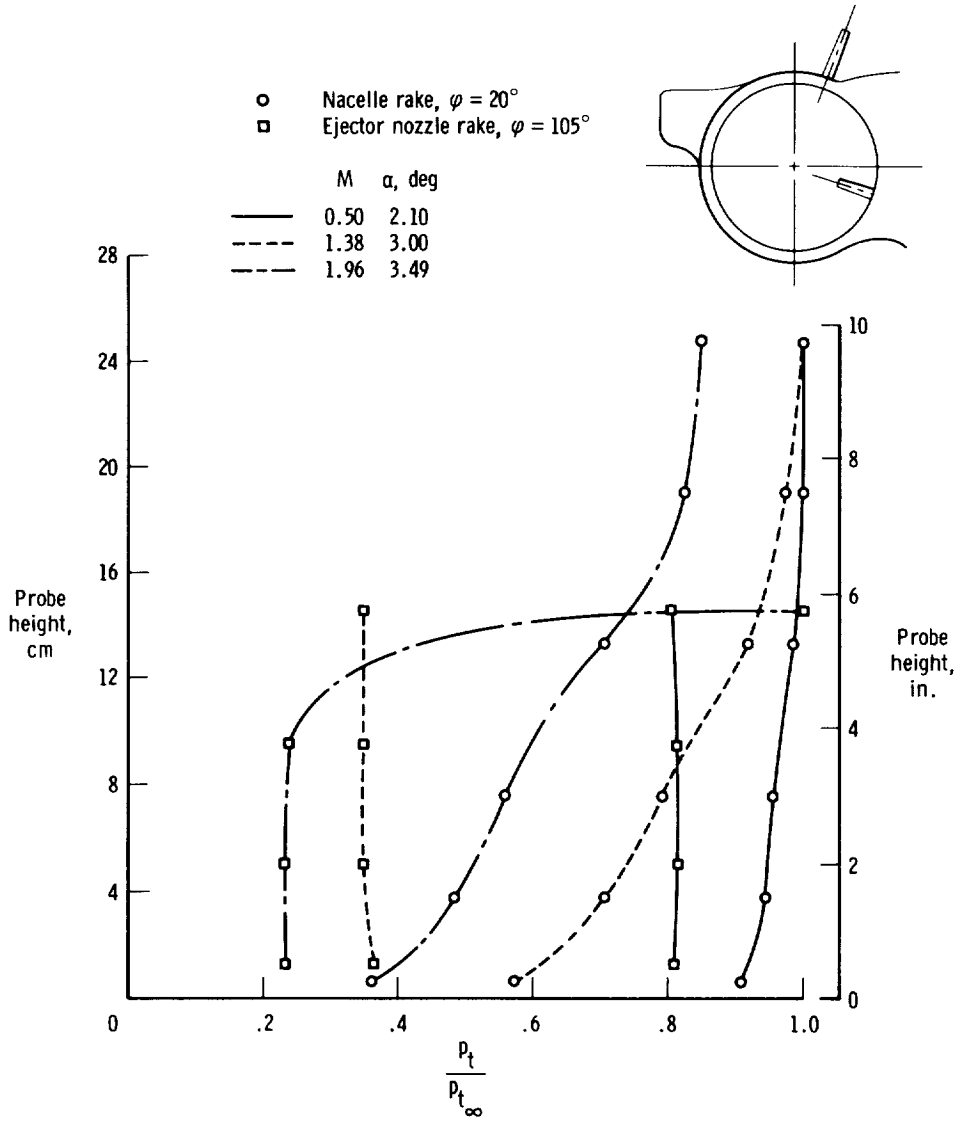

(a) Upper quadrant.

Figure 18. Comparison of nacelle and ejector nozzle boundary layer rake measurements at three representative Mach numbers.

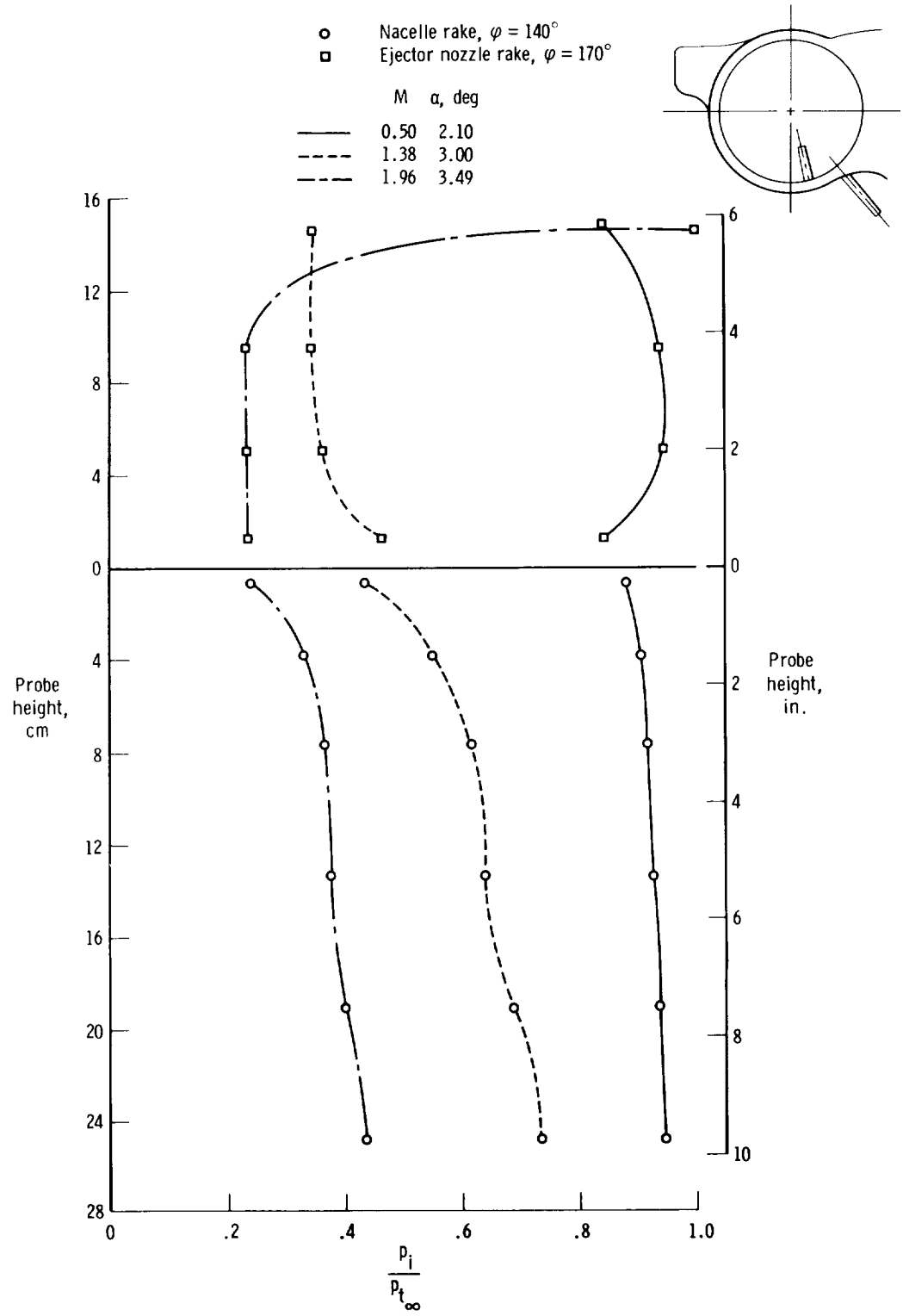

(b) Lower quadrant.

Figure 18. Concluded.

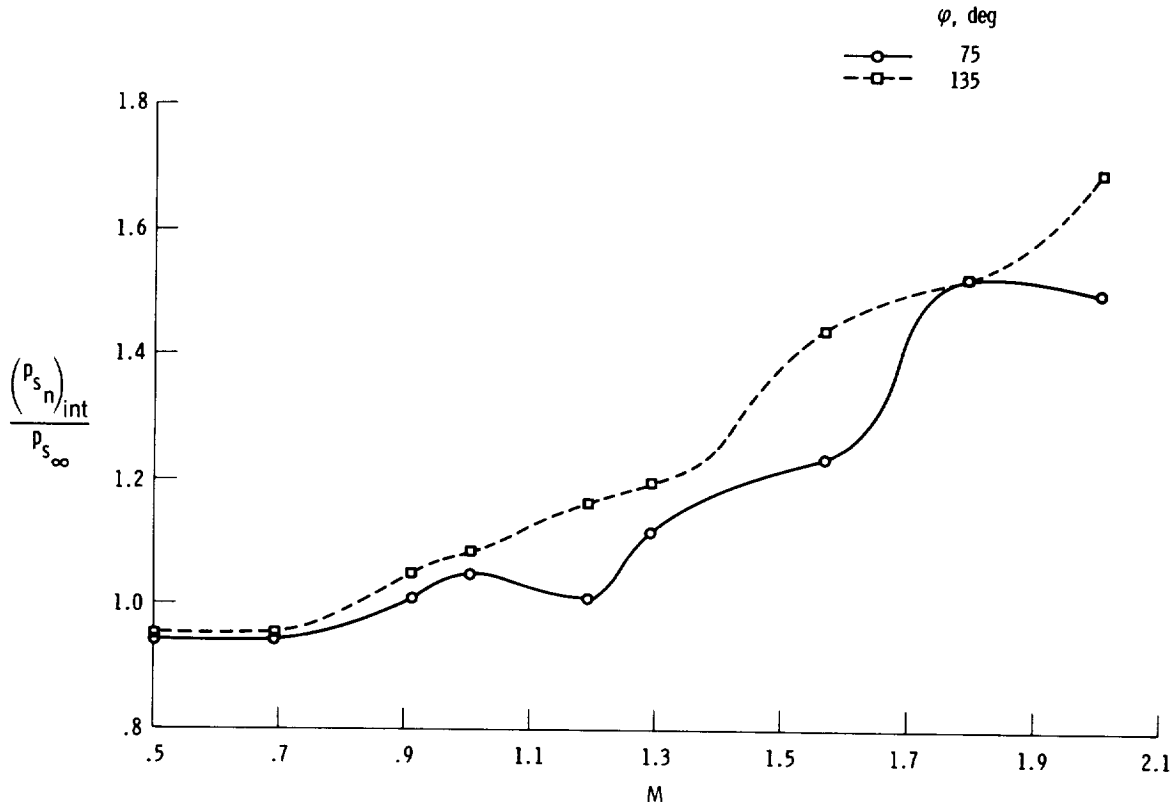

Figure 19. Ejector nozzle static pressure ratio.

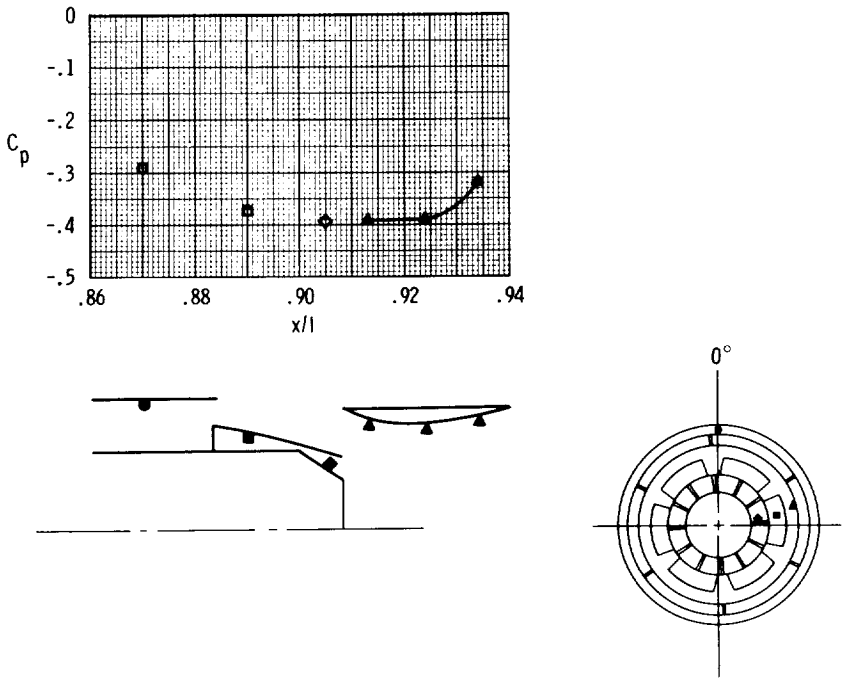

(a) M = 0.50, α = 2.10°, φ = 85°, blow-in door 87.5 percent open.

Figure 20. Internal pressure coefficients at three representative Mach numbers.

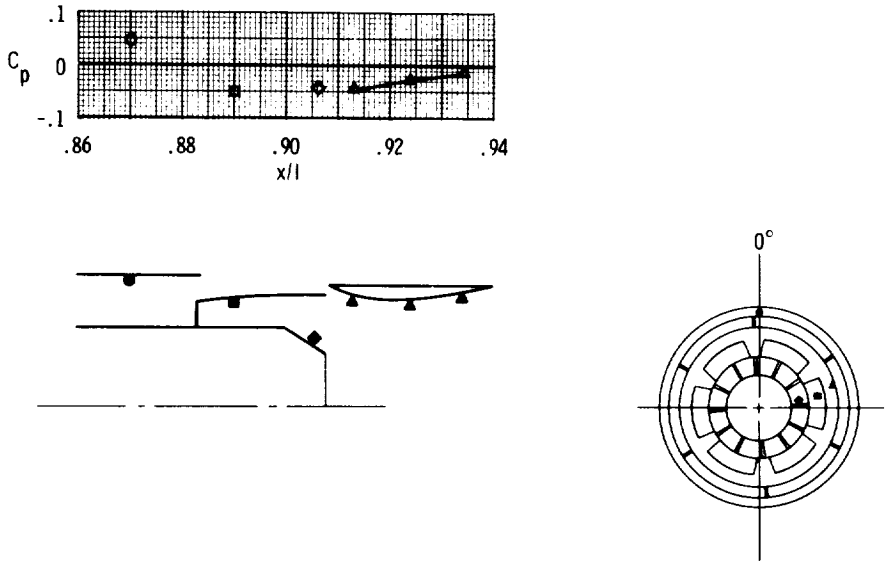

(b) M = 1.38, α = 3.00°, φ = 85°, blow-in door 13 percent open.

Figure 20. Continued.

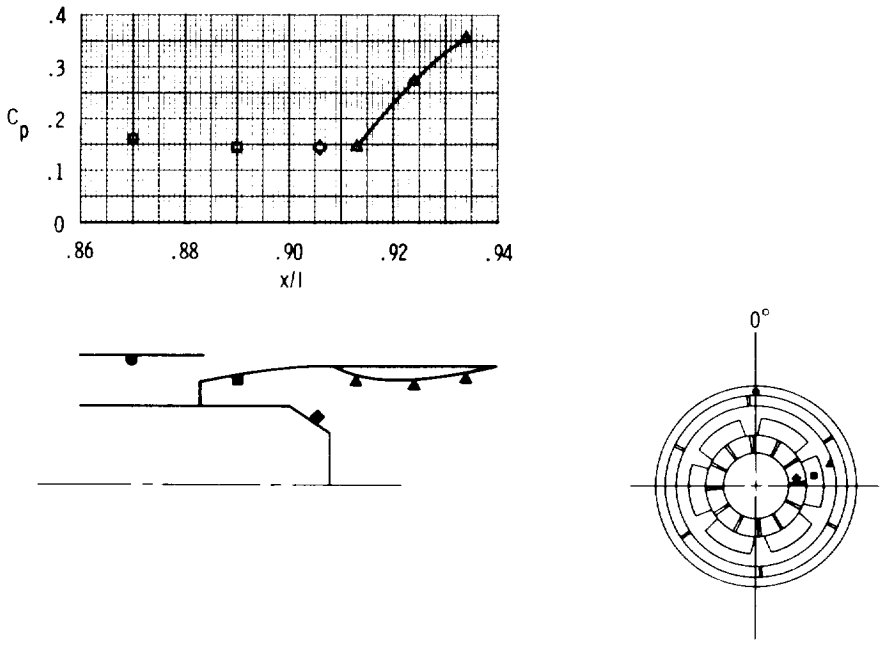

(c) M = 1.96, α = 3.49°, φ = 85°, blow-in door closed.

Figure 20. Concluded.

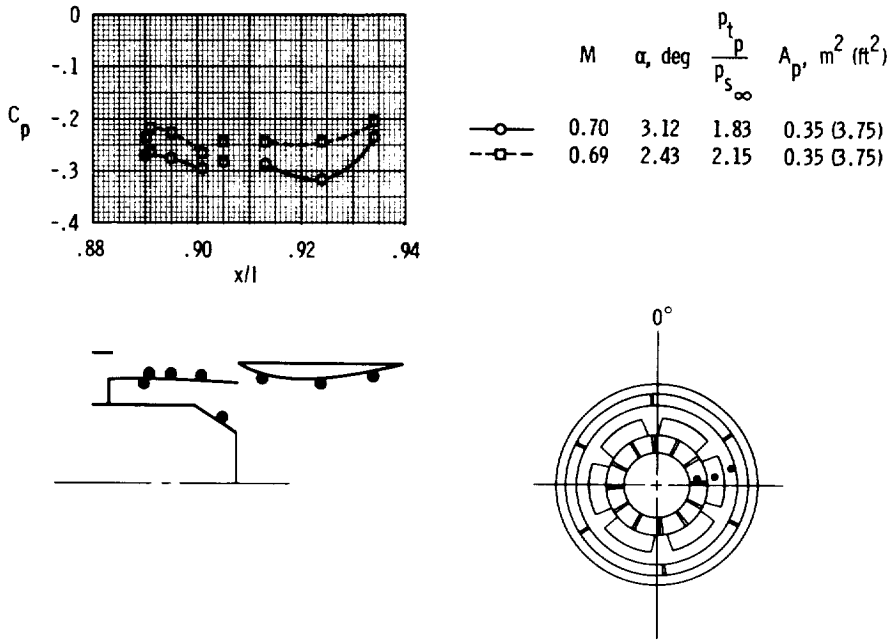

(a) Internal pressure coefficients.

Figure 21. Effect of primary nozzle total pressure ratio at a subsonic Mach number of approximately 0.7.

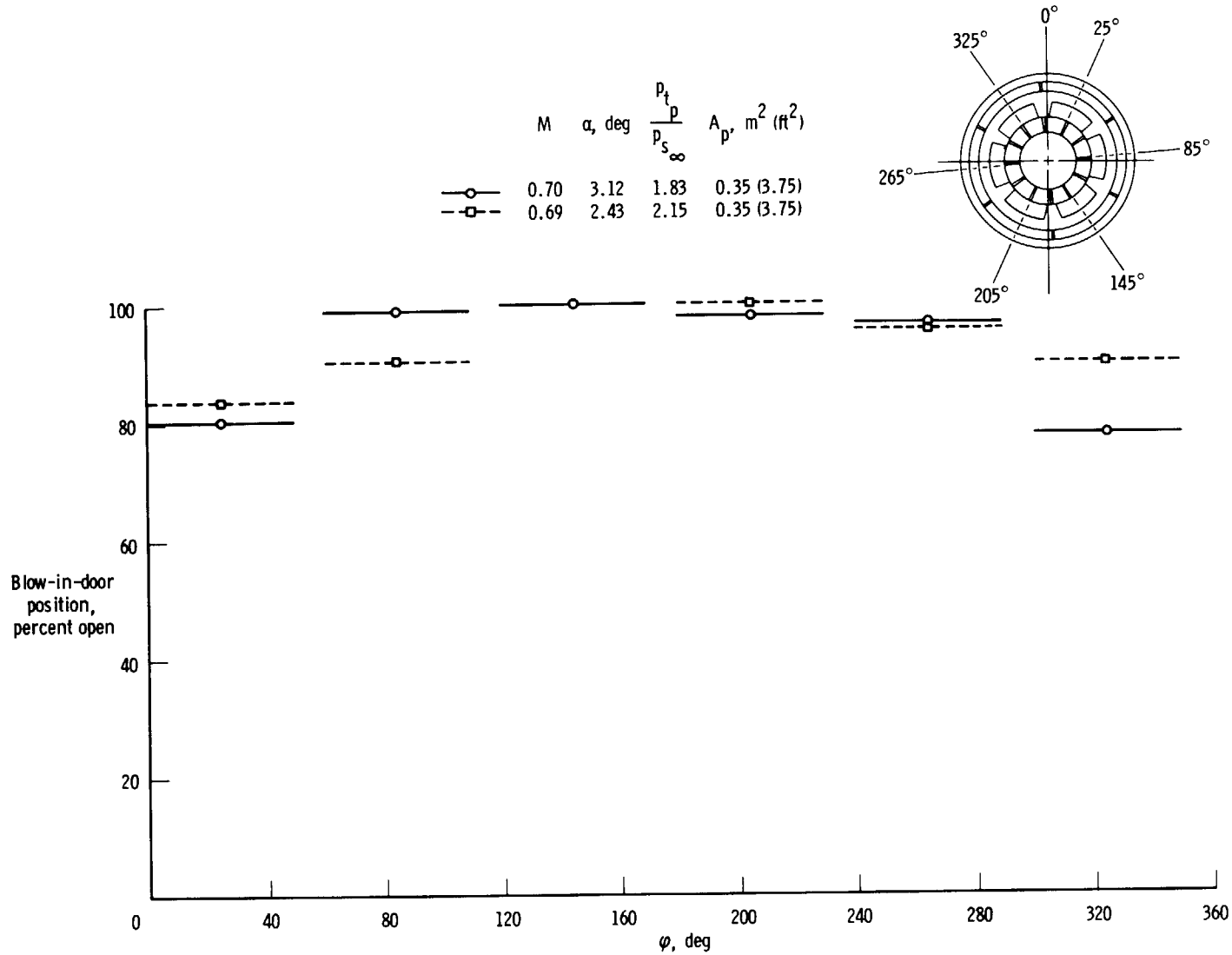

(b) Blow-in-door position.

Figure 21. Continued.

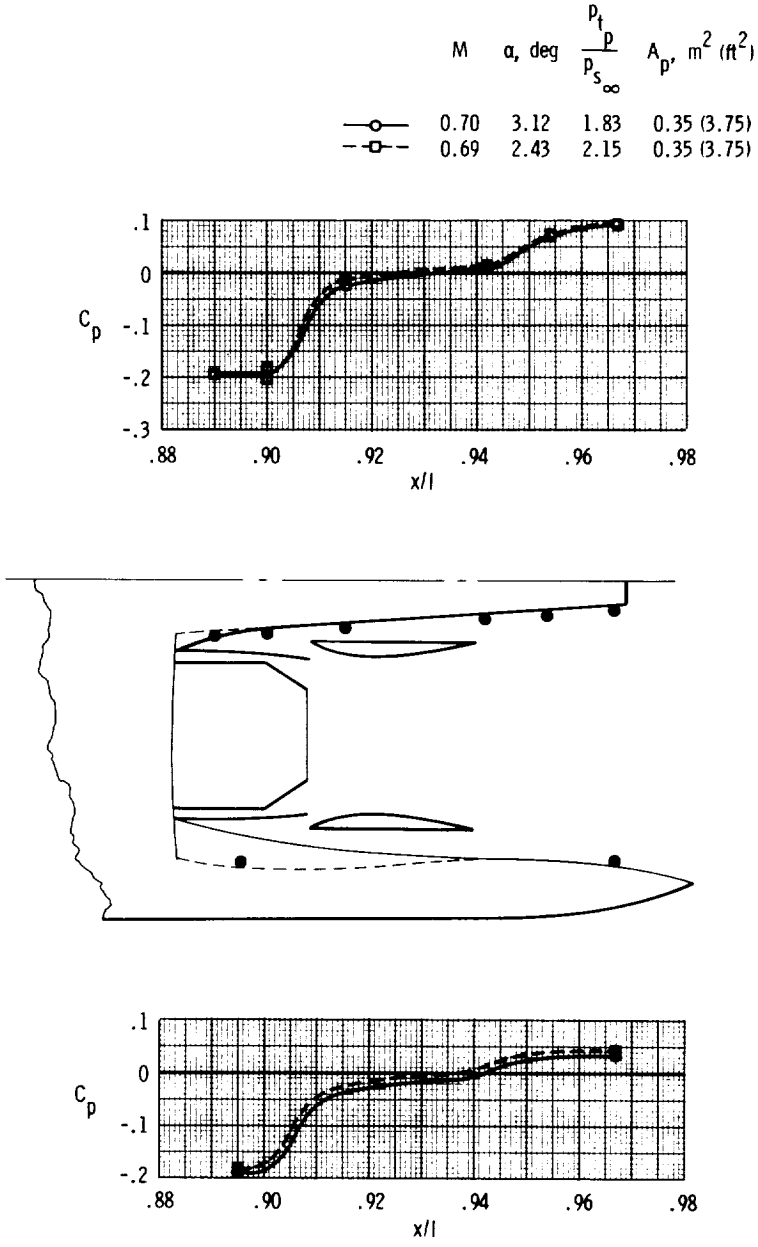

(c) Interfairing and speed bump pressure coefficients.

Figure 21. Continued.

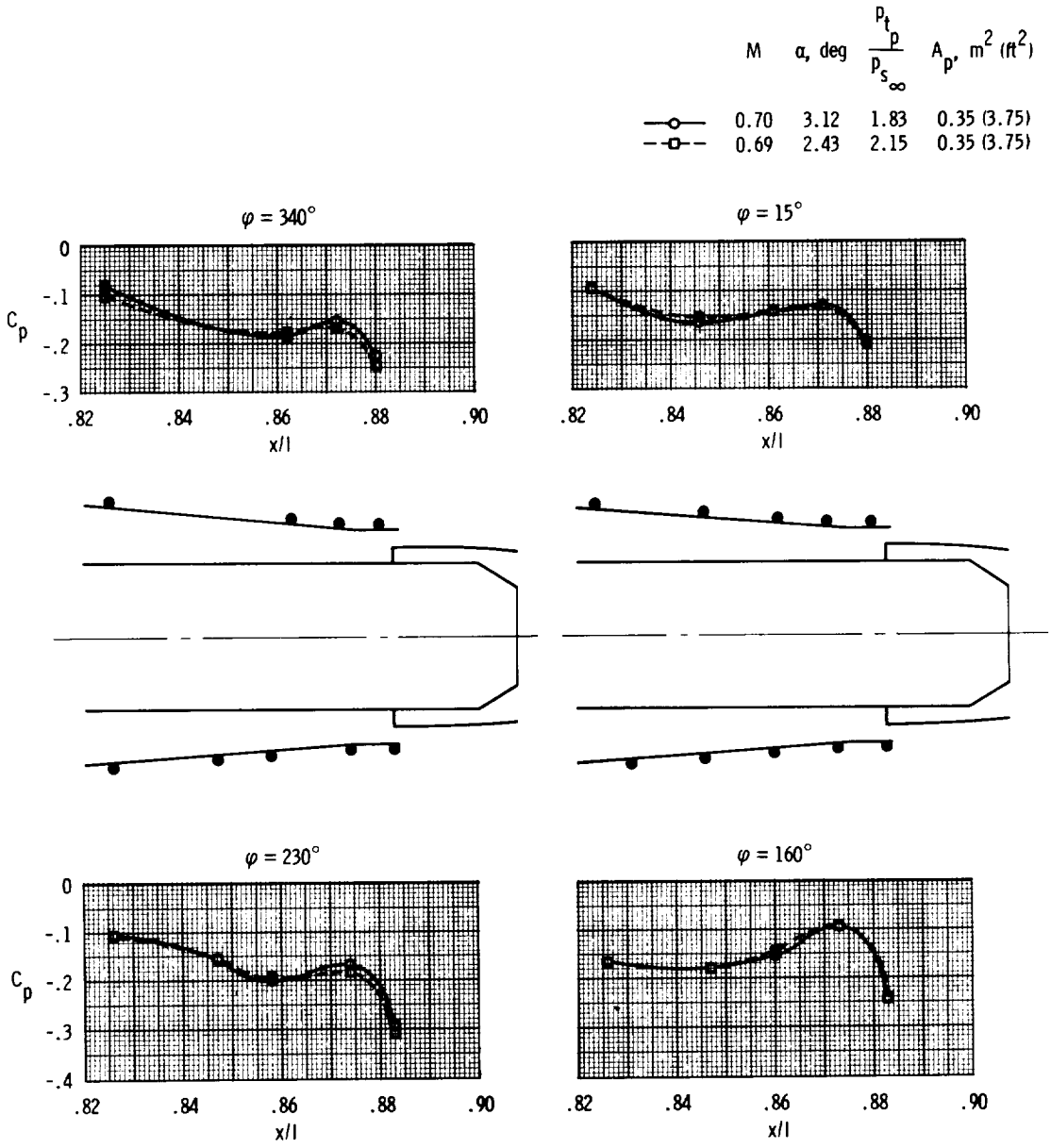

(d) Nacelle pressure coefficients.

Figure 21. Continued.

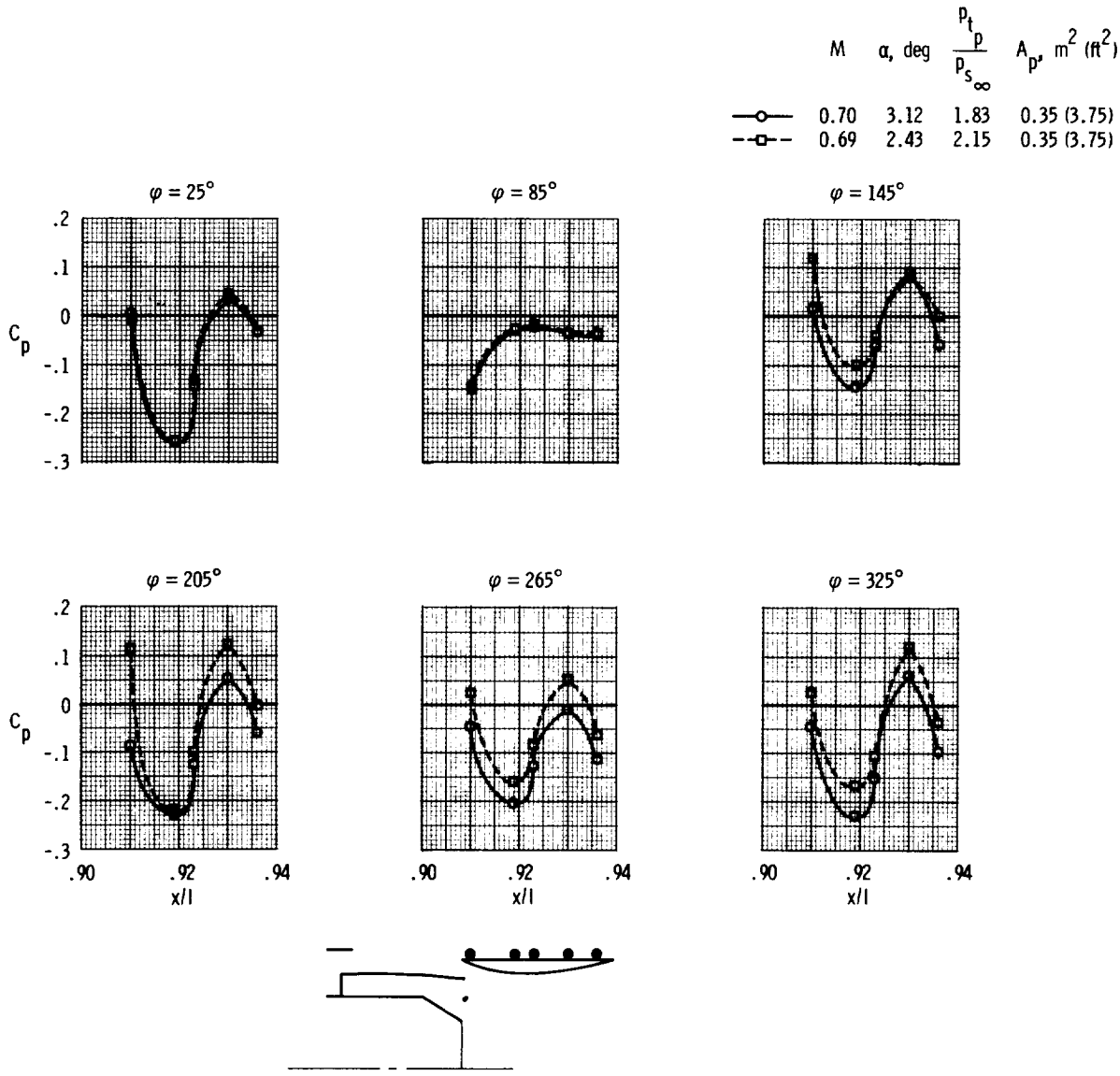

(e) Ejector nozzle pressure coefficients.

Figure 21. Concluded.

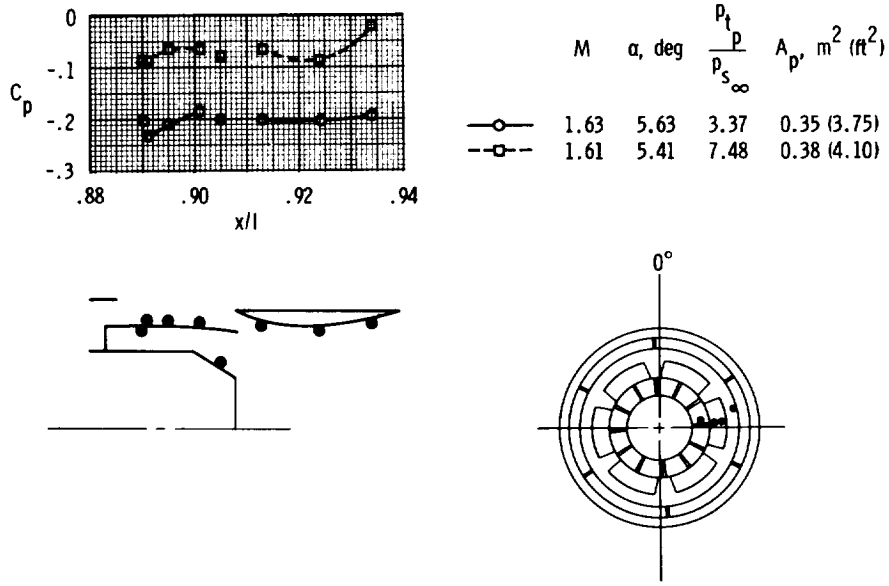

(a) Internal pressure coefficient.

Figure 22. Effect of primary nozzle total pressure ratio at a supersonic Mach number of approximately 1.6.

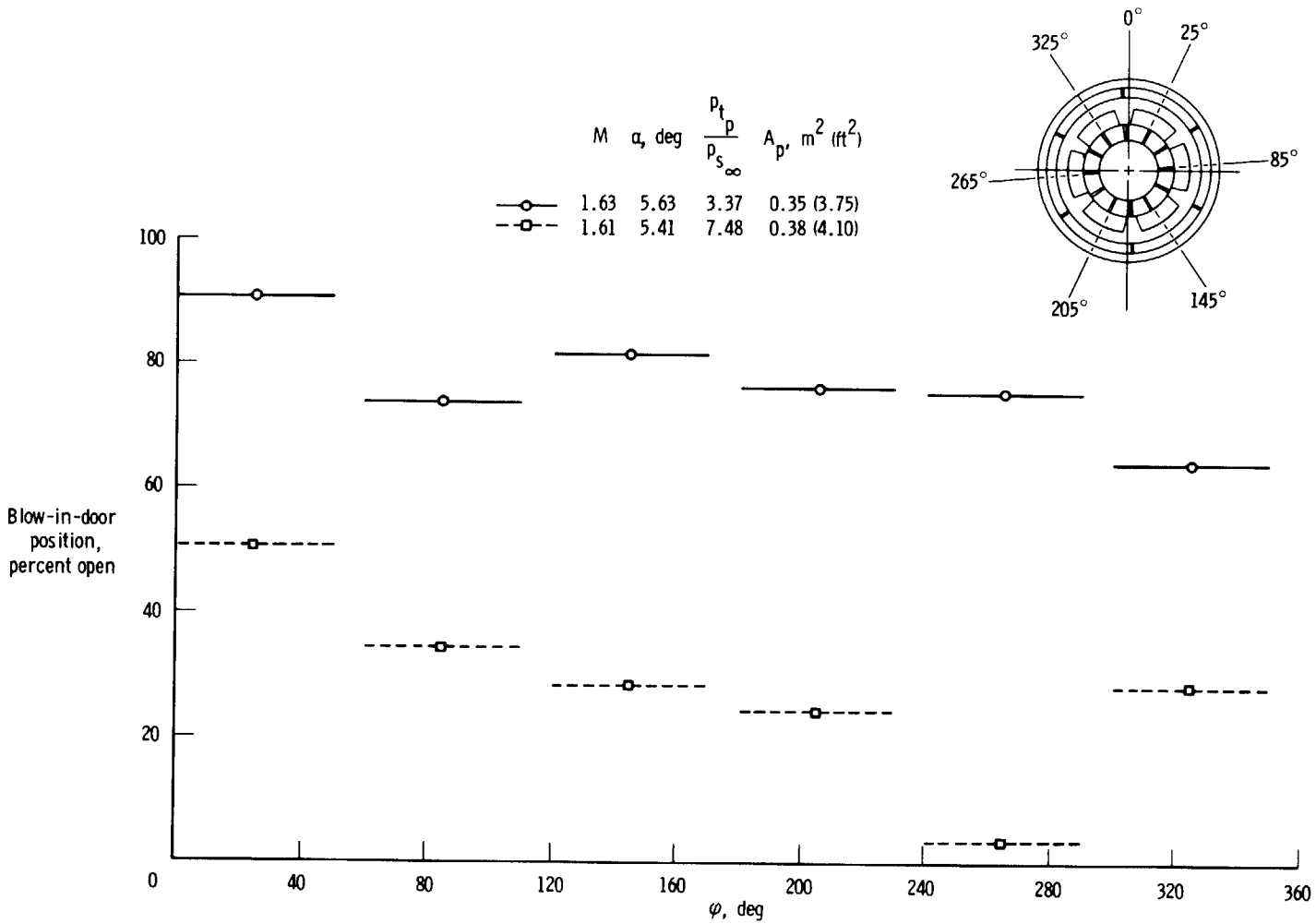

(b) Blow-in-door position.

Figure 22. Continued.

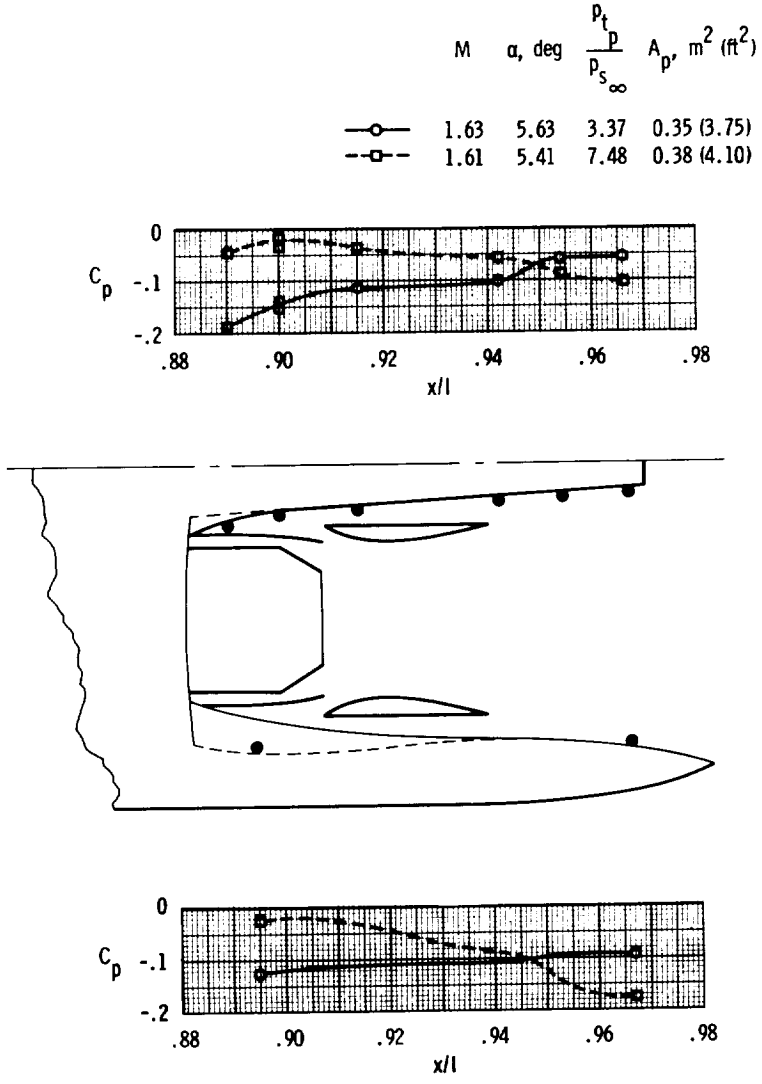

(c) Interfairing and speed bump pressure coefficients.

Figure 22. Continued.

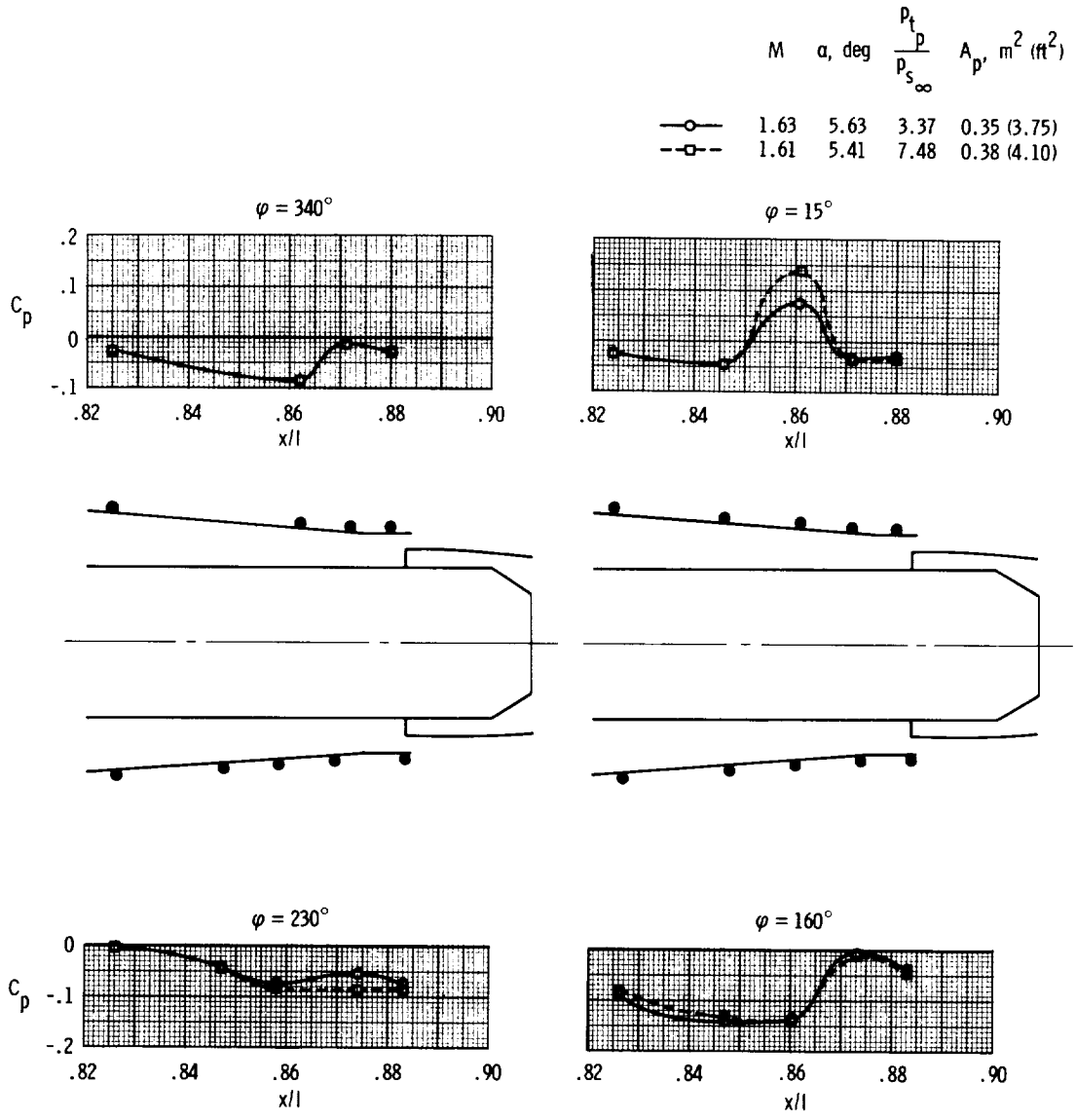

(d) Nacelle pressure coefficients.

Figure 22. Continued.

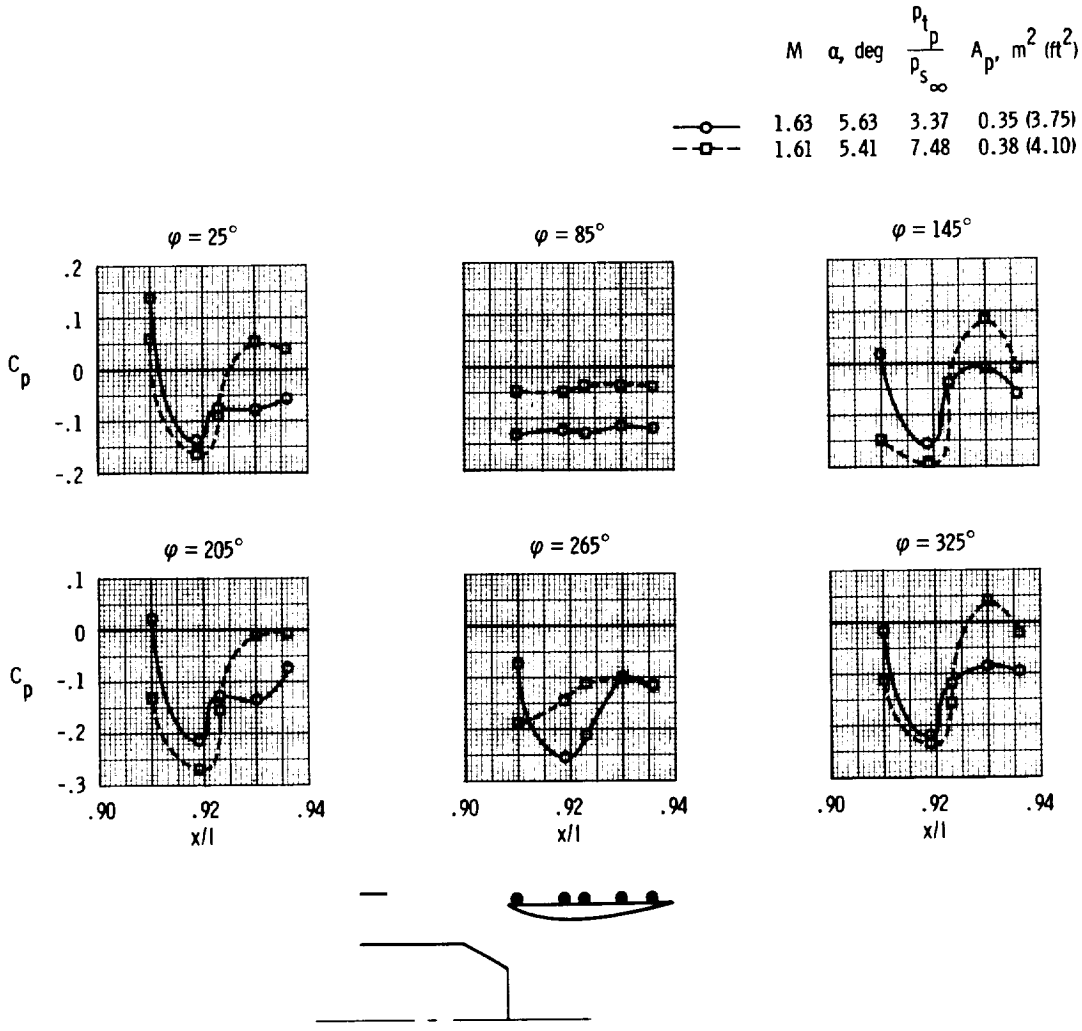

(e) Ejector nozzle pressure coefficients.

Figure 22. Concluded.

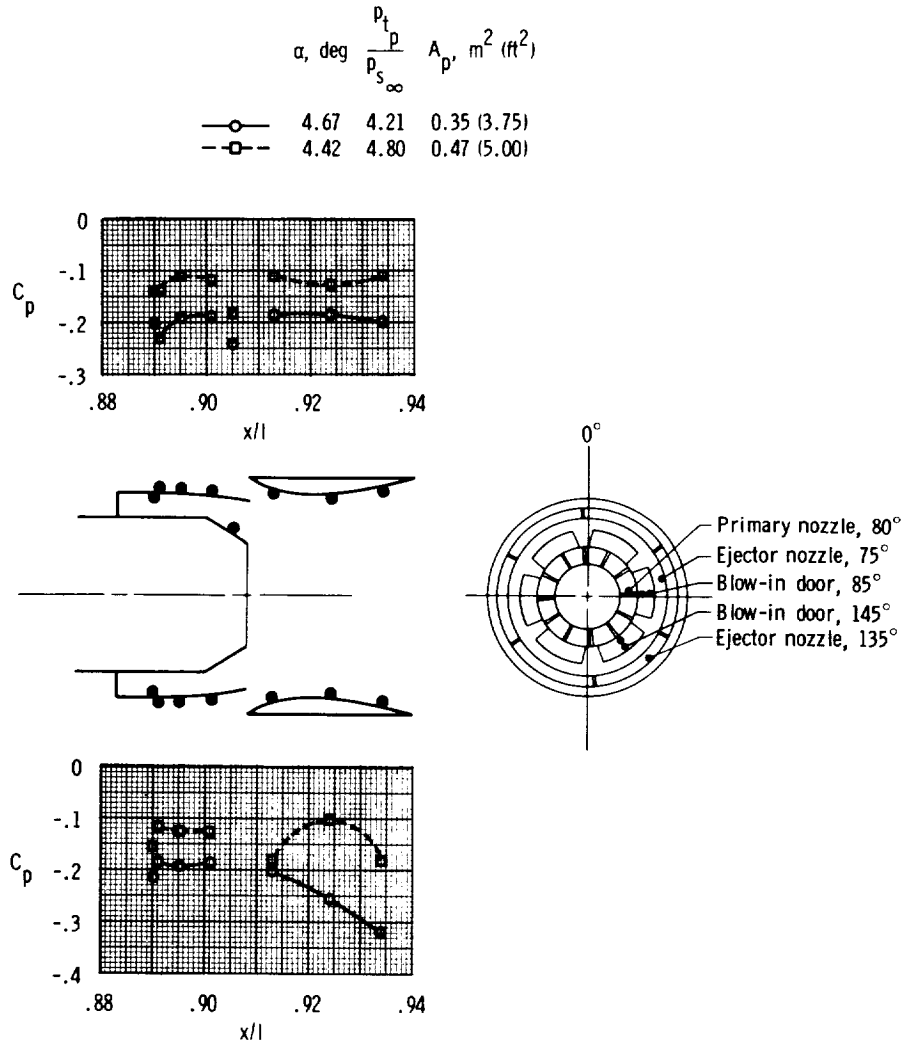

(a) Internal pressure coefficients.

Figure 23. Effect of primary nozzle area at a Mach number of 1.30.

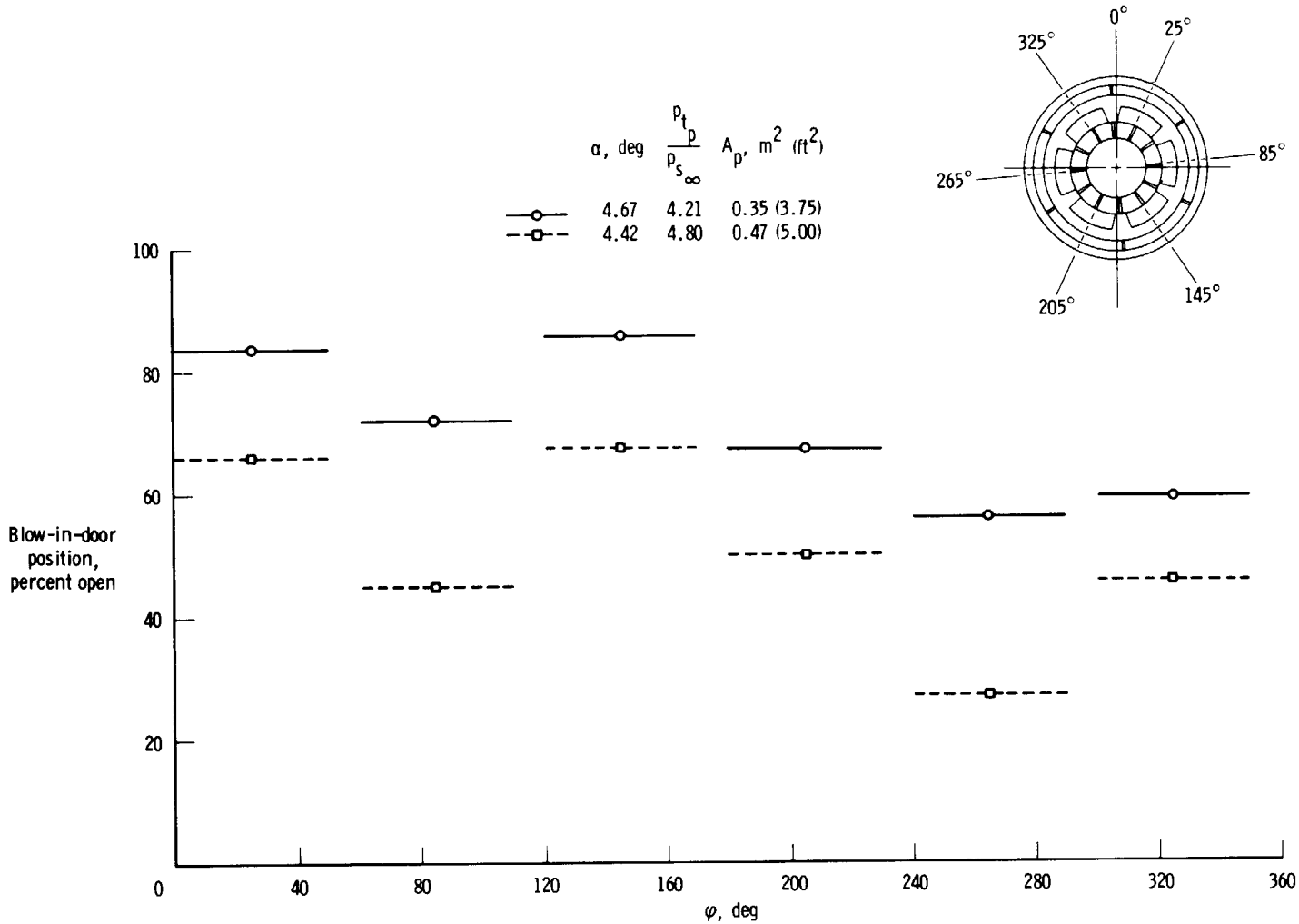

(b) Blow-in-door position.

Figure 23. Continued.

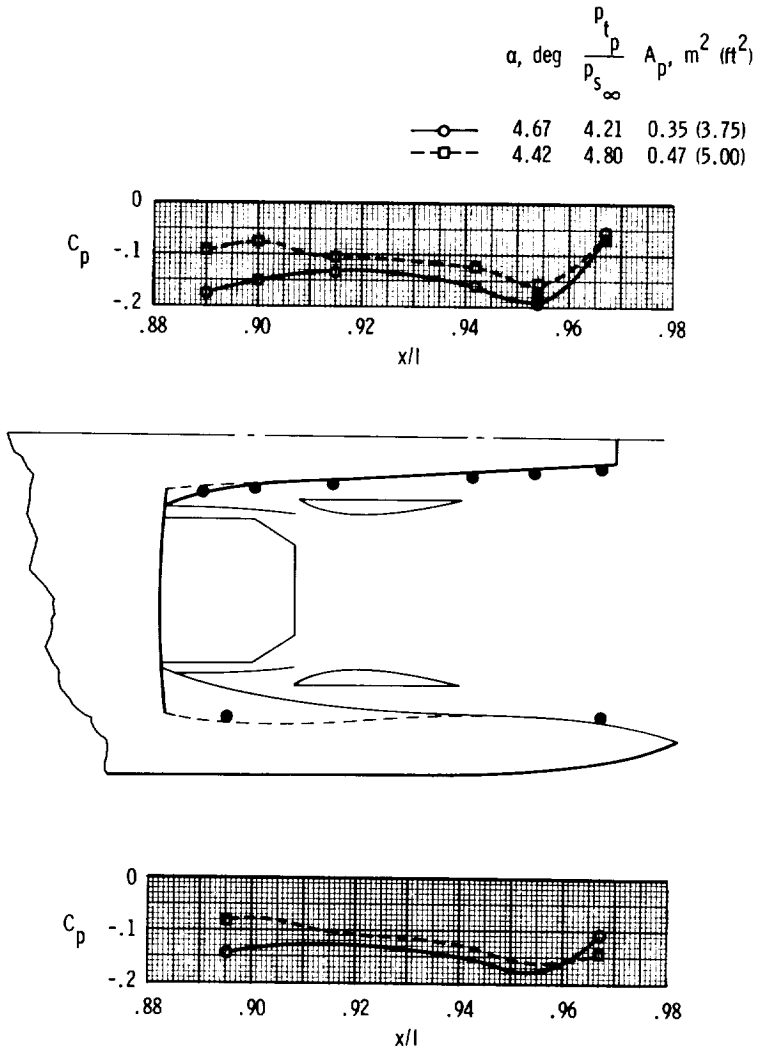

(c) Interfairing and speed bump pressure coefficients.

Figure 23. Continued.

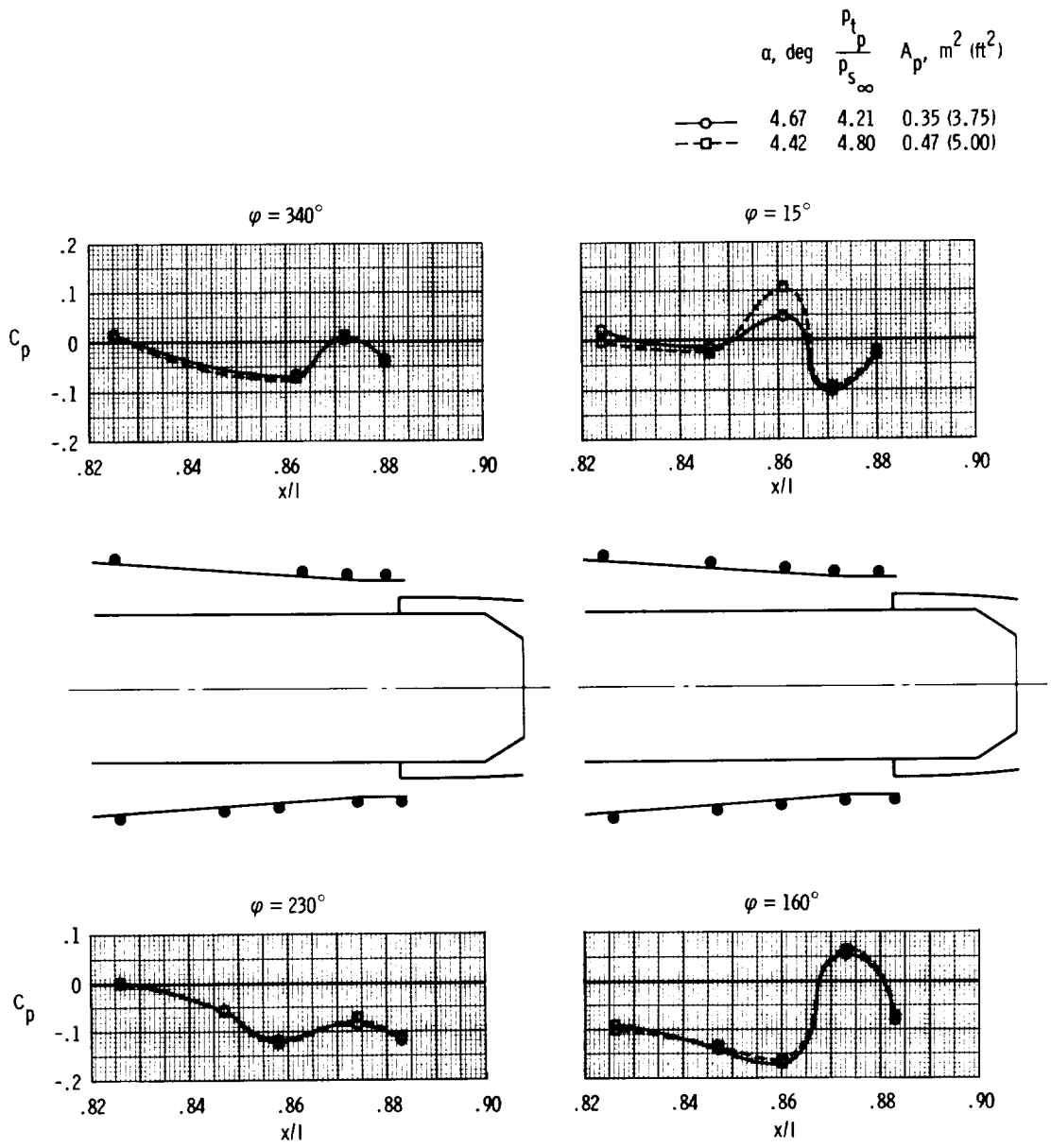

(d) Nacelle pressure coefficients.

Figure 23. Continued.

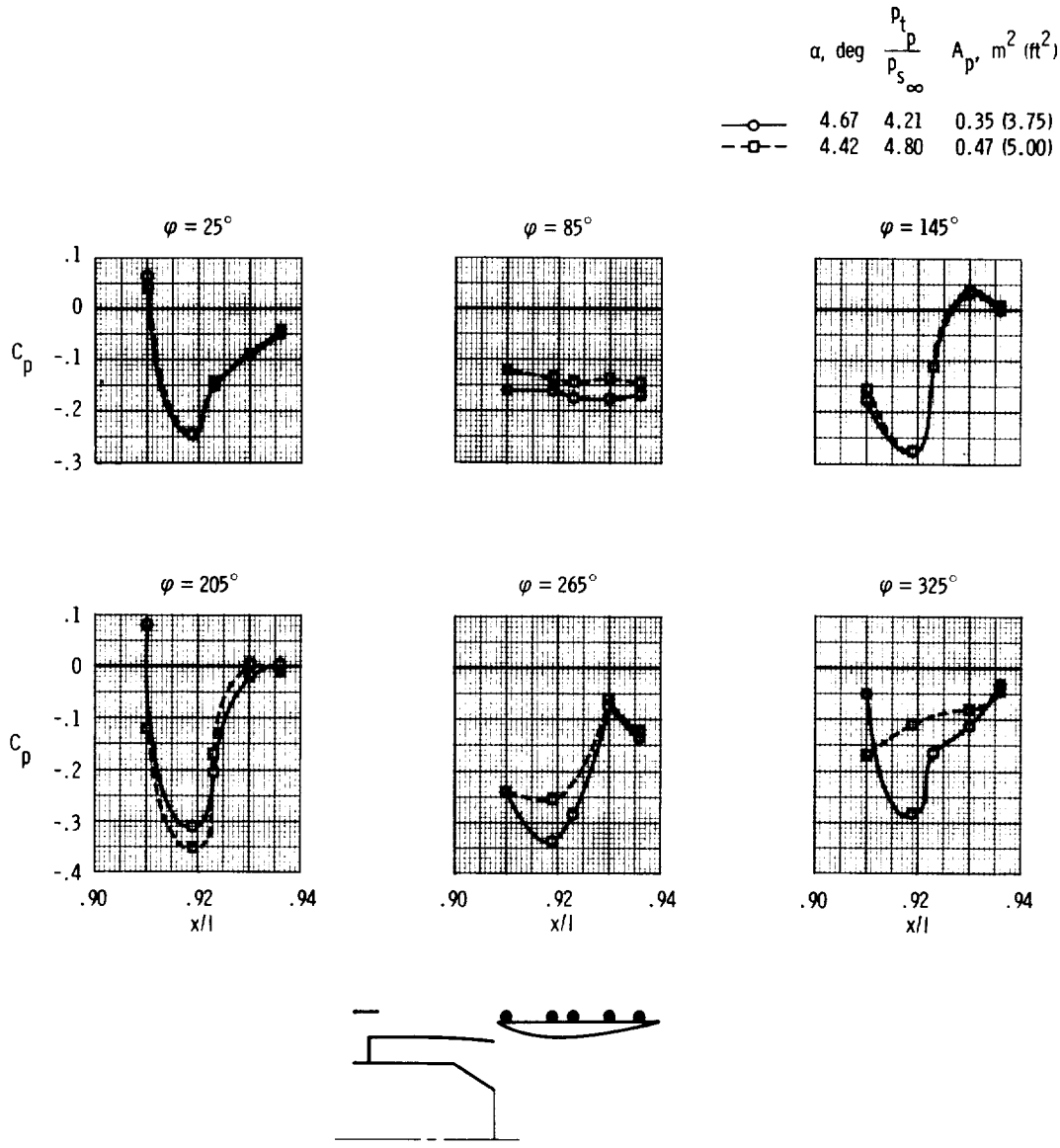

(e) Ejector nozzle pressure coefficients.

Figure 23. Concluded.

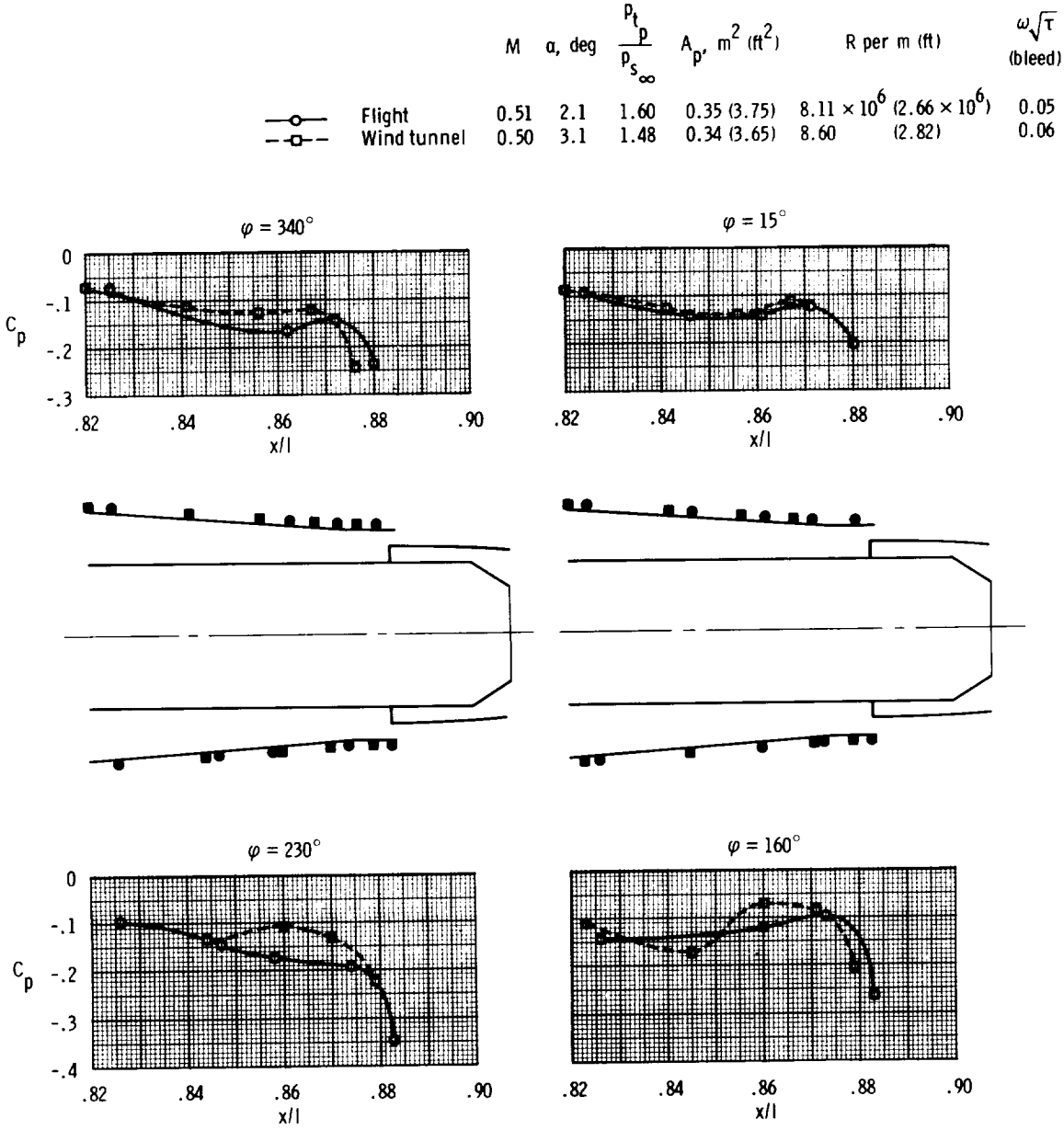

(a) Nacelle.

Figure 24. Comparison of flight and wind-tunnel pressure coefficients for $M \approx 0.50$.

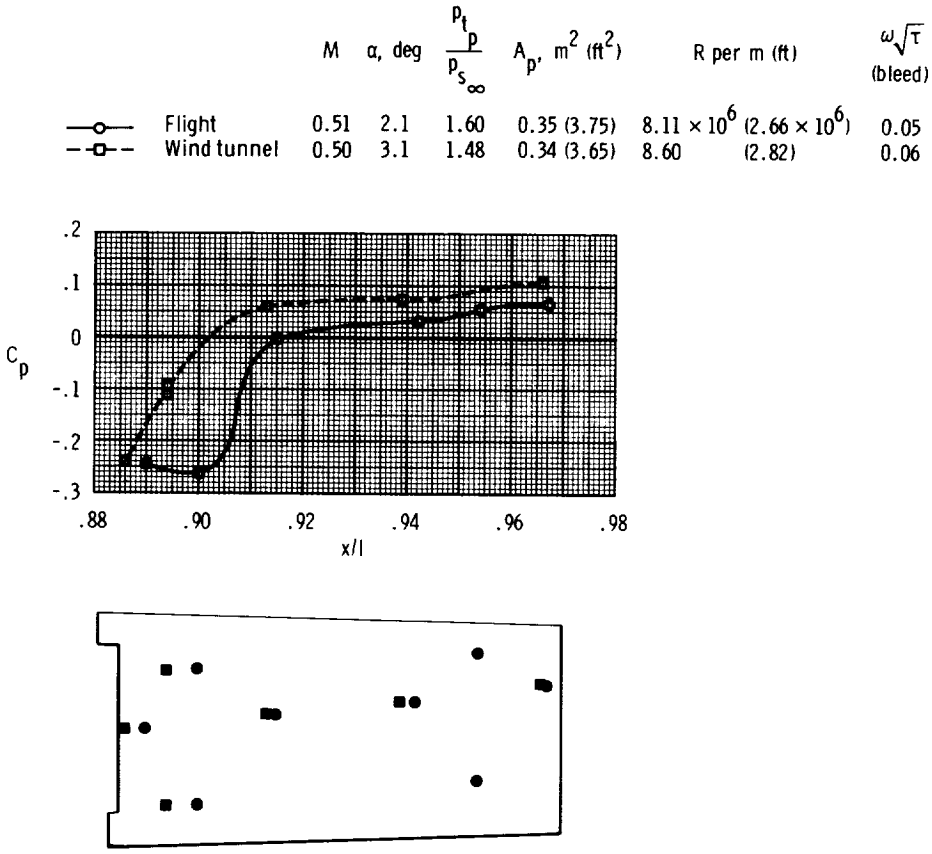

(b) Interfairing.

Figure 24. Continued.

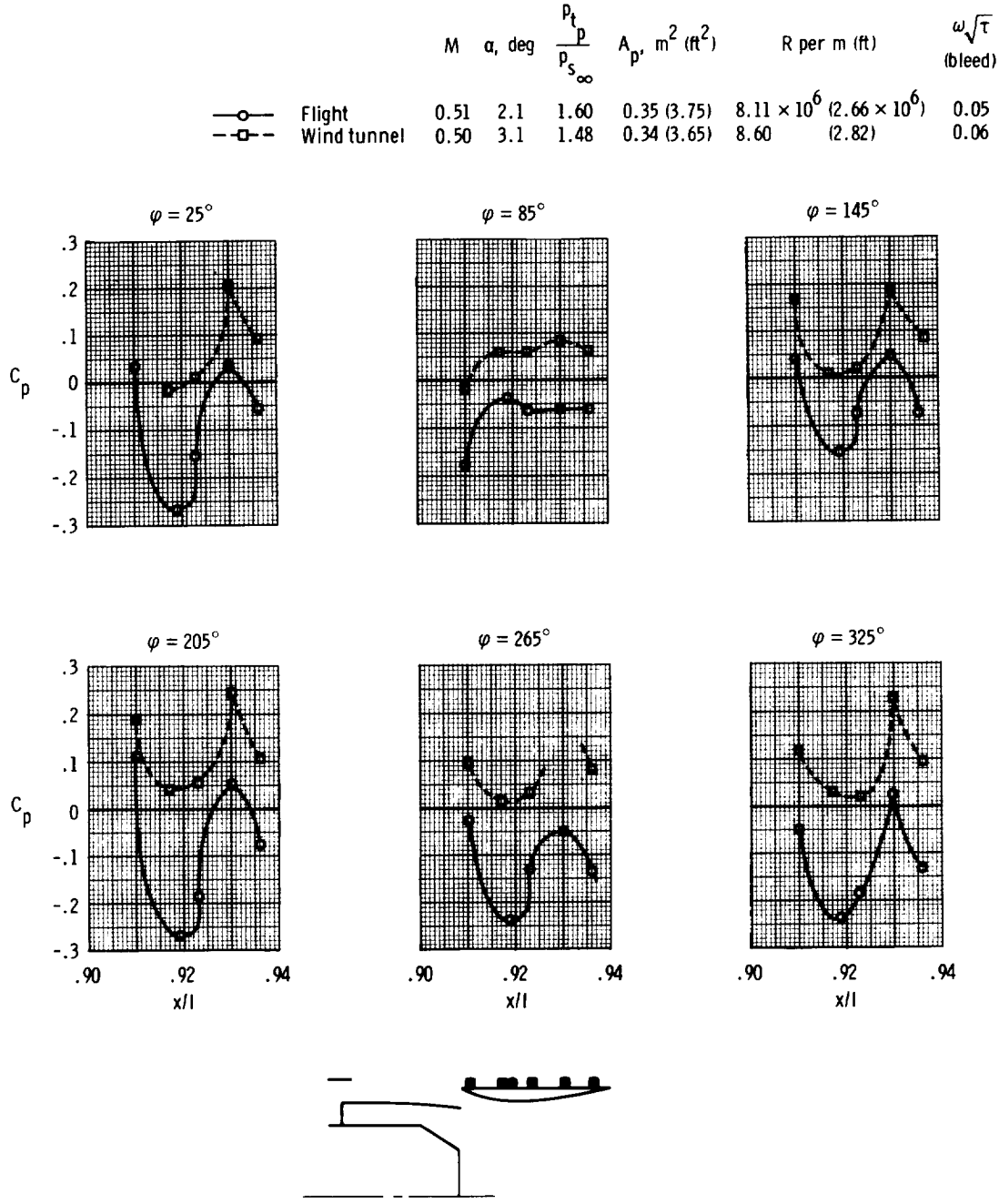

(c) Ejector nozzle.

Figure 24. Concluded.

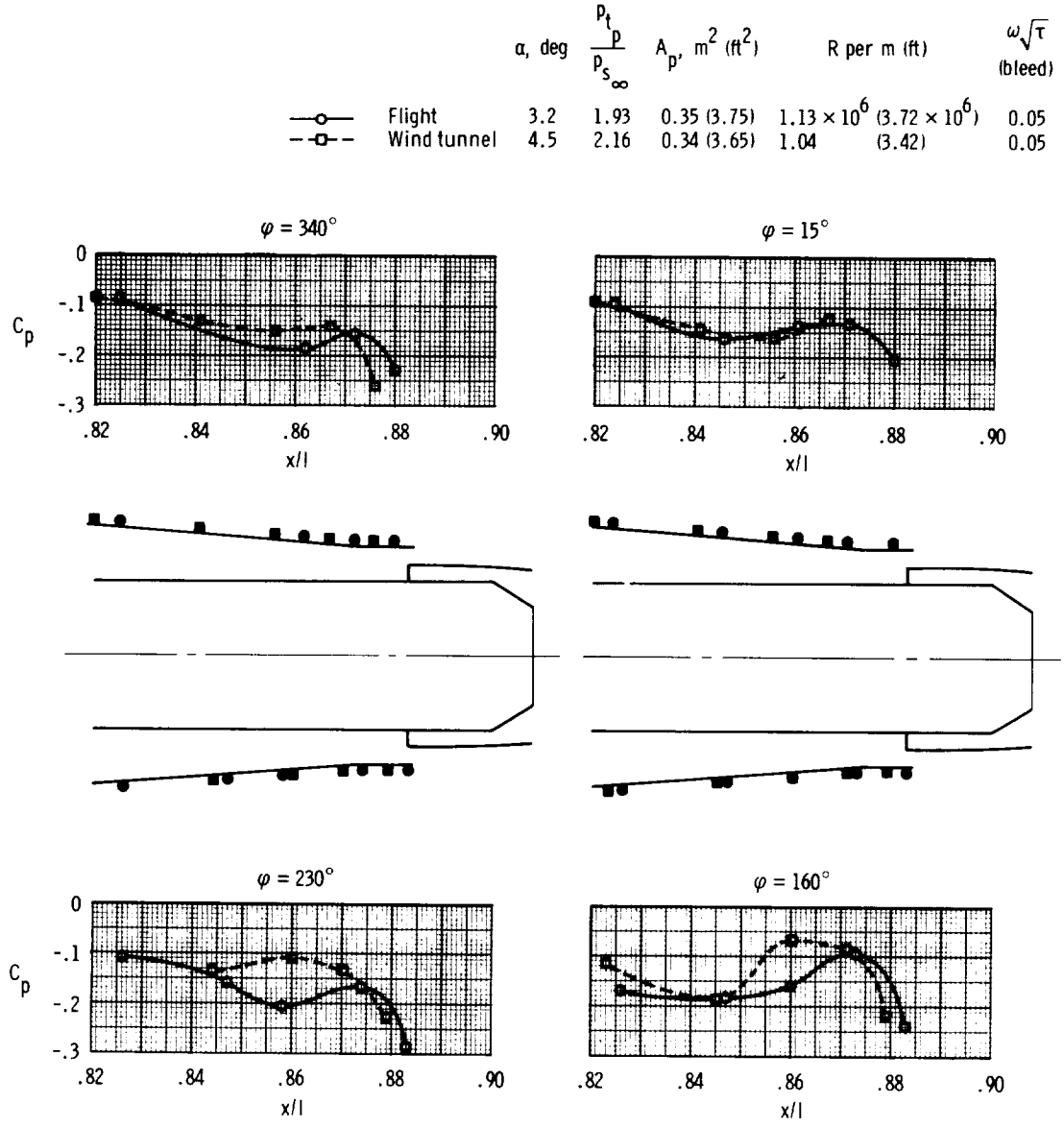

(a) Nacelle.

Figure 25. Comparison of flight and wind-tunnel pressure coefficients for M = 0.70.

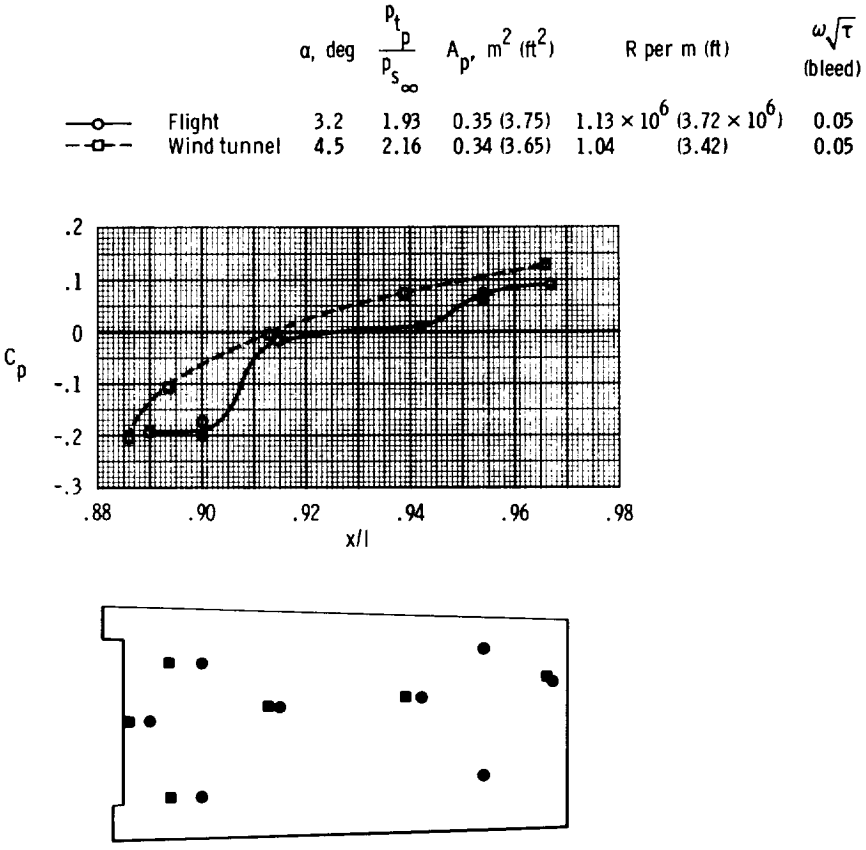

(b) Interfairing.

Figure 25. Continued.

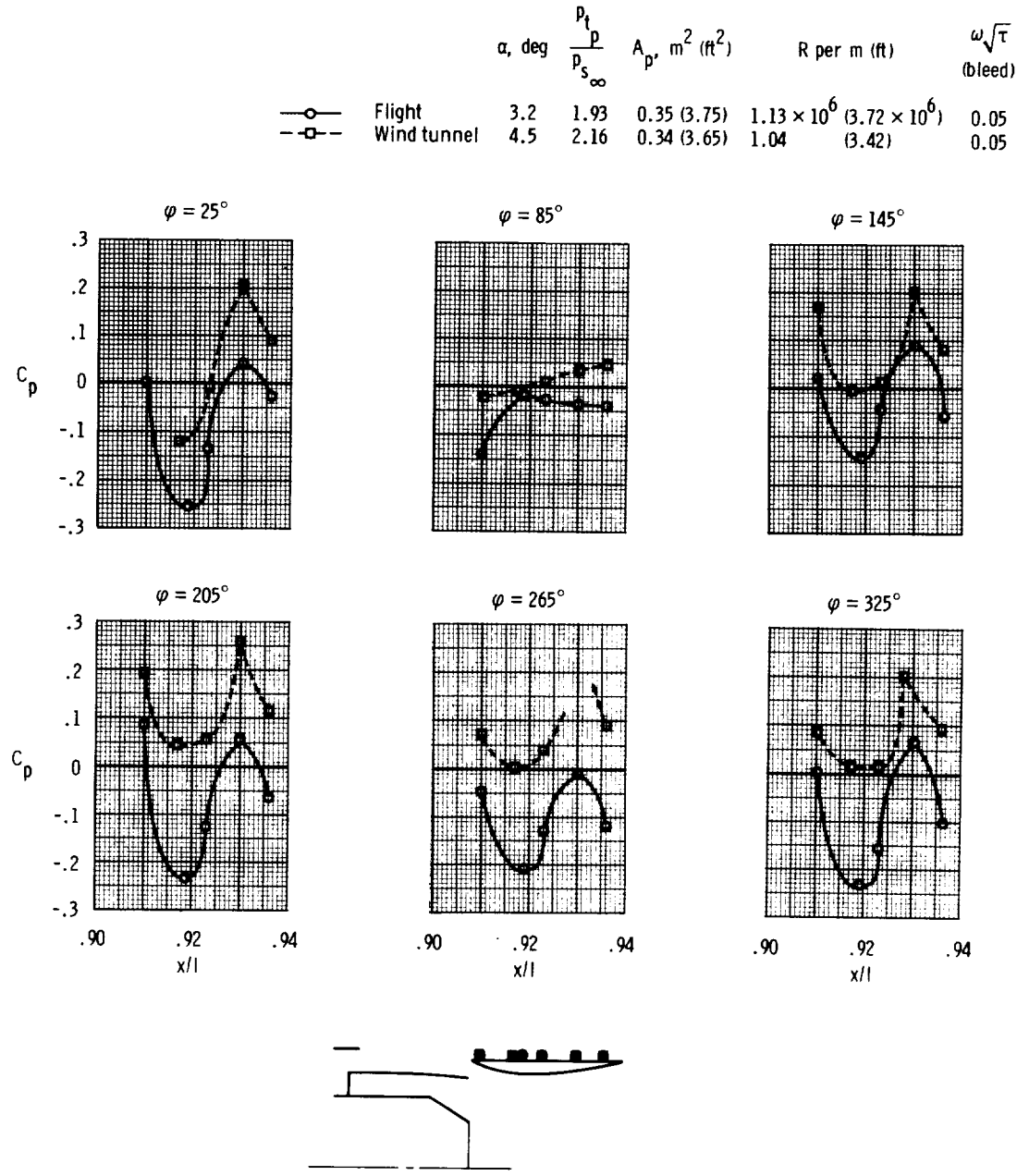

(c) Ejector nozzle.

Figure 25. Concluded.

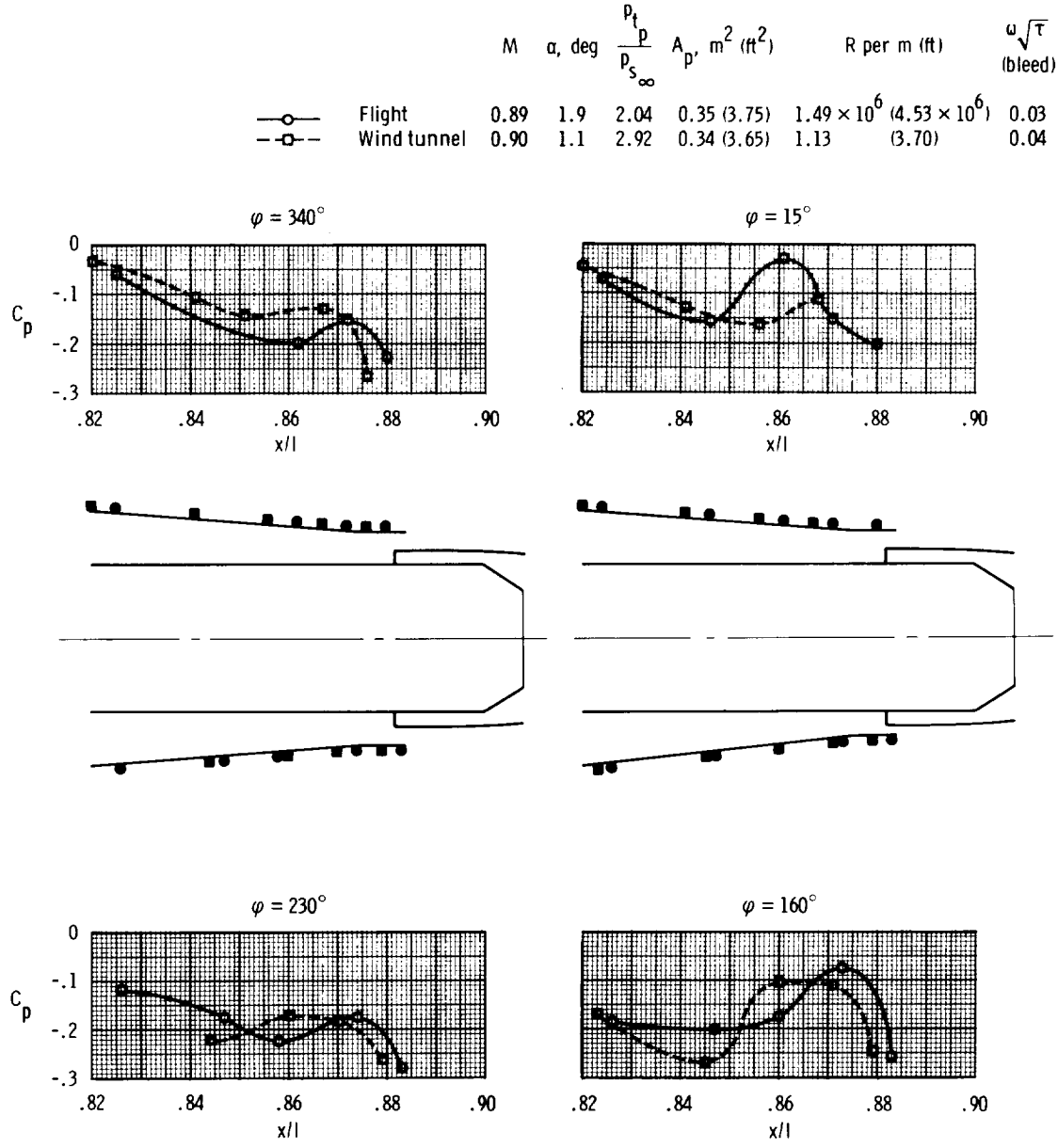

(a) Nacelle.

Figure 26. Comparison of flight and wind-tunnel pressure coefficients for $M \approx 0.90$.

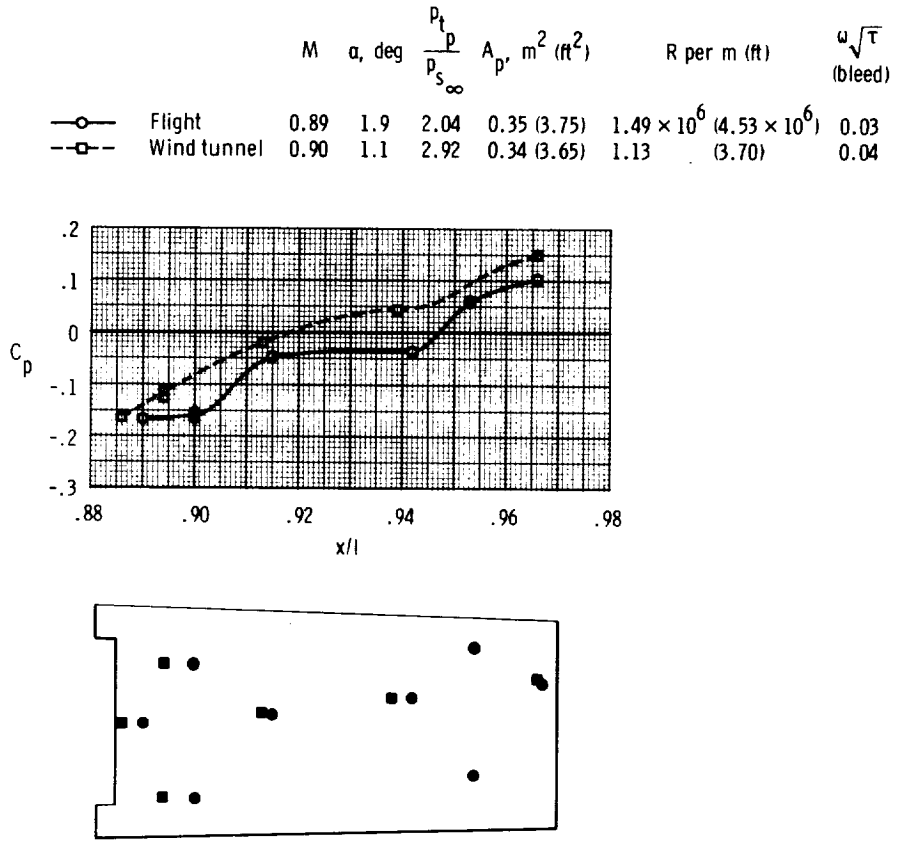

(b) Interfairing.

Figure 26. Continued.

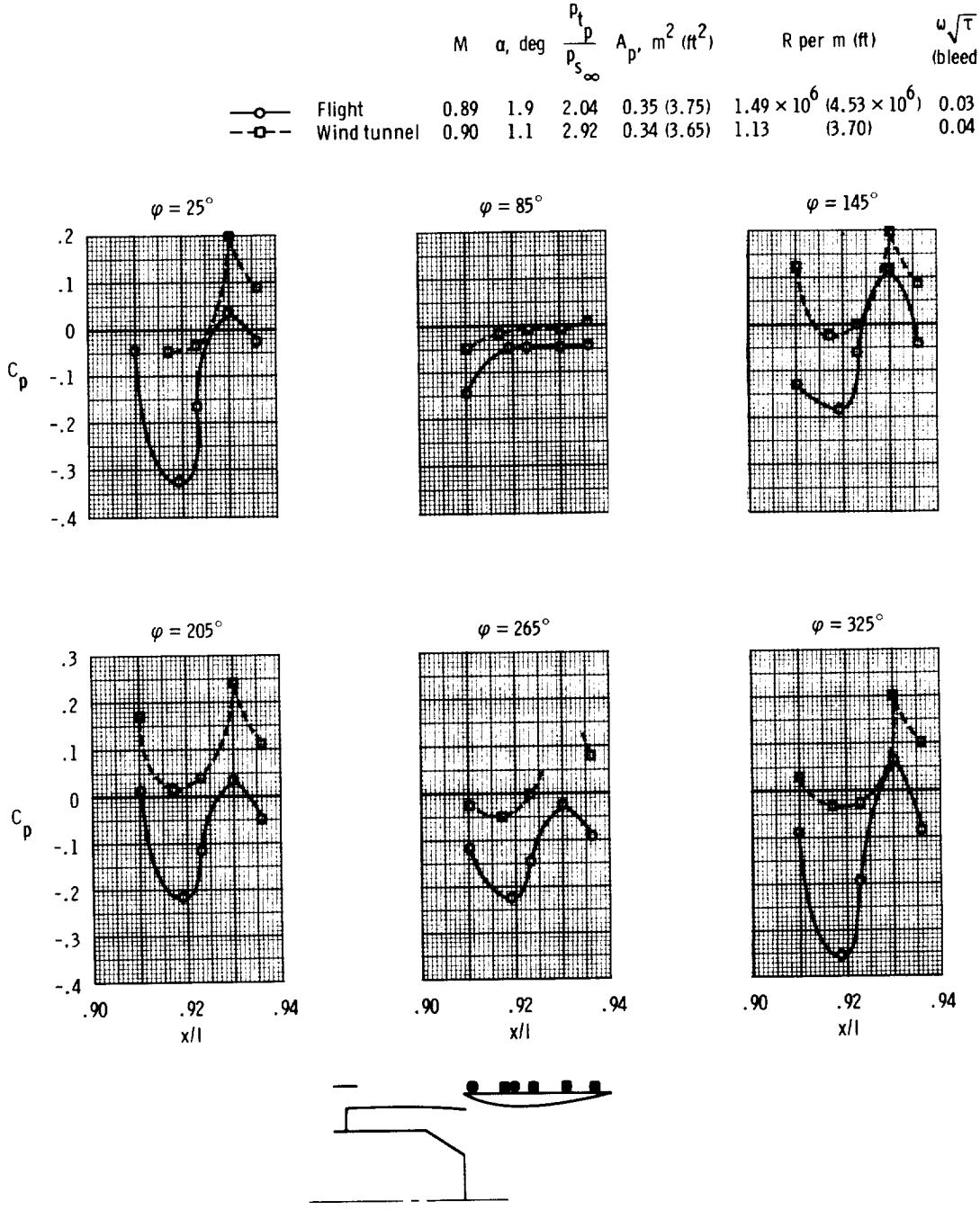

(c) Ejector nozzle.

Figure 26. Concluded.

U.S. Government Printing Office: 1974—737-360/50 Region No. 3-11